UNRAVELING THE DYNAMICS AND EQUILIBRIUM BEHAVIOR OF PURE AND MIXED MICELLES: INSIGHTS FROM MICROSCOPIC COARSE-GRAIN MODELING

Maria Pantelidou

UNIVERSITAT ROVIRA i VIRGILI

Unraveling the Dynamics and Equilibrium Behavior of Pure and Mixed Micelles:

Insights from Microscopic coarse-grain modeling

Doctoral Thesis

Maria S. Pantelidou

Supervised by Prof. Allan D. Mackie

Co-supervised by Prof. Josep Bonet Avalos

Universitat Rovira i Virgili
Departament d'Enginyeria Química
Tarragona, Spain

February, 2023

The University of Manchester

The International Distinction was awarded for the research conducted in collaboration with the University of Manchester.

UNIVERSITAT ROVIRA I VIRGILI
UNRAVELING THE DYNAMICS AND EQUILIBRIUM BEHAVIOR OF PURE AND MIXED MICELLES: INSIGHTS FROM MICROSCOPIC COARSE-GRAIN MODELING
Maria Pantelidou

WWW.URV.CAT

First edition, June 1, 2023

UNIVERSITAT ROVIRA i VIRGILI

FAIG CONSTAR que aquest treball, titulat "**Unraveling the Dynamics and Equilibrium Behavior of Pure and Mixed Micelles: Insights from Microscopic coarse-grain modeling**", que presenta **Pantelidou Maria** per a l'obtenció del títol de Doctor, ha estat realitzat sota la meva direcció al Departament **d'Enginyeria Química** d'aquesta universitat.

HAGO CONSTAR que el presente trabajo, titulado "**Unraveling the Dynamics and Equilibrium Behavior of Pure and Mixed Micelles: Insights from Microscopic coarse-grain modeling**", que presenta **Pantelidou Maria** para la obtención del título de Doctor, ha sido realizado bajo mi dirección en el Departamento **de Ingeniería Química** de esta universidad.

I STATE that the present study, entitled "**Unraveling the Dynamics and Equilibrium Behavior of Pure and Mixed Micelles: Insights from Microscopic coarse-rain modeling**", presented by **Pantelidou Maria** for the award of the degree of Doctor, has been carried out under my supervision at the Department of **Chemical Engineering** of this university.

Tarragona , 22/02/2023

El/s director/s de la tesi doctoral
El/los director/es de la tesis doctoral
Doctoral Thesis Supervisor/s

Allan Donald Mackie Walker - DNI 55227824V (TCAT)
Firmado digitalmente por Allan Donald Mackie Walker - DNI 55227824V (TCAT)
Fecha: 2023.02.21 10:46:20 +01'00'

Allan D. Mackie

Firmado por BONET AVALOS JOSE - 33912182Q el día

Josep Bonet Avalos

To my Family...

UNIVERSITAT ROVIRA I VIRGILI
UNRAVELING THE DYNAMICS AND EQUILIBRIUM BEHAVIOR OF PURE AND MIXED MICELLES: INSIGHTS FROM MICROSCOPIC COARSE-GRAIN MODELING
Maria Pantelidou

Acknowledgements

I would like to express my deep gratitude to my supervisor, Allan Mackie, for their invaluable guidance, support, and encouragement throughout my doctoral journey. Their expertise and dedication to my research were instrumental in shaping my work and providing valuable insights. I would also like to thank Josep Bonet for his continuous support and his valuable suggestions. I would like to extend my gratitude to Fabian Garcia for his unwavering support and assistance throughout my journey. He was always willing to troubleshoot issues and provide motivation when I needed it most. I am particularly thankful to Alexandro Patti for welcoming me into his team and for the wonderful hospitality during my time in Manchester.

I am also grateful for the support and guidance provided by Teresa Marmol, who was always willing to help and offer her support, both emotionally and practically. Also, many thanks to my colleague Fabricio Masullo, a great friend who was always lent an ear, shared his knowledge and provided valuable insights that helped me to navigate through my research work. Their support, encouragement and kind-heartedness made my stay in Tarragona more pleasant and productive.

I would also like to extend my gratitude to the scholarship program that made this journey possible. Without the financial support provided by the scholarship, I would not have been able to complete my Ph.D. I am truly grateful for the opportunity and support provided by the scholarship program and the people who administrate it.

I want to express my deepest gratitude to my partner, Giorgos, for his unwavering patience, understanding, and love throughout my entire PhD journey. His support and encouragement have been instrumental in helping me to achieve this important milestone. Lastly, I want to dedicate this Thesis to my Family, my parents and my brother, Simeon, Nikoleta and Lazaros, and to thank them for their love, support, and encouragement. Their belief in me has been a constant source of strength and motivation. I am deeply grateful to them for all that they have done for me, and for being my rock during my Ph.D journey.

Thank you all.

This thesis has received funding from the European Union's Horizon 2020 research and innovation programme under the Marie Skłodowska-Curie grant agreement No. 713679 and from the Universitat Rovira i Virgili (URV). JBA and ADM wish to thank the *Ministerio de Ciencia, Innovación y Universidades* (MCIU), of the Spanish Government for financial support, grant CTQ2017-84998-P *Segregación molecular a múltiples escalas en sistemas no tensioctivos para la obtención de materiales avanzados*.

Marie Skłodowska-Curie
Actions

Abstracts

English

This thesis focuses on exploring and controlling the mechanisms behind the formation and dynamic behavior of pure and mixed micelles, which are widely used across many industries. Single-Chain Mean-Field simulations of coarse-grain models are proposed as a quick and efficient way to explore these complex molecular systems. The thesis is divided into two parts, the first of which explores the dynamic behavior of micelles using time correlation functions and dynamic Single-Chain Mean-Field theory simulations. The results show that the exit of poloxamer copolymers from micelles exhibits four distinct regimes: a fast reorganization, a logarithmic intermediate regime, an exponential intermediate regime, and a final exponential decay. It was observed that the logarithmic response previously believed to be due to polydispersity can also arise from the degeneracy of energy states of the hydrophobic block in the micelle core. This finding suggests that the short-time dynamic response of these systems has an entropic origin rather than being influenced by polydispersity as previously thought. A modified Eyring equation was proposed to reproduce the observed dynamic behavior. The second section of the thesis delves into the examination of the equilibrium behavior of mixed micelles utilizing the Single-Chain Mean-Field method for binary systems. The study reveals that the formation of mixed micelles is greatly influenced by the ratio of total A and B surfactant concentrations, and the CMC of mixed micelles is lower than that of the shorter surfactant and falls between the CMCs of the pure A and B surfactants. The results were compared with existing experimental data, and a good match was observed, further validating the findings.

Spanish

Esta tesis se centra en explorar y controlar los mecanismos detrás de la formación y el comportamiento dinámico de micelas puras y mixtas, las cuales son ampliamente utilizadas en muchas industrias. Se proponen simulaciones de campo medio de una cadena única de modelos *coarse-grain* como una forma rápida y eficiente de explorar estos sistemas moleculares complejos. La tesis se divide en dos partes, la primera de las cuales explora el comportamiento dinámico de las micelas utilizando funciones de correlación temporal y simulaciones de la teoría dinámica de campo medio de una sola cadena. Los resultados muestran que la salida de copolímeros poloxámero de las micelas exhibe cuatro regímenes distintos: una rápida reorganización, un régimen intermedio logarítmico, un régimen intermedio exponencial, y una decadencia exponencial final. Se observó que la respuesta logarítmica previamente creída debido a la polidispersidad también puede surgir de la degeneración de estados de energía del bloque hidrofóbico en el núcleo de la micela. Este hallazgo sugiere que la respuesta dinámica a corto plazo de estos sistemas tiene un origen entrópico en lugar de ser influenciada por la polidispersidad, como se pensaba anteriormente. Se propuso una ecuación de Eyring modificada para reproducir el comportamiento dinámico observado. La segunda sección de la tesis se adentra en el examen del comportamiento de equilibrio de las micelas mixtas utilizando el método de campo medio de una sola cadena para sistemas binarios. El estudio revela que la formación de micelas mixtas está fuertemente influenciada por la relación de las concentraciones totales de tensioactivos A y B, y la CMC de las micelas mixtas es menor que la del tensioactivo más corto y se sitúa entre las CMC de los tensioactivos puros A y B. Los resultados se compararon con datos experimentales existentes y se observó una buena coincidencia, lo que valida aún más los hallazgos.

Catalan

Aquesta tesi es centra en explorar i controlar els mecanismes darrere de la formació i el comportament dinàmic de micel•les pures i mixtes, les quals són àmpliament utilitzades en moltes indústries. Es proposen simulacions de camp mitjà d'una cadena única de models *coarse-grain* com una forma ràpida i eficient d'explorar aquests sistemes moleculars complexos. La tesi es divideix en dues parts, la primera de les quals explora el comportament dinàmic de les micel•les utilitzant funcions de correlació temporal i simulacions de la teoria dinàmica de camp mitjà d'una sola cadena. Els resultats mostren que la sortida de copolímers poloxàmer de les micel•les exhibeix quatre règims distintius: una ràpida reorganització, un règim intermedi logarítmic, un règim intermedi exponencial i una decadència exponencial final. Es va observar que la resposta logarítmica prèviament creguda degut a la polidispersitat també pot sorgir de la degeneració d'estats d'energia del bloc hidrofòbic en el nucli de la micel•la. Aquesta troballa suggereix que la resposta dinàmica a curt termini d'aquests sistemes té un origen entròpic en lloc de ser influïda per la polidispersitat, com es pensava anteriorment. Es va proposar una equació d'Eyring modificada per reproduir el comportament dinàmic observat. La segona secció de la tesi es planteja l'examen del comportament d'equilibri de les micel•les mixtes utilitzant el mètode de camp mitjà d'una sola cadena per a sistemes binaris. L'estudi revela que la formació de micelles mixtes està fortament influenciada per la relació de les concentracions totals de tensioactius A i B, i la CMC de les micel•les mixtes és menor que la del tensioactiu més curt i es situa entre les CMC dels tensioactius purs A i B. Els resultats es van comparar amb dades experimentals existents i es va observar una bona coincidència, la qual cosa valida encara més els resultats.

Contents

List of Figures

List of Tables

1

Background

1.1 | Introduction

1.1.1 | Surfactants

Amphiphilic molecules are broadly defined as any compound with two distinct covalently bonded components that have different solvent affinities within the same molecule. One part has a strong affinity for nonpolar solvents like hydrocarbons, ethers, and esters and the other part has a strong affinity for polar solvents like water. The prefix "amphi-" comes from the Greek words "amphi ($\acute{\alpha}\mu\phi\iota$)", meaning "both", and the suffix "-philic" comes from "philos ($\phi\acute{\iota}\lambda o\varsigma$)", meaning "friend". Together, these words describe the dual nature of these molecules as having both hydrophobic (oil-like) and hydrophilic (water-like) parts. Surfactants are amphiphilic molecules, well known as surface active agents as they tend to lower the surface tension of a liquid or the interfacial tension between two liquids or between a liquid and a solid. They consist of hydrophobic (water-insoluble) tail groups and hydrophilic (water-soluble) head groups (Figure 1.1), where the hydrophobic ends are able to interact favorably with the hydrophobic substances, while the hydrophilic ends interact favorably with the water (4). This allows surfactants to solubilize hydrophobic substances in water, mix oils and water together in products like shampoo and soap, and lower the surface tension of water, making it easier to wet and spread over surfaces (5; 6; 7).

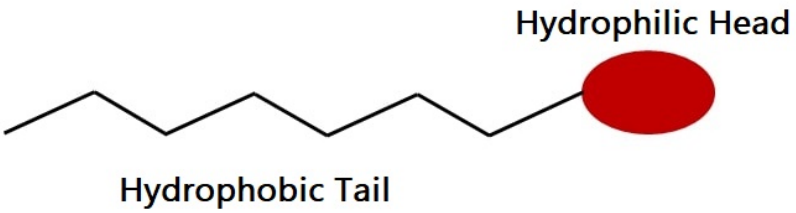

Figure 1.1: Schematic representation of the hydrophilic head group and the hydrophobic tail group of a surfactant molecule.

On account of this, surfactants are widely used in a variety of biological processes including cell mobility, cell communication etc. as well as in many industrial areas such as in petroleum industry for enhancing oil recovery and in cosmetics in health and beauty products such as emulsifiers, foaming agents, detergents, wetting agents etc. (8; 9; 10). For example, surfactants have been employed to create nanoparticles that possess properties such as stability, compatibility, and non-toxicity, making them suitable for use in drug delivery systems. They are also powerful inhibitors of P-glycoprotein, a trait that

is beneficial for increasing drug absorption and targeting specific tissues, as exemplified by their use in the delivery of anticancer drugs, steroids, HIV protease inhibitors, cardiovascular drugs, and beta-blockers (10). In addition, anionic surfactants, which are a type of surfactant that contain a negative charge on their hydrophilic, are widely utilized in laundry detergents as they are highly effective in removing dirt, clay, and oil stains. When these surfactants are dissolved in water, they become ionized, acquiring a negative charge. This allows them to effectively attract and bind to positively charged dirt, clay, and oil stains, resulting in their removal. Also, amphoteric surfactants, a type of surfactant that has both positive and negative charges on the hydrophilic head group, contain ions that can adapt their charge depending on changes in environmental conditions, such as pH, making them versatile and useful for various cleaning applications (9).

1.1.2 | Classification of Surfactants

The polar head group's charge can be positive, negative, or neutral, and depending on that charge, a surfactant's properties may vary under specific circumstances (11) (Figure 1.2). For instance, positively charged surfactants are not typically used as detergents since they are not good in cleaning. In contrast, studies have demonstrated that positively charged surfactants are more effective in cleaning oily dirt and oil/clay soil, but negatively charged surfactants are better at removing impurities that are positively charged. Neutral surfactants, on the other hand, could be more versatile and able to interact with both positively and negatively charged molecules (9; 12; 13). Therefore, depending on the charge of their polar head group surfactants are classified as follows:

- Nonionic surfactants have no electrical charge on the hydrophilic head group, and they are commonly used as emulsifiers and wetting agents. Examples include alkylphenol ethoxylates and polyethylene oxide.
- Cationic surfactants have a positive charge on the hydrophilic head group and are often used as fabric softeners and hair conditioners. Subtypes of cationic surfactants include alkyl amines, ethoxylated amines, alkyl imidazolines and quaternaries.
- Anionic surfactants contain a negative charge on their hydrophilic substance and can be used in a wide range of products, including detergents, dishwashing liquids, shampoos, body washes, and hand soaps. Examples of anionic surfactants include the sodium lauryl sulfate (SLS), sodium dodecylbenzene sulfonate (SDBS), sodium lauryl ether sulfate (SLES) and sodium linear alkylbenzene sulfonate (LAS).

- Amphoteric/Zwitterionic surfactants have both positive and negative charges on the hydrophilic head group. This means that they can behave like either anionic or cationic surfactants depending on the physical conditions such as the pH of the solution in which they are placed. At low pH, amphoteric surfactants can behave like cationic surfactants, while at high pH, they behave like anionic surfactants (14). Some examples of amphoteric surfactants include betaines and sultaines. These surfactants are often used in personal care products such as shampoos, body washes, and facial cleansers.

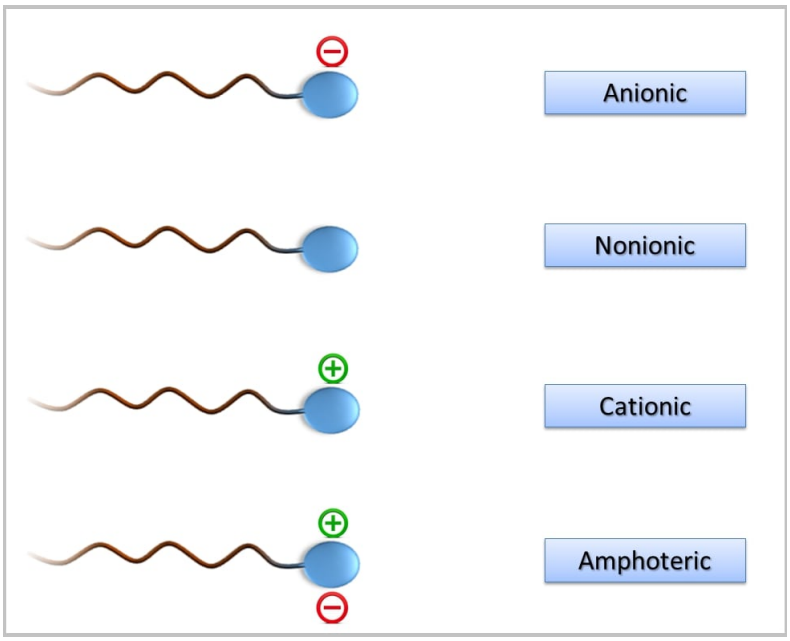

Figure 1.2: Classification of surfactants. Anionic surfactant polar heads are charged negatively, nonionic surfactants polar heads have no charge, cationic surfactants polar heads are charged positively, and amphoteric surfactants polar heads are charged positively or negatively depending on the circumstances of the solution in which they are dissolved.

Common surfactant molecules have molecular weights of 500 Da, which are considered small molecules. However, some block copolymers can also have an amphiphilic nature and are typically 10-1000 times larger than common surfactants (14). Examples of block copolymers include diblock and triblock copolymers. Polyethylene oxide-polypropylene oxide-polyethylene oxide (PEO-PPO-PEO) molecules are nonionic triblock copolymer surfactants that are known commercially as Pluronics ®. These molecules consist of a central hydrophobic polypropylene oxide chain connected to two hydrophilic

polyethylene oxide chains.

1.1.3 | Conditions under which Micelles can Appear in Solution

Because of their amphiphilic nature, surfactants tend to accumulate at the water-air interface when in solution. The hydrophilic group is found preferentially in the water solution, while the hydrophobic group is in the air. When the concentration of surfactants in the water is increased, the water-air interface becomes saturated, and the surfactants are forced into the solution and begin to self-assemble into aggregates known as micelles (15) (Figure 1.3).

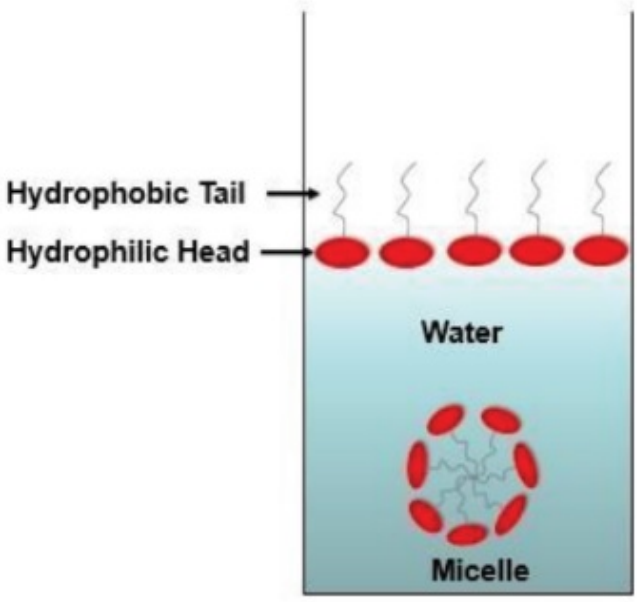

Figure 1.3: Surfactant behavior when dissolved in aqueous media.

This aggregation process is motivated by the the well-known Hydrophobic effect (16) and takes place due to the tendency of nonpolar molecules to avoid interacting with water. Namely, water molecules are polar, while the nonpolar tail groups of surfactants interact disfavorably with water. Since the tail groups of surfactants prefer to interact with each other, the formation of aggregates allows the surfactants to minimize the contact with water.

1.1.4 | Thermodynamics of the Hydrophobic Effect

The hydrophobic effect is driven by the need to minimize the standard Gibbs (eq. (1.1)) free energy of the surfactant solution, which involves balancing the enthalpy and entropy changes that occur during the formation of aggregates (17).

$$\Delta G = \Delta H - T\Delta S, \tag{1.1}$$

where ΔG is the change in the standard Gibbs free energy, ΔH is the enthalpic change, T is the temperature, and ΔS is the entropic change.

To further understand the hydrophobic effect, it is important to consider how surfactants interact with water. In order to minimize the free energy of the system, surfactants will begin to form aggregates, resulting in a decrease in the entropy of the system. As the surfactant molecules come together, the hydrophobic tails of the molecules are no longer exposed to water. This decrease in entropy is offset by the decrease in enthalpy. The enthalpy decreases as a result of the unfavorable interactions between the hydrophobic tails of the surfactant molecules in an aqueous environment, leading to a reduction in the overall energy of the system (18).

Due to the hydrophobic effect, surfactants tend to form aggregates that differ in shape and size depending on their structure and the solvents they are dissolved in. Some common examples of these aggregates include spherical and non-spherical micelles like worm-like micelles, while there is the possibility of forming larger structures such as bilayers which can lead to liposomes or vesicles (18; 19).

1.1.5 | Micelles

Micelles are very small 'clusters' that form when surfactants self-assemble in aqueous media once their concentration surpasses a certain value. They are nanostructures with sizes between 1-100 nanometers in diameter and they contain a hydrophobic core made of surfactant tails interacting with each other and a hydrophilic corona made of surfactant heads, in contact with the water.

Micelles are highly versatile and adaptable structures that can be used in a variety of applications. Depending on the chemical structure of surfactants or the solvent in which they are dissolved, they can take different shapes and have different sizes. Some of the most common types of micelles are spherical, cylindrical (worm-like), vesicular, and reversed micelles (Figure 1.4) (20; 21).

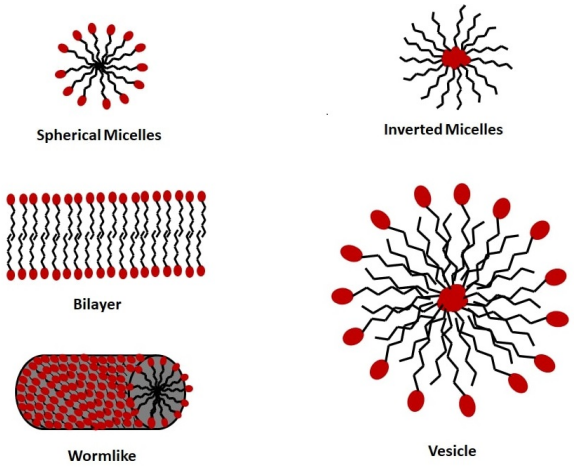

Figure 1.4: Surfactants can form micelles with different geometries when they are dissolved in a solvent above a specific concentration.

1.1.6 | Critical Micelle Concentration (CMC)

As mentioned before, the formation of micelles begins above a specific concentration of surfactants in water. This concentration is called Critical Micelle Concentration (CMC) and it is one of the most important characteristics of the micellization process.

The CMC has been defined by several theoretical and experimental methods as the concentration at which the slope of a given physicochemical property versus concentration changes sharply within a narrow concentration range (22), as illustrated in Figure 1.5.

1.1.7 | Applications and Future of Micelles

Over the past few decades, micelles have gained significant importance due to their widespread usage in a variety of very important applications including drug delivery systems, food applications etc. For example, drug delivery systems have shown micelles to be important due to their solubility, stability, and non-toxicity. In recent years, they have been used as carriers for several drugs in the treatment of various diseases, as well as for imaging and diagnostic purposes. Micelles are able to solubilize drugs in their core and deliver them to specific tissues or cells within the body without affecting any healthy neighboring tissues. Finally, they are able to control the release rate of the drug through coating with polymeric matrices.(21; 23; 24; 25; 26; 27; 28; 29).

In the food industry, micelles can be used for oil and protein extraction, as well as for the development of effective antioxidants, the separation and purification of enzymes,

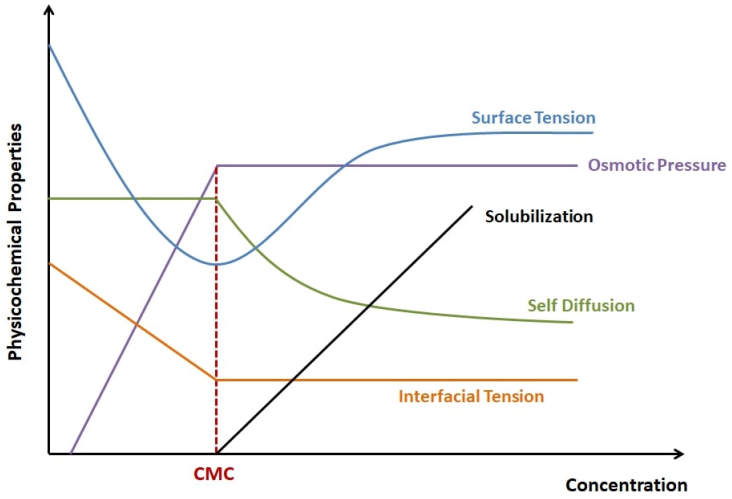

Figure 1.5: Schematic representation of the CMC, which is defined as the value at which the slope of a physicochemical property versus concentration changes.

the fabrication of enzyme-immobilized magnetic nanoparticles, and the enrichment of food-derived components for analysis and quantification (30).

Future research and development on micelles is expected to focus on finding new and improved applications for these structures. The creation of innovative micelles with enhanced drug delivery capabilities, the use of micelles in food processing to improve the quality of food products, and the development of micelles for use in environmental cleaning and oil recovery are a few prospective study fields.

1.2 | Micellization Behavior: Literature Review

The behavior of surfactants, the micellization process, and the dynamic behavior of micelles have all been the subject of numerous theoretical and experimental studies over the past few years.

1.2.1 | Experimental Studies

From the experimental point of view, the methods used include dynamic light scattering (31; 32; 33; 34), small-angle X-ray scattering (35; 36; 37; 38; 39), nuclear magnetic resonance spectroscopy (40; 41), fluorescence spectroscopy (42; 43; 44) etc. Specifically, dynamic light scattering identifies the size and shape of micelles by using lasers that are scattered on interacting with any aggregates in the solution. Researchers can measure

these properties by monitoring the intensity and the frequency of the scattered light over time (45). Nuclear magnetic resonance spectroscopy (NMR) uses magnetic fields and energy transfer to measure various properties such as phase changes, conformational and configurational changes, solubility, and diffusion potential (46; 47). Finally, Fluorescence spectroscopy uses fluorescent probes to identify the properties of the micelles, by measuring the intensity and wavelength of fluorescence emitted by the probes associated with any micelles in solution (42).

1.2.2 | Theoretical Studies

Simulations can be a valuable tool for studying surfactant systems, as they enable researchers to investigate the properties and interactions between molecules at the atomic level. They use mathematical models, usually based on statistical mechanics and are able both to test different theories in a fast and low-cost way (48) and more fully understand the experimental results.

Three types of simulation models may be used to examine how structure develops in surfactant solutions: atomistic, coarse grain models and mesoscale models (49) (Figure 1.6).

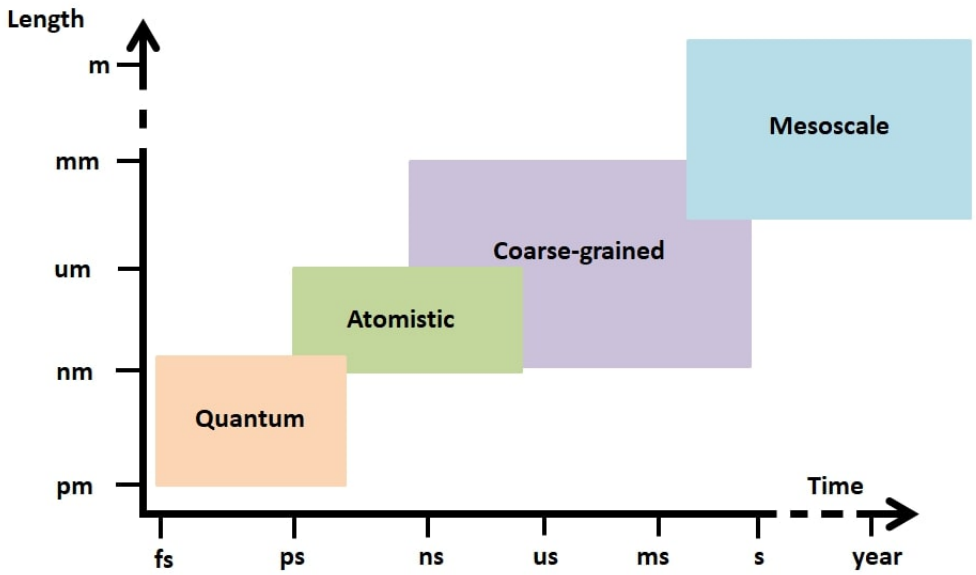

Figure 1.6: Computer simulation models depending on the properties under study.

Molecular dynamics simulation using atomistic models (50) by either “all atom” or “united atom” where pseudoatoms are used which are small groups of atoms repre-

sented by individual site. These models account for interactions between atoms using, typically, the Lennard-Jones potential for the non-bonded non-electrostatic interactions, (eq. (1.2)).

$$V_{LJ}(r_{ij}) = 4 \cdot \varepsilon_{ij} \left[\left(\sigma_{ij}/r_{ij}\right)^{12} - \left(\sigma_{ij}/r_{ij}\right)^{6} \right], \tag{1.2}$$

where r_{ij} is the distance between two particles (i and j), while ε_{ij} and σ_{ij} are constants and depend on the nature of the interacting particles.

This is a very powerful methodology but has limitations when studying surfactant systems due to the large computational resources required. Consequently, it can accurately predict properties of aggregates only close to equilibrium and has severe limitations in predicting their dynamic behavior for large time scales. On the other hand, with Coarse Grain models (49), the surfactant molecules are grouped together at a coarser level of detail, as well as the solvent molecules. These models are often used to study the micellization process through both lattice (51; 52; 53) and off-lattice models (48; 54; 55). Lattice models restrict the movement of the molecules, resulting in a significant reduction in computational time. In contrast, off-lattice models use continuous space rather than discrete points, allowing more flexibility in the motion of the molecules, leading to more realistic models, but at the cost of increased computational time. Additionally, mesoscale modeling frequently employs Dissipative Particle Dynamics (DPD), which generally uses a larger scale compared to coarse grain models. DPD simulations allow for larger groups of atoms to be modeled by a single site, which results in soft-conservative interaction potentials. This allows for the use of relatively large time steps, resulting in more efficient computation for the longer time scales typically required for micellar processes (49). In recent years several simulation methods have been implemented to study surfactant systems, including Molecular dynamics (MD) simulations (20; 50; 54; 56; 57), Monte Carlo simulations (MC) (51; 52; 53; 58; 59; 60; 61; 62; 63; 64; 65), Brownian Dynamics (BD) (66; 67; 68), Dissipative Particle Dynamics (DPD) (69; 70; 71; 72; 73; 74) as well as Mean Field theories (1; 75; 76; 77; 78). The appropriate method depends on the properties being studied. Molecular dynamics (MD) is a computational method that uses force fields to introduce interactions between particles. There are three types of interactions between the particles: bonded, non-bonded, and external field interactions. Subsequently, Newton's equations of motion are integrated to calculate the new position and velocity of the particles, while controlling the thermodynamic parameters.

$$F = m \cdot \mathbf{a} \Rightarrow \tag{1.3}$$

$$-\frac{dV}{d\mathbf{r}} = m\frac{d^2\mathbf{r}}{dt^2}. \tag{1.4}$$

The MD simulation traces out a trajectory in phase space as the system evolves over time, moving from one point in phase space to another. Specifically, Newton's equation of motion is integrated by taking a short timestep to get the position (r) of each particle at time (t) given the initial coordinate (r_0) at time (t_0). Different initial conditions calculate different trajectories. The entire process is repeated for a chosen number of steps and averages over the different trajectories. From the MD simulation the time average of any property under study can be extracted as follows:

$$\langle A \rangle = \lim_{\tau \to \infty} \frac{1}{T} \int_{t=0}^{T} A\left(\mathbf{p}(t), \mathbf{r}(t)\right)\, dt. \tag{1.5}$$

The integration is completed by averaging over all M time steps.

$$\langle A \rangle = \frac{1}{M} \sum_{i=1}^{M} A\left(\mathbf{p}, \mathbf{r}\right) \tag{1.6}$$

MD simulations are limited in the length of time they can reach due to the extensive computation time required to simulate the evolution of the system. This can make it challenging to reach equilibrium in certain complex systems.

In contrast, the Monte Carlo (MC) simulation method has previously been used to study complex systems (51; 52; 53; 58; 59; 60; 61; 62; 63; 65). Monte Carlo is a stochastic computational method that involves the use of random numbers. It generates random movements of particles, creating different states until the system reaches equilibrium. These movements are accepted within a certain probability associated with the Boltzmann distribution, which states that only low energy configurations are the most probable. Specifically, MC tries to find and sample the low energy configurations until it covers the whole phase space. In this manner, MC simulations are capable of approximating a complicated system using a statistical sample.

The probability distribution in the canonical ensemble (NVT) is given by

$$P(i) = \frac{1}{Q}\exp\left(-\frac{E_i}{k_b T}\right), \tag{1.7}$$

where E_i is the total energy of the system at state i and Q is the partition function, which is the sum of the Boltzmann factors for all possible states i. Consequently, any property (A) of the system can be computed as an average over all states i, as follows

$$\langle A \rangle = \sum_{i=1}^{i=N} A_i \exp\left(-\frac{E_i}{k_b T}\right) A(\mathbf{r_1}, ..., \mathbf{r_N}) d\mathbf{r_1} ..... d\mathbf{r_N}, \tag{1.8}$$

Where k is the Boltzmann's constant and r_i the positions of the particles. In addition to MC and MD simulations, Brownian Dynamics (BD) simulations consider the mass of the particles and the forces acting on them, including friction and inter-particle interactions. To describe the motion of the particles, the Langevin equation, which accounts for these particle interactions, is used in this method as follows

$$m\dot{v}(t) = -\gamma m v(t) + f(t) + R(t), \tag{1.9}$$

where m is the particle mass, γ is the friction coefficient that represents a non-conservative, non-systematic force induced by the solvent, such as frictional forces. The inter-particle potential is represented by the force $f(t)$, which is a conservative, systematic force. Finally, $R(t)$ denotes the conserved random force, and is responsible for the random Gaussian motion of the particles, known as Brownian motion.

Dissipative Particle Dynamics (DPD) is another relevant method where simulations are performed in continuous space using particles (74). It takes into account the forces acting on each particle, including conservative, dissipative, and stochastic random forces that only affect particles within a certain distance of each other defined by a cut-off distance. A conservative force can be included which is typically represented by a simple soft-core potential. This feature of DPD makes it computationally efficient, allowing for larger time steps and faster computation times.

In recent years there has also been considerable interest in simulation methods based on Mean field theories, such as the self-consistent field (SCF) and Single Chain Mean Field (SCMF) theories, which have been used to predict the properties of surfactant systems (1; 75; 76; 77; 78; 79; 80). These theories are particularly effective for these types of studies because they reduce the many-body problem to a one-body problem, substantially reducing computational time. They do so by considering the interactions between particles through an average interaction represented by mean molecular fields.

1.2.3 | Methods used in this Study

In this thesis, a Single-Chain Mean-Field (SCMF) Theory is implemented to study the surfactant behavior in aqueous media. Specifically, triblock copolymer surfactants well known as Pluronics are modeled using a coarse grain model in continuous space to study their equilibrium and dynamic properties over time through a dynamic version of the SCMF scheme. Finally, an extended version of SCMF, which includes three components rather than two (namely two different kinds of surfactants and water molecules), is used to study the equilibrium properties of mixed micelles systems.

1.3 | Summary of the chapter-thesis outline

This Chapter provides an overview of surfactants, their behavior when surrounded by water molecules; how and under which conditions micelles are formed. In addition, it addressed the importance of surfactants and their behavior in modern times, as well as the various applications that use them. Finally, this chapter reviewed the recent theoretical and experimental methods used to study these kinds of molecules, including their advantages and limitations. A brief introduction to the method used in this thesis is also provided, along with its advantages and limitations. The next chapter, **Chapter 2**, analyses the theoretical basis of this study and includes a comprehensive description of the simulation method and model used in this research. Subsequently, Chapter 3 and Chapter 4 include the results and the analysis of two cases of study. Namely, **Chapter 3**, discusses the *Exit Dynamics of Block Copolymers from Micelles at Short and Long Time Scales*, while **Chapter 4** explores the *Equilibrium Properties of Binary mixtures*. Finally, the thesis' main points are outlined in **Chapter 5** along with the implications of the findings for future research.

UNIVERSITAT ROVIRA I VIRGILI
UNRAVELING THE DYNAMICS AND EQUILIBRIUM BEHAVIOR OF PURE AND MIXED MICELLES: INSIGHTS FROM MICROSCOPIC COARSE-GRAIN MODELING
Maria Pantelidou

2

Simulation Methodology

2.1 | Single-Chain Mean-Field (SCMF)Theory

The Single-Chain Mean-Field (SCMF) simulation method has previously been employed to analyze the equilibrium properties of micelle systems, including the impact of surfactant chain architecture on the micellization (81). By utilizing a coarse grain model, the Critical Micelle Concentration (CMC), and the aggregation number of poly(ethylene oxide) surfactants with varying chain geometry and length, in water at a constant temperature have been calculated. The results showed that the CMC values are responsive to the degree of branching in the hydrophilic head of surfactants, while the aggregation number is also impacted by the variation in the length of the hydrophobic tail of surfactants.

Moreover, a dynamic version of the SCMF simulation method was applied to investigate the micellar kinetic exchange of these triblock copolymer surfactants over a broad range of time-scales (75; 82). Results showed that the kinetics of these micelles exhibit three different regimes: a fast rearrangement of the chains, followed by a peculiar logarithmic relaxation, and eventually an exponential decay.

In this thesis the same model will be used to further understand the logarithmic behavior observed in the dynamic exchange of these micelles by changing the surfactant chain flexibility. Furthermore, an expanded version of the static equilibrium formulation of the SCMF method is used to study the equilibrium behavior of mixed micelle systems.

The Single-Chain Mean-Field (SCMF) theory was first introduced by Ben-Shaul, Szleifer, and Gelbart (83; 84; 85) as a way to describe micellization of low-molecular weight block copolymer surfactants. Since then, it has been further developed and applied to study a wide range of systems, including the structure of phospholipid membranes (86; 87), homopolymer adsorption onto flat interfaces (88), binary surfactant solutions (77), and more recently the behavior of semiflexible polymer brushes (89).

The Single-Chain Mean-Field (SCMF) theory describes the behavior of a single molecule within a complex system of interacting molecules. The basic idea behind this theory is to simplify the analysis of complex systems made up of many interacting molecules by reducing the many chain-problem to one of a representative central chain. This central chain interacts with the surrounding molecules through a mean field approximation. The mean fields determine the most probable conformations of the molecule through the probabilities of the individual molecule (Figure 2.1). The properties of the representative molecule are then determined by solving a set of nonlinear equations defined by the self-consistent closure of the model. These equations take into account the probabilities of individual conformations of the representative molecule and the mean field. By

solving these equations, all the equilibrium properties can be obtained.

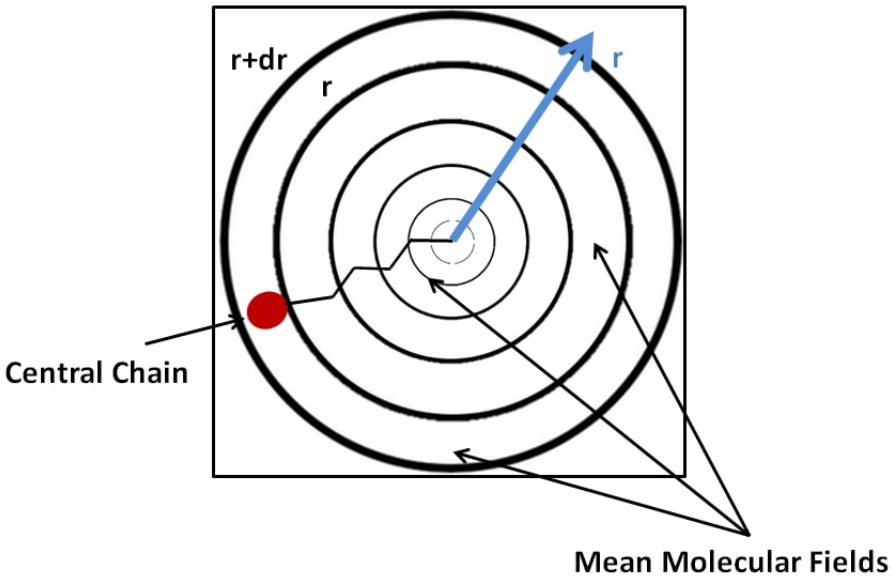

Figure 2.1: Schematic of the SCMF with a central chain and the mean molecular fields as concentric spherical layers. Each layer has a radius r and thickness dr, within which the densities of the surfactants and solvent are assumed to be uniform.

2.1.1 | SCMF Theory: Theoretical Background

As already mentioned, the Single-Chain Mean-Field Theory considers a central chain, with a set of conformations $\{\alpha\}$ and calculates the interactions between this central chain with the environment. A chain's conformation is represented by the positions of all its monomers, which are expressed as a collection $[\alpha]=(\mathbf{r}_1, \mathbf{r}_2, \ldots, \mathbf{r}_{\mathcal{N}})$, where $\mathcal{N}$ is the total number of monomers in the chain, and $\mathbf{r}$ denotes the position of each individual monomer. The referred interactions include both intramolecular interactions, which are calculated precisely, and intermolecular interactions, which involve the interactions of the central chain with the solvent molecules and the remaining chains. These interactions are determined by using mean molecular fields and defined by the probability distribution functions of the chain conformations $P[\alpha]$ and the distribution of the solvent molecules, through the minimization of the free energy of the system.

2.1.2 | Thermodynamic Formalism of the SCMF Theory

The core concept of the SCMF theory is determining the probability distribution function (pdf) of conformation α, $P[\alpha]$, together with the concentration fields of the solvent molecules. We assume that our systems is incompressible, which implies that space is completely filled with the surfactant chains and solvent molecules. (See Appendix I for more details.) Consequently,

$$\phi_s(\mathbf{r}) + N\langle\phi(\mathbf{r})\rangle = 1. \tag{2.1}$$

Where the volume fraction of the solvent is represented by $\phi_s(\mathbf{r})$, and the average volume fraction of all possible conformations of the surfactant is represented by $N\langle\phi(\mathbf{r})\rangle = N\sum_\alpha P[\alpha]\phi(\alpha,\mathbf{r})$, with N to be the number of chains representing the surfactants in the system.

To properly describe the thermodynamic properties of the system being studied, it is essential to identify surfactant profiles that comply with this incompressibility condition expressed in the equation mentioned above. As already mentioned, this approach involves determining the pdf and the concentration fields of the solvent molecules. This can be accomplished by minimizing the free energy of the system, while adhering to the incompressibility condition. The free energy of the system is provided by

$$F = \langle E\rangle - T\langle S\rangle, \tag{2.2}$$

where E is the total energy, T the temperature and S the entropy of the system. The total energy of the system E is equivalent to the sum of the intramolecular energy, $(u_{intra}(\alpha))$ and the intermolecular energy, $(u_{inter}(\alpha))$ within a system consisting of N surfactant chains.

$$\langle E\rangle = N\int d\alpha P[\alpha]\left(u_{intra}(\alpha) + u_{inter}(\alpha)\right). \tag{2.3}$$

The **intramolecular energy** is calculated by the ensemble average of the probability distribution function (*pdf*) and the internal energies of each individual chain, as follows

$$\langle u_{intra}\rangle = N\int d\alpha P[\alpha]u_{intra}(\alpha), \tag{2.4}$$

While the **intermolecular energy** ($\langle u_{inter}\rangle = N\int d\alpha P[\alpha]u(\alpha)$) is computed based on the individual contributions of the chains, which are determined by their interaction volumes and the surrounding mean molecular fields. Thus, it is calculated taking into account both chain-chain and chain-solvent interactions, by the following equation

$$\langle u_{inter} \rangle = N \int d\alpha P[\alpha] \left[\frac{N-1}{2} \epsilon_{cc} \int d\mathbf{r} \Phi_{int}^{cc}(\alpha, \mathbf{r}) \langle c(\mathbf{r}) \rangle + \epsilon_{cs} \int d\mathbf{r} \Phi_{int}^{cs}(\alpha, \mathbf{r}) c_s(\mathbf{r}) \right]. \quad (2.5)$$

The interaction parameters for chain-chain and chain-solvent interactions are represented by ϵ_{cc} and ϵ_{cs}, respectively. The available volume for the central chain to interact with other chains and the solvent, at a specific position $\mathbf{r}$, is represented by $d\mathbf{r}\Phi_{int}^{CC}(\alpha, \mathbf{r})$ and $d\mathbf{r}\Phi_{int}^{CS}(\alpha, \mathbf{r})$, respectively. This available volume interacts with the average concentration fields of the other chains and solvent, represented by $\langle c(\mathbf{r}) \rangle$ and $c_s(\mathbf{r})$, respectively. The number of interaction parameters as well as the number of species represented by the concentration fields will vary depending on the number of different species present in the coarse grain model used.

With respect to the entropy of the system, two contributions are considered:

- The **conformational entropy** of the surfactant chains

$$\langle S_c \rangle = -kN \int d\alpha P[\alpha] \log P[\alpha] \quad (2.6)$$

- The **translational entropy** of the solvent molecules

$$\langle S_T \rangle = -k \int d\mathbf{r} c_s(\mathbf{r}) \log \phi_s(\mathbf{r}). \quad (2.7)$$

Upon examining each component of the free energy equation, and using eqs. (2.3), (2.4), (2.5), (2.6) and (2.7), eq. (2.2), takes on the following form:

$$F = N \int d\alpha P[\alpha] \left(u_{intra}(\alpha) + u_{inter}(\alpha) \right) + kT \left(N \int d\alpha P[\alpha] \log P[\alpha] + \int d\mathbf{r} c_s(\mathbf{r}) \log \phi_s(\mathbf{r}) \right). \quad (2.8)$$

By minimizing the free energy F and taking into account the the incompressibility constraint using eq. (2.1), the probability distribution function and the solvent concentration at position $\mathbf{r}$, denoted as $c_s(\mathbf{r})$, are determined. This is done by introducing a set of Lagrange multipliers, $\pi(\mathbf{r})$, into the free energy expression. Once the procedure is finished, the set of chain probabilities $P[\alpha]$ can be obtained by setting the partial derivative of F with respect to $P[\alpha]$ and $c_s(\mathbf{r})$ equal to zero. Namely,

$$\frac{\partial F}{\partial P[\alpha]} = 0, \frac{\partial F}{\partial c_s(\mathbf{r})} = 0 \Rightarrow \quad (2.9)$$

$$P[\alpha] = \frac{1}{Q} \exp \left[-\beta \left(u_{intra}(\alpha) + u_{inter}(\alpha) + \int d\mathbf{r} \pi(\mathbf{r}) \phi(\alpha, \mathbf{r}) \right) \right], \quad (2.10)$$

and

$$\pi(\mathbf{r}) \approx -\frac{kT}{v_s}\log\phi_s(\mathbf{r}). \tag{2.11}$$

where Q in eq. (2.10), is the partition function, which ensures the proper normalization of probabilities, such that the integral of the probability distribution function over all possible states is equal to 1.

Eq. (2.11) implies that the quantity of $\phi_s(\mathbf{r})$ is approximately equal to $e^{-\beta v_s \pi(\mathbf{r})}$, where v_s represents the volume of a solvent molecule. This provides a physical interpretation for the Lagrange Multipliers $\pi(\mathbf{r})$, which act as the osmotic pressure required to maintain the chemical potential of the solvent constant. They can also be understood as the average repulsive energy between the chains caused by the presence of the solvent and surfactant molecules in the surrounding area, since the Lagrange Multipliers $\pi(\mathbf{r})$ arise from the incompressibility assumption.

The set of non-linear equations represented by eqs. (2.1), (2.10) and (2.11), can be used to determine any thermodynamic quantity in equilibrium, $\langle A\rangle$, using

$$\langle A\rangle = \int d\alpha P[\alpha]A(\alpha). \tag{2.12}$$

In this thesis,we wish to connect these microscopic equilibrium properties to macroscopic observables such as the CMC once the equations are solved. This can be done by relating the Mass Action Model (MAM) to the quantities determined by the SCMF theory such as the chemical potential. This connection will be outlined in the next section.

2.1.3 | Mass Action Model (MAM)

Micelles form when surfactants in a solvent self-assemble under specific conditions. The Mass Action model assumes that free surfactants and micelles are in thermodynamic equilibrium. This can be described in terms of the chemical potentials (Figure 2.2), namely the chemical potential of free surfactants (μ_1) should be equal to the chemical potentials of surfactants in a micelle which consists of N surfactant chains (μ_2, ..., μ_N)

$$\mu_1 = \mu_2 = \ldots = \mu_{N-1} = \mu_N. \tag{2.13}$$

Any thermodynamic property can be defined as the summation of the excess property and the ideal property, $\mu = \mu^{id} + \mu^{exc}$ (90; 91; 92). The ideal chemical potential is the chemical potential value of an ideal solution at the same temperature, pressure and concentration and it is given by

$$\mu_1^{id} = \mu_1^0 + kTlogX_1, \tag{2.14}$$

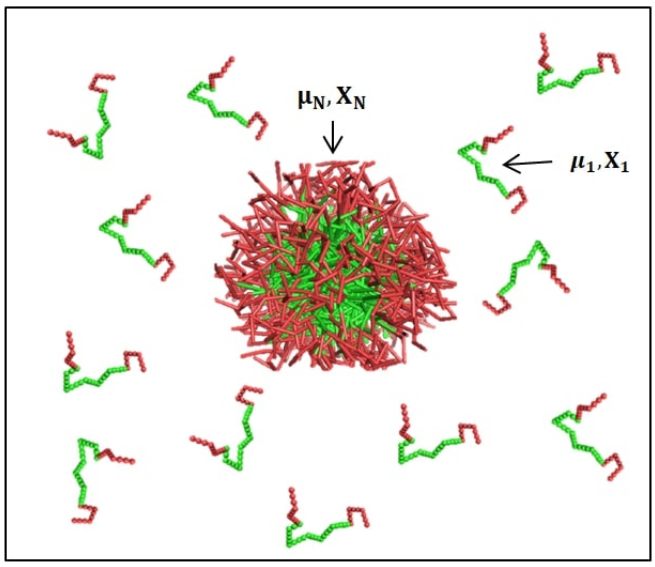

Figure 2.2: Schematic illustration of micelles and free surfactant in a solvent.

where μ_1^0 is the standard chemical potential of the free surfactants in the system, k is the Boltzmann constant, T the temperature and X_1 the concentration of free surfactants in bulk solution, in mole fraction. If we consider that $\mu^* = \mu_1^0 + \mu^{exc}$, eq. (2.13) becomes

$$\mu_1 = \mu_1^* + kT \log X_1. \tag{2.15}$$

Similarly for surfactants in micelles of size N,

$$\mu_N = \mu_N^* + \frac{kT}{N} \log \frac{X_N}{N}, \tag{2.16}$$

where μ_N^0 is the standard chemical potential of surfactant in micelles and X_N is the concentration of surfactant in micelles of size N in mole fraction, while $\mu_N = \mu_N^0 + \mu_N^{exc}$.

The second term on the right side of eq. (2.15) is known as the translational entropy and implies that single chains are free to move independently in space In contrast, the analogous term in eq. (2.16) infers that all surfactants in aggregates are forced to move together. It can be observed that as the micelle size increases, the translational entropy per chain decreases.

If we consider that the surfactant system behaves in an ideal manner, with no interactions between free surfactants ($\mu_1^* = \mu_1^0$) and no interactions between aggregates ($\mu_N^0 = \mu_N^0$), eqs. (2.13), (2.15) and (2.16), can be used to derive the following relationship

$$X_N = N \left(X_1 e^{-(\mu_N^0 - \mu_1^0)/kT} \right)^N. \tag{2.17}$$

The equation presented above is the expression of the mass action model (MAM). The standard chemical potential difference, represented by the term $e^{-(\mu_N^0-\mu_1^0/kT)}$ is crucial for understanding the formation of micelles. It indicates that when the standard chemical potential of free surfactants is larger than the standard chemical potential of surfactants in aggregates, micelles may form. It also defines the concentration at which the addition of surfactants in solution leads to the formation of aggregates. This concentration is called the Critical Micelle Concentration (CMC), and is described below.

2.1.4 | Critical Micelle Concentration (CMC) Calculations

The critical micelle concentration (CMC) is defined as the concentration of surfactants at which micelles start to appear. It is calculated by analyzing the free energy of the system, in terms of chemical potential differences, described by the term $e^{-(\mu_N^0-\mu_1^0/kT)}$. In general terms CMC can be calculated through the equation

$$(X_1)_{Crit} = CMC \approx e^{(\Delta\mu/kT)_{min}}, \tag{2.18}$$

while the total surfactant concentration in solution is given by

$$X_T = \sum_N X_N. \tag{2.19}$$

As depicted in Figure 2.3, there is a correlation between the concentration of free surfactants in the bulk solution (X_1) and the total concentration of surfactants in the solution (X_T). As the concentration of free surfactants increases, the total concentration also increases up until a point at which free surfactants prefer to form aggregates rather than remain in the bulk solution. This point, where X_1 reaches its peak, is known as the Critical Micelle Concentration (CMC).

The size distribution of micelles is given by $X_N/N = \left(X_1 e^{-(\mu_N^0-\mu_1^0)/kT}\right)^N$.

To relate the macroscopic quantities X_N to the microscopic thermodynamic quantities obtained from the SCMF theory, it is necessary to use the Partition function (Q), which is given by

$$Q = N\, e^{-\mu/kT}. \tag{2.20}$$

As mentioned before, the Partition function (Q) is calculated through the normalization of the chain probabilities, according to $P[\alpha] = \frac{1}{Q} e^{H[\alpha]/kT}$, where $H[\alpha]$ is the Hamiltonian of a configuration α and it is given in terms of the intermolecular, intramolecular and repulsive interactions.

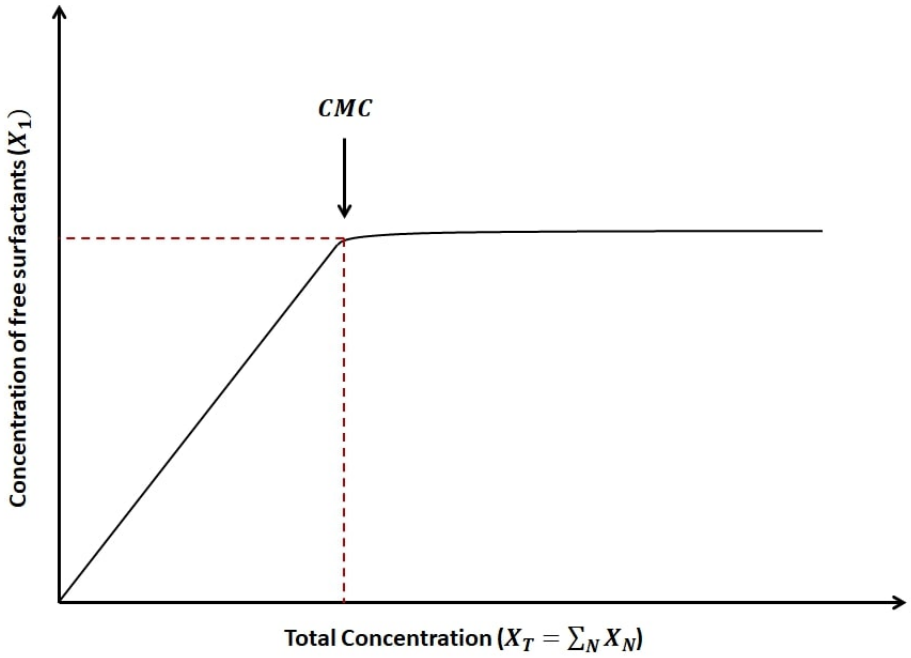

Figure 2.3: CMC illustration based on the MAM. As the free surfactant concentration X_1 increases, the value of X_T increases too until reaches a saturation point known as the Critical Micelle Concentration (CMC). Beyond this point, any additional surfactant added to the system will preferentially form aggregates rather than remain in the bulk solution, resulting in no further increase in the value of X_1.

$$H[\alpha] = u_{intra}(\alpha) + u_{inter}(\alpha) + \int d\mathbf{r}\pi(\mathbf{r})\phi(\alpha, \mathbf{r}). \tag{2.21}$$

Thus the partition function takes the following form

$$Q = \int d\alpha e^{-H[\alpha]/kT}. \tag{2.22}$$

From eqs. (2.20) and (2.22), it can be inferred that

$$e^{-\mu/kT} = \frac{1}{N}\int d\alpha e^{-H[\alpha]/kT}. \tag{2.23}$$

and taking into account that micelles are fixed in space-in our simulation cell by the definition of the mean fields, namely $\mu_N = \mu_N^0$,

$$e^{-\mu_N^0/kT} = \frac{1}{N}\int d\alpha e^{-H_N[\alpha]/kT}. \tag{2.24}$$

In order to ensure that surfactants in micelles and free surfactants have the same degrees of freedom, it is necessary to remove the translational contribution in the chem-

ical potential of the free surfactants and take into account the volume of the system, as follows

$$e^{-\mu_1^0/kT} = \frac{1}{V}\int d\alpha e^{-H_1[\alpha]/kT}. \tag{2.25}$$

By combining eqs. (2.24) and (2.25) the following relationship can be derived

$$e^{-(\mu_N^0-\mu_1^0)/kT} = \frac{V}{N}\frac{\int d\alpha e^{-H_N[\alpha]/kT}/W(\alpha)}{\int d\alpha e^{-H_1[\alpha]/kT}/W(\alpha)}. \tag{2.26}$$

The term $W(\alpha)$ accounts for any bias included from the algorithm that generates the chain configurations. In this work we use only Self-Avoiding Random walks for the chain configurations in the SCMF which we generate using the Rosenbluth algorithm. Consequently, $W(\alpha)$ is here the corresponding Rosenbluth weight for each chain configuration.

2.2 | Single-Chain Mean-Field: Dynamic Scheme

The SCMF dynamic scheme is a dynamic methodology that has been applied in previous studies to investigate the relaxation of surfactants in micelles (75; 82). This method involves generating a series of explicit moves for a set of sampling chains $\alpha = (\alpha_1, \alpha_2, \ldots, \alpha_N)$, with each chain considered as independent and evolving separately within the established mean fields. These moves are generated simultaneously for each chain, and they are accepted or rejected based on the relative change in the conformation energy as determined by the Metropolis formulation.

2.2.1 | Metropolis Algorithm

The Metropolis formulation is a statistical mechanics algorithm used to generate a sequence of configurations for a system in thermal equilibrium. The algorithm is based on a Markov Chain Monte Carlo method and is used to generate configurations that are distributed according to the Boltzmann distribution, which describes the probability of a system being in a particular state at a given temperature. More specificly, the key concept of the Metropolis algorithm is to randomly generate a new configuration for the system and then accept or reject this configuration based on the energy of the old (α_N) and the new (α_0) conformation. The probability of accepting a move from an old (0) to a new state (n) is given by the Metropolis criterion determined by

$$p(\alpha_{o\to n}) = \min\left(1, \exp\left(-\Delta H\left[\alpha_{o\to n}\right]/kT\right)\right), \tag{2.27}$$

where k is the Boltzmann constant, T the temperature, and $\Delta H\left[\alpha_{o\to n}\right] = H[\alpha_n] - H[\alpha_0]$ is the change in the SCMF Hamiltonian during the proposed move, which is given by eq. (2.21).

The dynamic methodology for generating the moves includes:

- Considering a representative number of configurations of the central chain α_0 through a set of independent sampling chains $\{\alpha_0\}$.
- Generating a trial move simultaneously for each chain, while keeping the average fields fixed.
- Each chain move is then accepted or rejected depending on the calculated probability based on the Metropolis formulation, eq. (2.27).
- Updating the concentration fields $\langle c(\mathbf{r})\rangle$, $\langle \phi(\mathbf{r})\rangle$, $c_s(\mathbf{r})$, $\phi_s(\mathbf{r})$ by solving the SCMF corresponding equations and repeating the process until equilibrium is reached.

The dynamic SCMF approach, which is a stochastic method, does not incorporate a physical time. To make the simulation results comparable to experimental data, the physical time must be inferred in some way, for instance by comparing the diffusivity of a single chain in the dynamic SCMF to the experimental value.

2.2.1.1 | Micelle Chain Exchange Correlation Function

The dynamics of surfactant chain, namely the insertion/extraction to/from micelles can be studied using the correlation function $F(t)$, which has been previously utilized in TR-SANS (Time-Resolved Small-Angle Neutron Scattering) studies (93; 94). It is based on the direct observation of labelled changes in a micelle over time. Namely,

$$F(t) = \frac{f(t)}{f(0)}, \tag{2.28}$$

where $f(t)$ and $f(0)$ represent the number of labelled surfactant chains in the micelle at time t and at time t=0, respectively. To track the number of chains over time, chains initially present in the micelle are labeled,$f(0)$. The number $f(t)$ is calculated by taking into account any labeled chains in the micelle. If a labeled chain leaves the micelle, it is no longer counted towards the number $f(t)$, but if it returns, it is once again included in the overall number. To compare the simulation results to experimental data, it is crucial to estimate the physical time of the simulation. This can be achieved by determining the

diffusion of free chains in the simulation (D_{SCMF}) and comparing it to the diffusion observed in experiments. The diffusion of a free chain in the simulation can be quantified using the number of Monte Carlo cycles (t_{cyc}), as follows

$$D_{\mathrm{SCMF}} = \lim_{t_{\mathrm{cyc}} \to \infty} \frac{\langle \Delta \mathbf{r}(t_{\mathrm{cyc}})^2 \rangle}{6 t_{\mathrm{cyc}}}, \tag{2.29}$$

where $\langle \Delta \mathbf{r}(t_{\mathrm{cyc}})^2 \rangle = \langle \left(\mathbf{r}(t_{\mathrm{cyc}}) - \mathbf{r}(0) \right)^2 \rangle_{N_\alpha}$ is the average displacement of the center of mass of the set of sampling chains (N_α). The conversion from Monte Carlo cycles (MC) to experimental time (t) was derived by

$$\frac{D_{\mathrm{SCMF}}}{\sigma^2} t_{\mathrm{cyc}} = \frac{D}{l^2} t, \tag{2.30}$$

where the diffusion D_{SCMF} is given in units of $\sigma^2/cycle$, l is the physical dimension of the monomers and D is calculated from the Stokes-Einstein expression which relates the diffusion of small particles in solutions with the temperature (T), the viscosity (η), and the hydrodynamic radius a, as follows

$$D = \frac{k_B T}{6 \pi \eta a}. \tag{2.31}$$

In this work, the exchange behavior of surfactants can be further explained in terms of a modified Eyring's equation which can be related to the correlation function.

2.2.2 | Modified Eyring's Equation

Previous research has shown that the micelle chain exchange correlation function described in the previous section for the exit of surfactant copolymers from equilibrated micelles exhibits a specific behavior that can be divided into different regimes. This behavior can be explained by incorporating an additional term into Eyring's equation, which accounts for the entire range of surfactant exit behavior. Note that the unmodified equation is typically used to study non-linear relaxation in polymers (95; 96). As previously stated, the release rate of surfactants exhibits a behavior that can be divided into three distinct regimes. In particular, an initial rapid reorganization can be identified, followed by a logarithmic intermediate stage, and then a final exponential decay. To further analyze this behavior, a modified version of Eyring's equation, which includes an additional parameter, is proposed in this thesis. Namely

$$\frac{dF(t)}{dt} + k_1 \left(e^{\frac{F(t)}{\epsilon}} - 1 \right) + k_2 \left(1 - e^{-\frac{F(t)}{\epsilon}} \right) = 0 \tag{2.32}$$

In this modified Eyring equation, k_1 represents the specific kinetic constant for the initial and intermediate regimes, k_2 represents the kinetic constant in the final exponential regime, and ϵ is a crossover value of the correlation function. These constants can be determined by using either the simulation data from the correlation function, $F(t)$, or experimental data for the same quantity. It is important to note that this modified version of the Eyring equation includes a third term with constant k_2, which allows for the three distinct regimes observed in the simulation to be accounted. The equation can be analytically solved to yield the following result.

$$F(t) = -\epsilon \ln \left(\frac{1 - k\, e^{-\frac{k_1+k_2}{\epsilon} t}}{\frac{k_2}{k_1}\, k\, e^{-\frac{k_1+k_2}{\epsilon} t} + 1} \right) \tag{2.33}$$

where

$$k \equiv \frac{e^{1/\epsilon} - 1}{e^{1/\epsilon} + \frac{k_2}{k_1}}. \tag{2.34}$$

On fitting eq. (2.32) to the correlation function simulation data, the parameters ϵ, k_1, k_2 of the modified Eyring equation can be extracted. With the information from the fitting of the values of the parameters, the process of surfactant copolymers exiting from micelles becomes more comprehensible.

2.3 | Single-Chain Mean-Field for Binary Systems

The Single-Chain Mean-Field method for binary systems is an extension of the SCMF equilibrium theory discussed in section 2.1. It has been modified to include the presence of two distinct surfactant chains in solution in order to investigate their equilibrium behavior when forming mixed micelles. The key point is to modify the free energy of the system, by including the intermolecular interactions of the second type of surfactant, with the solvent and the other chains.

2.3.1 | Thermodynamic Formalism

The SCMF theory reduces the complex problem of many interacting bodies in a binary system to a simpler problem of two central chains, with different conformations α, β respectively which represent two different types of surfactants A and B. The theory considers a system of N_A and N_B surfactant chains surrounded by solvent molecules and follows the calculations of the SCMF discussed in section 2.1.2. Thus the goal is to minimize the free energy of the system, subject to the **incompressibility condition**, which in this case takes into account the two central single Chains A and B

$$\phi_s(\mathbf{r}) + N_A\langle\phi(\mathbf{r},\alpha)\rangle + N_B\langle\phi(\mathbf{r},\beta)\rangle = 1, \tag{2.35}$$

where $\phi_s(\mathbf{r})$ is the volume fraction of the solvent molecules while $\langle\phi(\mathbf{r},\alpha)\rangle$ and $\langle\phi(\mathbf{r},\beta)\rangle$ are the ensemble average volume fractions of chains A and B respectively, meaning that all available space is occupied by A, B surfactant chains and solvent molecules.

The **internal energy** is modified, to include the intramolecular and the intermolecular interactions of the second component B together with its concentration fields, $\langle c(\mathbf{r})\rangle_B = \int d\beta P[\beta] c(\beta,\mathbf{r})$,

$$< E >= N_A \int d\alpha P[\alpha](U_{intra}(\alpha) + U_{inter}(\alpha)) + N_B \int d\beta P[\beta](U_{intra}(\beta) + U_{inter}(\beta)), \tag{2.36}$$

while the **entropy** is given by the sum of the conformational entropies of the A and B chains respectively and the translational entropy of the solvent molecules, as follows

$$< S >= -k_B \left[(N_A \int d\alpha P(\alpha) lnP(\alpha) + N_B \int d\beta P(\beta) lnP(\beta) + \int d\mathbf{r} c_s(\mathbf{r}) ln\phi_s(\mathbf{r}) \right]. \tag{2.37}$$

From eqs. (2.35), (2.36) and (2.37), the **free energy** of the system, given by eq. (2.2) takes the following form

$$F = N_A \int d\alpha P[\alpha](U_{intra}(\alpha) + U_{inter}(\alpha)) + N_B \int d\beta P[\beta](U_{intra}(\beta) + U_{inter}(\beta))$$

$$+ k_B T \left[(N_A \int d\alpha P(\alpha) lnP(\alpha) + N_B \int d\beta P(\beta) lnP(\beta) + \int d\mathbf{r} c_s(\mathbf{r}) ln\phi_s(\mathbf{r}) \right] \tag{2.38}$$

Through the minimization of eq. (2.38), with respect to $P[\alpha]$, $P[\beta]$ and $c_s(\mathbf{r})$,namely

$$\frac{\partial F}{\partial P[\alpha]} = 0, \frac{\partial F}{\partial P[\beta]} = 0, \frac{\partial F}{\partial c_s(\mathbf{r})} = 0, \tag{2.39}$$

and taking into account the Lagrange multipliers $\pi(\mathbf{r})$, subject to the incomprehensibility condition (eq. (2.35)) any thermodynamic property of the system can be calculated through the following set of equations

$$P(\alpha) = \frac{1}{Q_A} e^{\frac{-H(\alpha)}{kT}}, \tag{2.40}$$

$$P(\beta) = \frac{1}{Q_B} e^{\frac{-H(\beta)}{kT}}, \tag{2.41}$$

$$\pi(\mathbf{r}) = -\frac{kT}{v_s} log\phi_s(\mathbf{r}). \tag{2.42}$$

Where Q_A and Q_B are the partition functions of the SCMF scheme and $H(\alpha)$ and $H(\beta)$ are the Hamiltonians of the system which are given by

$$H[\alpha] = U_{intra}(\alpha) + U_{inter}(\alpha) + k_B T \int d\mathbf{r}\pi(\mathbf{r})\phi(\alpha, \mathbf{r}). \tag{2.43}$$

$$H[\beta] = U_{intra}(\beta) + U_{inter}(\beta) + k_B T \int d\mathbf{r}\pi(\mathbf{r})\phi(\beta, \mathbf{r}). \tag{2.44}$$

2.3.2 | Mass Action Model (MAM) for Binary Systems

As mentioned in section 2.3.2., the Mass Action Model is used to link the microscopic quantities calculated from the SCMF with the macroscopic equilibrium quantities of the system of interest. In this case we consider that there are two concentrations of surfactant free chains in solution. X_1^A is the free surfactant concentration of species A while X_1^B is the concentration of surfactants B (Figure 2.4).

Following the assumptions of the mass action model calculations discussed in the previous section, the chemical potentials of free surfactants A and B will be given by:

$$\begin{aligned} \mu_1^A &= \mu_1^{0,A} + KTlnX_1^A, \\ \mu_1^B &= \mu_1^{0,B} + KTlnX_1^B, \end{aligned} \tag{2.45}$$

where $\mu_1^{0,A}$ and $\mu_1^{0,B}$ are the standard chemical potentials of surfactant A and B, respectively.

In thermodynamic equilibrium, the chemical potentials of free surfactants A and B are equal to the chemical potential of the aggregate made of $N_A + N_B$ surfactant chains, namely

$$\begin{aligned} \mu_1^A &= \mu_{N_A+N_B}^A \\ \mu_1^B &= \mu_{N_A+N_B}^B \end{aligned} \tag{2.46}$$

$$\Rightarrow N_A\mu_1^A + N_B\mu_1^B = N_A\mu_{N_A+N_B}^A + N_B\mu_{N_A+N_B}^B \tag{2.47}$$

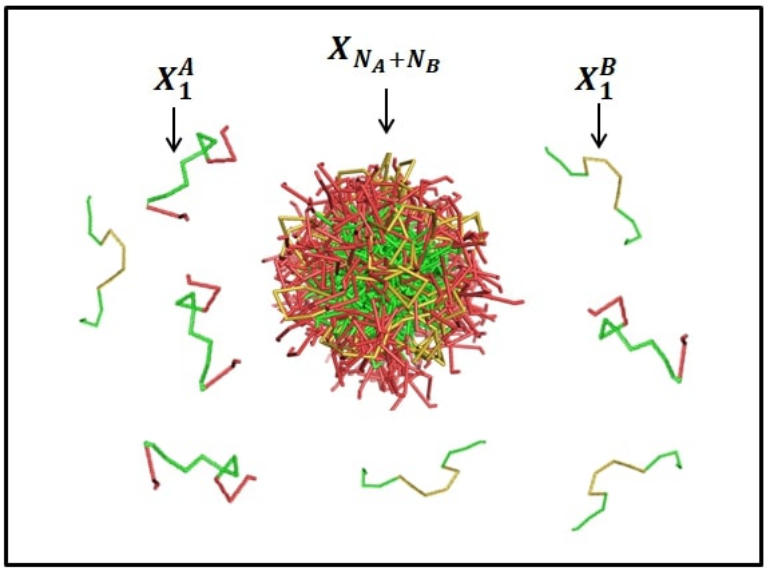

Figure 2.4: Schematic representation of mass action model with two kinds of Pluronics in water. X_1^A, X_1^B denote the concentration of free surfactants A and B respectively, in water while $X_{N_A+N_B}$ denotes the concentration of the aggregated surfactants in a micelle of $N_A + N_B$ surfactant chains.

From eqs. (2.45) and (2.47), the mass action model for a system containing two types of surfactants can be formulated as

$$X_{N_A+N_B} = (X_1^A)^{N_A} \cdot (X_1^B)^{N_B} e^{-\frac{1}{KT}[N_A(\mu^{0,A}_{N_A+N_B} - \mu_1^{0,A}) + N_B(\mu^{0,B}_{N_A+N_B} - \mu_1^{0,B})]} \tag{2.48}$$

If $N_B = 0$, so that only surfactants of species A will be present in a solvent, then the MAM eq.(2.48) takes its original form, given by eq. (2.17).

To be apply the mass action model given in eq. (2.48) and calculate the concentrations of micelles as a function of the free chain concentrations, it is necessary to determine the changes in the standard chemical potentials, namely, the $\Delta\mu^{0,A}$ and $\Delta\mu^{0,B}$. These chemical potentials differences are calculated within SCMF as follows by taking into account the partition functions Q_A and Q_B, which according to eq. (2.22), take the form

$$\begin{aligned} Q_A &= \int d\alpha e^{-H[\alpha]/kT}, \\ Q_B &= \int d\beta^{-H[\beta]/kT}, \end{aligned} \tag{2.49}$$

where $H[\alpha]$ and $H[\beta]$ are the Hamiltonians of the A and B molecule chains, respectively and are given by

$$H[\alpha] = u_{intra}(\alpha) + u_{inter}(\alpha) + \int d\mathbf{r}\pi(\mathbf{r})\phi(\alpha,\mathbf{r}),$$
$$H[\beta] = u_{intra}(\beta) + u_{inter}(\beta) + \int d\mathbf{r}\pi(\mathbf{r})\phi(\beta,\mathbf{r}). \tag{2.50}$$

Eq. (2.24), for 2 compounds takes the form

$$e^{-\mu^{0,A}_{N_A+N_B}/kT} = \frac{1}{N_A}\int d\alpha e^{-H_{N_A}[\alpha]/kT},$$
$$e^{-\mu^{0,B}_{N_A+N_B}/kT} = \frac{1}{N_B}\int d\beta e^{-H_{N_B}[\beta]/kT}. \tag{2.51}$$

By taking into account the volume of the system, according to eq. (2.25),

$$e^{-\mu^{0,A}_{1}/kT} = \frac{1}{V}\int d\alpha e^{-H_{1}[\alpha]/kT},$$
$$e^{-\mu^{0,B}_{1}/kT} = \frac{1}{V}\int d\beta e^{-H_{1}[\beta]/kT} \tag{2.52}$$

Finally, from eqs. (2.51), (2.52), the standard chemical potential differences can be obtained through the following equations

$$e^{-\left(\mu^{0,A}_{N_A+N_B}-\mu^{0,A}_{1}\right)} = \frac{V}{N_A+N_B}\frac{\int d\alpha\cdot e^{-\frac{H^A_{N_A}[\alpha]}{KT}}}{\int d\alpha\cdot e^{-\frac{H^A_{1}[\alpha]}{KT}}},$$
$$e^{-\left(\mu^{0,B}_{N_A+N_B}-\mu^{0,B}_{1}\right)} = \frac{V}{N_A+N_B}\frac{\int d\beta\cdot e^{-\frac{H^B_{N_B}[\beta])}{KT}}}{\int d\beta\cdot e^{-\frac{H^B_{1}[\beta]}{KT}}}. \tag{2.53}$$

2.3.3 | Simulation Details

The simulation code used in this study was developed by the Molecular Simulation Group in Tarragona and was originally designed to describe the micellization of block copolymers (83; 84; 85). It has since been expanded to investigate the structure of phospholipid membranes at the molecular level (86; 87).

Continuing its development, the code was further extended to include a dynamic version to allow for the study of micellization dynamics (81; 82). For this thesis, the SCMF code was modified to incorporate a second surfactant in the system, enabling the study of equilibrium properties of mixed micelles.

The code was implemented in the C programming language with parallelization using OpenMP, and it incorporated various algorithms and methodologies to accurately model and simulate the phenomena under investigation.

In all cases under study, the simulations were executed on 12-core Intel nodes and 24-core AMD nodes, each equipped with RAM capacities of 64 GB and 32 GB, respectively.

2.3.3.1 | Equilibrium SCMF

The calculation of equilibrium properties of single-component micelles involved a two-part simulation. The first part focused on generating the sampling chains, which included determining the number of chains, concentrations, volume fractions, interaction volumes, sizes, and number of beads. In the second part, the code used these initial parameters and chain statistics to find solutions to the SCMF equations through an iterative method. The parameters specific to this stage of the method could be adjusted in the second part of the simulation.

After configuring the necessary input files, running the simulations provided important outputs. These outputs included equilibrium densities for a given aggregation number (N) for all the species, such as solvent, tails, heads, and total heads and tails, as functions of the distance from the center of the simulation box. Additionally, the standard chemical potential difference as a function of the aggregation number was determined.

To ensure reliable results with minimal statistical errors, the simulation parameters were carefully selected for this thesis. The box size ranged from 40x40x40 to 100x100x100 in units of the bead diameter σ, depending on the Pluronic under study. Between 5 and 10 million conformations $\{\alpha\}$ were generated for each Pluronic. The simulation runtime varied depending on the surfactant being investigated but typically completed within a week.

2.3.3.2 | Dynamic SCMF

For dynamic SCMF simulations, a total of 500 sampling chains, $N\{\alpha\}$, were employed for all Pluronic molecules. It should be noted that this number of sampling chains is independent from the number of physical chains chosen for any given system. The

simulations were carried out within boxes with volumes ranging from 70x70x70 to 100x100x100 in units of σ, employing periodic boundary conditions The simulation runtime lasted approximately 3-5 weeks.

2.3.3.3 | SCMF for Binary Mixtures

For mixed micelles, the equilibrium SCMF simulation method was employed, incorporating the generation of sampling chains for both Pluronics present in the system, $\{\alpha\}$ and $\{\beta\}$. In this scenario, 3-5 million conformations were generated for each chain. Depending on the system under study the simulations required a duration of 3-6 weeks to calculate the standard chemical potential for all the binary systems of interest, typically about 200*200=40000 systems (for each Pluronic a range of up to 200 physical chains in the system).

UNIVERSITAT ROVIRA I VIRGILI
UNRAVELING THE DYNAMICS AND EQUILIBRIUM BEHAVIOR OF PURE AND MIXED MICELLES: INSIGHTS FROM MICROSCOPIC COARSE-GRAIN MODELING
Maria Pantelidou

3

Universal scaling for the exit dynamics of block copolymers from micelles at short and long time scales

This study has been publinshed in Macromolecules Journal
Macromolecules 2022 55 (3), 914-927 DOI: 10.1021/acs.macromol.1c02387

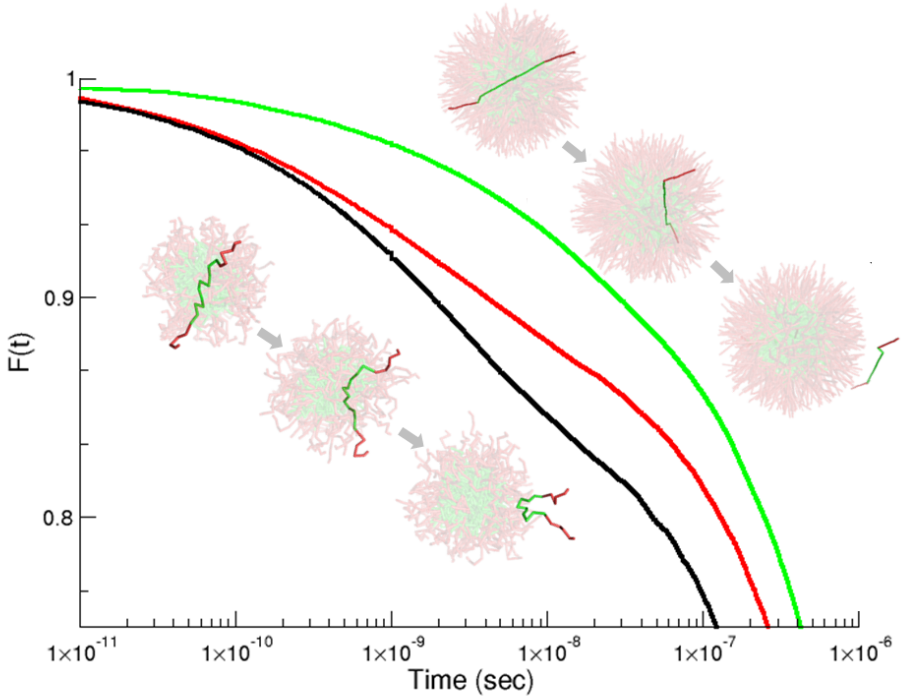

3.1 | Introduction

Poloxamers are triblock copolymers with a central hydrophobic polyoxypropylene block (PPO) between two external hydrophilic polyoxyethylene blocks (PEO). These copolymers are also available commercially under the trade name of Pluronics. Due to their amphiphilic nature, when they are surrounded by solvent molecules above a specific concentration called the CMC, they are able to self-assemble into aggregates known as micelles, driven by the hydrophobic effect (16; 97). Even after reaching thermal equilibrium, the micelles are constantly evolving in shape and composition, due to the low aggregation free energy involved in the hydrophobic effect. In the standard interpretation of this equilibrium, two different dynamic processes are proposed. The first is a fast process characterized by the insertion and expulsion of single surfactant chains from the micelles (98). On the other hand, the second is much slower and is characterized by the fusion and fission of the micelles (99; 100; 101; 102; 103; 104; 105). Typically, there is a difference of approximately 6 orders of magnitude between the timescales involved in these two processes (106; 107). Micelle relaxation is of particular importance because it controls micellar stability, which is important in many applications involving processes such as foaming, emulsification, detergency, wetting, and solubilization (108). Consequently, a detailed understanding of the associated molecular mechanism is expected to contribute key insights into micelle behavior, as well as to serve as a basis for future experimental studies and applications.

Over the last few decades, numerous experimental and theoretical studies have focused on both dynamical processes (98; 109; 110). However, in this work we are particularly interested in the faster process where individual chains are exchanged with the bulk solution. In this case, the most established theory is the one developed by Aniansson and Wall (99; 100; 111), whose step-wise model assumes that for short surfactants the exchange between the bulk solution and micellar aggregates undergoes a single exponential decay. Later, Halperin and Alexander (98) adapted the same model, but with diblock copolymers as surfactants in a solvent of low molecular weight. They also proposed a single exponential decay in the relaxation curves. Subsequently, much research on micelle kinetics has been done by using different experimental techniques such as: temperature jump (98), fluorescence (112), ultrasonic absorption spectrometry (113) and time-resolved small angle neutron (TR-SANS) (94; 114; 115). In these experiments a single exponential decay in the relaxation process was observed, which allegedly confirmed the validity of these models for micelle dynamics.

However, more recent experimental works have found a much richer behavior, including a broad logarithmic time-dependence at shorter times instead of the expected

exponential decay (94; 116). In an attempt to explain this logarithmic relaxation, Lund and co-workers (94; 116; 117) ascribed this behavior to the polydispersity of the triblock copolymers. In their model, surfactants have to overcome an energetic barrier in order to leave the micelle and so copolymers with different chain lengths are expected to face different barrier heights. However, it is not clearly explained why this should give rise specifically to a logarithmic decay, since the distribution of chain lengths due to polydispersity is somehow arbitrary. Simulation methods such as Monte Carlo (MC) (118), molecular dynamics (109; 110), and dissipative particle dynamics (119; 120; 121) have been used to provide additional insight into the dynamics of micelles. In particular, a dynamic Single Chain Mean-Field (SCMF) theory has been used to simulate the behavior of poly(ethylene oxide)-poly(propylene oxide)-poly(ethylene oxide) triblock copolymer systems (75; 82). The dynamic SCMF has similarities to other dynamic mean-field density functional theories found in the literature (122). However, SCMF uses explicit non-overlapping configurations, instead of Gaussian statistics for the chain conformations, which significantly changes the resulting equilibrium and dynamic behavior (88; 123). Despite using a strictly monodisperse distribution of chain lengths in the simulations, a similar logarithmic decay to the experiments was found. This suggests that the observed behavior must be caused by an inherent physical property of polymeric micelles and not to a particular polydispersity in the size distribution of the samples. The observed logarithmic decay was speculated to arise from a degeneracy of energy states arising from the conformational space of the hydrophobic block of the copolymer in the core. This degeneracy is broken on exiting the micelle, giving rise to an effective energetic barrier distribution. Although this hypothesis is valid for the chains escaping at short times, at longer times the exit time of the copolymer is of the same order of magnitude as the diffusion in conformational space and, therefore, it cannot be expected for the chain to be expelled from the micelle without a change in conformation, as required by the hypothesis. Hence, the observed non-exponential decay must be related to the coupling of at least two different dynamic processes, rather than to merely an energy barrier distribution. The view that we develop in this article is based on the following two points: a) as indicated in our previous work (75; 82), different chain conformations experience different barrier heights to exit the micelle, therefore hairpin conformations of the triblock copolymer are more likely to exit the micelle than more extended conformations, b) there is an entropic barrier to reach such a hairpin shape, whose height depends on the initial chain conformation.

These hairpin conformations are depleted during the initial stages, and other chains have to diffuse through the entropic barrier in conformational space until they can become ready to exit the micelle. Such a diffusive process introduces additional dynamics,

which does not depend on the height of the exit energetic barrier. Although the hypothesis is oversimplified, it contains the main ingredients needed to explain the different regimes observed experimentally. In addition, this hypothesis allows the relevance of such an intermediate non-exponential decay to be related to the size of the chain conformational space. For example, stiffer triblock copolymers with longer Kuhn segments have their conformational diffusion suppressed, and their behavior should be dominated by a purely exponential decay. On the other hand, more flexible chains of the same length should display a broad intermediate non-exponential behavior. The simulations conducted in this article show that the breadth of the non-exponential decay is directly related to such a chain property.

Interestingly, a recent article (124) has further explored the consistency of literature models based on polydispersity to explain their experimental results. The authors used Förster resonance energy transfer (FRET) to study the exchange dynamics of complex coacervate core micelles and found that the literature models required energies below the one expected for their system, and speculate on the need for additional factors besides polydispersity to properly describe the observed experimental dynamics. In a further twist to their discussion, they noted that in experiments with monodisperse core blocks no logarithmic relaxation had been observed, but rather a single exponential time decay in agreement with the standard Halperin and Alexander model. At first sight, these monodisperse experimental results might appear to contradict the conclusions of the SCMF dynamic simulations already commented on (75; 82). However, it should be noted that these experimental works use only poly(ethylene oxide) polymers (PEO) with n-alkyl ethers: $C_n - EO_5$ and $C_n - EO_{10} - C_n$, where n=18, 22, 24, 28, 30. Given that the Kuhn segment length for polyethylene is about 4 ethylene monomers (C_2H_4) (125), this indicates that the hydrophobic block of these polymers have a very reduced conformational space since they range from about only 2 to almost 4 Kuhn segments. In order to have a distribution of degenerate energy states of the hydrophobic block in the core, it is reasonable to assume that a sufficiently large number of Kuhn segments would be needed in the hydrophobic block. The question thus arises if such a low number of segments is enough to display the required degeneracy. On the contrary, a low number of hydrophobic segments could potentially cause the observed single exponential time decay rather than a lack of polydispersity, as suggested by the authors of these works. The question about whether the size of the conformational space, with conformations separated by entropic barriers, affects the existence of the intermediate logarithmic regime is the main subject of this article.

To help shed some light on this matter, in this study we have carried out several simulations using a dynamic SCMF simulation method. In particular, we have chosen to

investigate the behavior of the L44 triblock copolymer $EO_{10}PO_{23}EO_{10}$ in water at 37 °C. In order to explore the effect of the number of Kuhn segments on the relaxation dynamics of single chains, we have artificially changed the flexibility of the L44 chains. Three cases are considered: the standard experimental chain flexibility, a more rigid chain, and a more flexible chain. We first study the equilibrium behavior for the formation of micelles as a function of their flexibility, and then model the chain dynamics to observe if the flexibility can cause the logarithmic decay to disappear as is found in the experiments. In addition, we follow the conformational behavior of the chains as they leave the micelle to check for any shrinking or swelling of the chains.

Last but not least, we propose a phenomenological equation to describe the evolution of the population of tagged surfactants inside the micelle. This phenomenological equation is a modified Eyring equation, with three parameters, which are related to: the kinetic constant for the intermediate logarithmic regime, the kinetic constant of the ultimate exponential regime, and a crossover surfactant number. The simulation as well as the available experimental data are fitted to this equation. As a result, we obtain a collapse of all data to a master curve, which reinforces the idea of the universality of the observed behavior.

The article is organized as follows, in the next section a brief description of the simulation methodology is given as well as the main features of the coarse-grain model. In the section on Results and discussion, the simulation results are presented for the chosen L44 Pluronic surfactant with varying Kuhn lengths that allow us to model the same molecule with different chain flexibilities. An analysis of these results allows us to follow changes in the chain configurations on exiting the micelle and propose a modified Eyring equation that shows that all the experimental data follows the same master equation. We finish the article in the Conclusions section with a summary of the most important findings.

3.2 | Simulation Methodology and Model Details

The simulation methodology used in this work has already been fully described in previous publications (1; 81; 85; 126) and so in this section only the most important details are included. First of all, a description of the Single Chain Mean-Field theory is given, as well as the dynamic version of the same theory. This is followed by an introduction of the coarse-grain model that was developed for the L44 triblock copolymer (1) and the manner in which we have introduced the different chain flexibilities into the polymer (Details on the chain flexibility can be found in Appendix B).

3.2.1 | Single Chain Mean-Field theory (SCMF)

The main idea behind the SCMF theory is to simulate a specific linear chain which interacts with the other surrounding molecules by way of mean molecular fields (see Figure 3.1). Consequently, a representative set of conformations $\{\alpha\}$ of this central chain needs to be sampled to self-consistently generate the statistical weight of each chain conformation α, from which the average fields are calculated. A given chain conformation is expressed as the collection of positions of all its monomers, $[\alpha] = (\mathbf{r}_1, \mathbf{r}_2, \ldots, \mathbf{r}_{\mathcal{N}})$, where $\mathcal{N}$ is the number of monomers of the chain. Finally, $\mathbf{r}_i[\alpha]$ stands for the position of the i^{th} monomer in the configuration α.

The intramolecular interactions of the central chain, $U_{\text{intra}}(\alpha)$, are calculated in an exact way whereas the intermolecular interactions with the solvent and other surfactants, $U_{inter}(\alpha)$, are calculated within a mean-field approximation. The exact evaluation of the intra-chain interactions allows us to keep track of the self-avoidance and conformational restrictions, which are very important for the kinetic problem that we address. The mean molecular fields are calculated by minimizing the system free energy ($\mathcal{F}$) in a self-consistent manner using the set of chain configurations. This yields the probabilities of the different configurations, $P[\alpha]$, and any other property of interest.

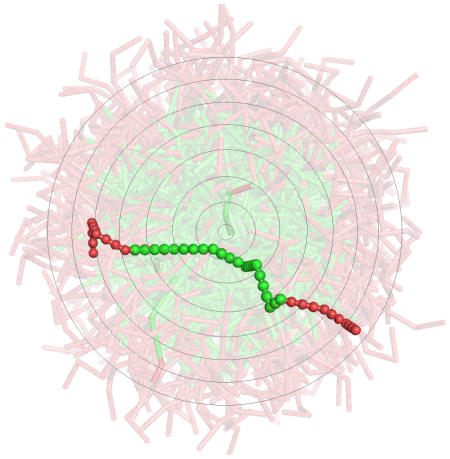

Figure 3.1: A schematic diagram of a specific surfactant chain interacting with the mean molecular fields of a micelle where the EO monomers are shaded red and the more hydrophobic PO monomers green. The circles indicate the one dimensional discretization of the molecular densities used in this work.

The free energy functional is analogous to a Density Functional Theory in conforma-

tional space, and is expressed as follows,

$$\mathcal{F} = N \int d\alpha P[\alpha] \left(U_{\text{intra}}(\alpha) + U_{\text{inter}}(\alpha) \right) + k_{\text{B}}T \left(N \int d\alpha P[\alpha] \log P[\alpha] + \int d\mathbf{r} c_{\text{s}}(\mathbf{r}) \log \phi_{\text{s}}(\mathbf{r}) \right) \tag{3.1}$$

where N is the number of chains in the simulated system, k_{B} is Boltzmann's constant, T is the temperature, $\phi_{\text{s}}(\mathbf{r})$ is the solvent volume fraction, $c_{\text{s}}(\mathbf{r})$ is the solvent number concentration as a function of the position $\mathbf{r}$, and $d\alpha = d\mathbf{r}_1 d\mathbf{r}_2 \dots d\mathbf{r}_{\mathcal{N}}$. The first term in this equation is the energy of the system, whereas the second and third terms account for the configurational and translational entropies of the chains and solvent, respectively. The solvent volume fraction is given as $\phi_{\text{s}}(\mathbf{r}) = c_{\text{s}}(\mathbf{r}) v_{\text{s}}$ where v_{s} is the volume of a solvent molecule.

The free energy in eq (3.1) is minimized subject to the incompressibility condition, which imposes that the available volume is completely filled by the solvent and surfactant molecules at any position $\mathbf{r}$,

$$\phi_{\text{s}}(\mathbf{r}) + N \int d\alpha P[\alpha] \phi(\alpha, \mathbf{r}) = 1 \tag{3.2}$$

where $\phi(\alpha, \mathbf{r})$ is the volume fraction of chain conformation α at a position $\mathbf{r}$, which is given by $v_p c_p = \sum_{i=1}^{\mathcal{N}} v_p \delta(\mathbf{r} - \mathbf{r}_i[\alpha])$, where v_p and c_p refer to the volume and concentration of the chain monomers.

The volume-filling constraint in eq (3.2), which accounts for the repulsive short-range forces, is introduced in the minimization of the free energy *via* a Lagrange multiplier field $\pi(\mathbf{r})$. After evaluating $\delta\mathcal{F}/\delta P[\alpha] = 0$ and $\delta\mathcal{F}/\delta c_{\text{s}}(\mathbf{r}) = 0$, we obtain the corresponding chain probabilities, $P[\alpha]$, and the solvent number concentration, $c_{\text{s}}(\mathbf{r})$, as follows:

$$P[\alpha] = \frac{e^{-H[\alpha]/k_{\text{B}}T}}{\int_V d\alpha \, e^{-H[\alpha]/k_{\text{B}}T}} \tag{3.3}$$

$$c_{\text{s}}(\mathbf{r}) = N_{\text{s}} \frac{e^{-v_{\text{s}}\pi(\mathbf{r})/k_{\text{B}}T}}{\int_V d\mathbf{r} \, e^{-v_{\text{s}}\pi(\mathbf{r})/k_{\text{B}}T}} \tag{3.4}$$

where V is the volume of the system and N_{s} is the total number of solvent molecules. $H[\alpha]$ is the SCMF Hamiltonian, which contains the total intramolecular and intermolecular interactions of conformation α with the surrounding fields. An analytical form of this Hamiltonian reads:

$$H[\alpha] = U_{\text{intra}}(\alpha) + U_{\text{inter}}(\alpha) + k_{\text{B}}T \int d\mathbf{r} \, \pi(\mathbf{r}) \phi(\alpha, \mathbf{r}) \tag{3.5}$$

A more detailed expression of the Hamiltonian for the Pluronic surfactants in water is given later in the section on model details. In this work we are only interested in the

behavior of spherical micelles and so the mean-fields were discretized into concentric spherical layers starting from the center of the simulation cell. A schematic diagram of these spherical shells is given in Figure 3.1.

3.2.2 | Dynamic SCMF scheme

To study the relaxation of the surfactants in the micelle, we use a dynamic version of the SCMF scheme which has already been applied in previous studies (75; 82). This scheme is based on the generation of local displacements of an initial ensemble of sampling chains, $\{\alpha_o\}$, within the already generated mean-fields. New chain configurations are generated independently of each other, in agreement with our mean-field approach, using a random movement in the spirit of dynamic Monte Carlo. Each new conformation is then accepted or rejected with a given probability, following the Metropolis algorithm eq (3.6), according to the change in the energy between the new and old conformations, α_n and α_o, respectively. In this way, detailed balance is maintained and the correct sampling of the equilibrium Canonical distribution for chain conformations is achieved. The probability of acceptance can be written as,

$$p\left(\alpha_o \rightarrow \alpha_n\right) = \min\left(1, e^{-\frac{H[\alpha_n]-H[\alpha_o]}{k_B T}}\right) \tag{3.6}$$

In every cycle a new set of conformations, $\{\alpha_n\}$, is generated, after which the mean-field concentration fields are updated by solving the SCMF equations. This cycle is equivalent to a step forward in time, Δt, the size of which needs to be determined independently in order to relate the simulation cycles to a physical time scale.

3.2.3 | Model details

In this work we implement a coarse-grain model for the triblock copolymer surfactant L44 Pluronic (1) ($EO_{10}PO_{23}EO_{10}$) which has a relatively low molecular weight of 2200. L44 is a linear chain for which we choose to model both the EO and PO monomers as beads of the same diameter σ. Figure 3.2 depicts a typical chain configuration where the green spheres correspond to the hydrophobic propylene oxide monomers (PO, $CH(CH_3)CH_2O$) and the red spheres correspond to the hydrophilic ethylene oxide head monomers (EO, CH_2CH_2O). The distance between consecutive beads is chosen to be equal to σ, while the monomer interactions are modeled by square well potentials at the center of each bead with inner radius σ, outer radius 1.62σ, and a well depth which depends on the particular interaction that is to be modeled. The chain flexibility is taken into account by using Kuhn segments, where a chosen number of monomers are taken

to form a rigid block although we allow complete flexibility between consecutive blocks. A larger number of rigid monomers embedded in each Kuhn segment leads to a more rigid chain with a smaller conformational space.

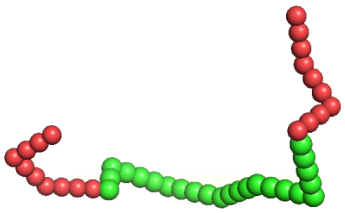

Figure 3.2: A typical chain configuration of the L44 triblock copolymer $(EO_{10}PO_{23}EO_{10})$ with a *Semiflexible* chain where the hydrophilic EO monomers are shaded red and the hydrophobic PO monomers green.

The details of the SCMF Hamiltonian already given in Eq. 3.5 depends on the model being considered. In this particular case, the Hamiltonian includes the interactions between the EO, PO, and water solvent molecules, together with the steric interactions. Hence, the Hamiltonian takes the following form,

$$\begin{aligned} H[\alpha] = U_{\text{intra}}(\alpha) + (N-1)\epsilon_{\text{EO,PO}} \int d\mathbf{r}\, (\Phi_{\text{EO}}(\alpha,\mathbf{r})\langle c_{\text{PO}}(\mathbf{r})\rangle + \Phi_{\text{PO}}(\alpha,\mathbf{r})\langle c_{\text{EO}}(\mathbf{r})\rangle) \\ + \epsilon_{\text{EO},s} \int d\mathbf{r}\, \Phi_{\text{EO}}(\alpha,\mathbf{r}) c_{\text{s}}(\mathbf{r}) + \epsilon_{\text{PO},s} \int d\mathbf{r}\, \Phi_{\text{PO}}(\alpha,\mathbf{r}) c_{\text{s}}(\mathbf{r}) \\ + k_{\text{B}}T \int d\mathbf{r} \left(\frac{\log \phi_{\text{s}}(\mathbf{r})}{v_{\text{s}}} \left[\phi_{\text{EO}}(\alpha,\mathbf{r}) + \phi_{\text{PO}}(\alpha,\mathbf{r})\right] \right) \end{aligned} \quad (3.7)$$

where the first term corresponds to the intramolecular interactions; the second, third, and fourth terms are the intermolecular interactions between EO-PO, EO-solvent, and PO-solvent molecules, respectively, together with their corresponding average concentration fields $\langle c_{\text{EO}}(\mathbf{r})\rangle = \int d\alpha\, P[\alpha] c_{\text{EO}}(\alpha,\mathbf{r})$, $\langle c_{\text{PO}}(\mathbf{r})\rangle = \int d\alpha\, P[\alpha] c_{\text{PO}}(\alpha,\mathbf{r})$, $c_{\text{s}}(\mathbf{r})$, and their available interaction volumes $\Phi_{\text{EO}}(\alpha,\mathbf{r})$ and $\Phi_{\text{PO}}(\alpha,\mathbf{r})$. Finally, the last term represents the steric interactions, arising from the hard core repulsion (or excluded volume) of the different molecules, expressed here as an incompressibility condition. The values of the interaction energy parameters were taken from our previous work (1), where an optimization procedure was carried out to reproduce the available experimental CMC literature values. The values are: $\epsilon_{\text{EO,PO}} = 0.006 k_{\text{B}}T/z$, $\epsilon_{\text{EO},s} = 0.5 k_{\text{B}}T/z$, $\epsilon_{\text{PO},s} = 2.1 k_{\text{B}}T/z$, with $z = 26$ as the coordination number. These values are closely related to the equivalent Flory-Huggins parameters. The coarse-grain nature of our model

prohibits its applicability over a range of temperatures and is limited to the temperature of 37 °C of the experiments to which the parameters were optimized.

The stochastic character of our dynamic SCMF has no physical time scale as such. Consequently, for the purpose of comparing with experimental data, we estimate the physical time scale of our simulations, t. To this end, we compare the diffusion of the free chains in the simulations, D_{SCMF}, to the one expected experimentally, D. The diffusion of a free chain in our simulation can be estimated in terms of the MC cycles, t_{cyc},

$$D_{\mathrm{SCMF}} = \lim_{t_{\mathrm{cyc}}\to\infty} \frac{\langle \Delta \mathbf{r}(t_{\mathrm{cyc}})^2 \rangle}{6 t_{\mathrm{cyc}}} \tag{3.8}$$

where $\langle \Delta \mathbf{r}(t_{\mathrm{cyc}})^2 \rangle = \langle \left(\mathbf{r}(t_{\mathrm{cyc}}) - \mathbf{r}(0)\right)^2 \rangle_{N_{\{\alpha\}}}$ is the average displacement of the center of mass of the $N_{\{\alpha\}}$ chains in the set $\{\alpha\}$. Furthermore, we used the following dimensionless equation to convert the MC cycles into experimental time t,

$$\frac{D_{\mathrm{SCMF}}}{\sigma^2} t_{\mathrm{cyc}} = \frac{D}{l^2} t \tag{3.9}$$

The diffusion constant D_{SCMF} is given in units of σ^2/cycle, whereas l is the physical dimension of the monomers. In our case the monomers have a diameter σ of approximately 0.2 nm which followed from a comparison of available experimental data and the diffusion constant calculated from the Stokes-Einstein expression,

$$D = \frac{k_B T}{6\pi\eta a} \tag{3.10}$$

where the viscosity of the solvent (water) was taken to be $\eta = 6.91 \times 10^{-4}$ kg m^{-1} s^{-1} and the hydrodynamic radius a is taken from the Rouse model, where $a = \mathcal{N}\sigma/2$.

3.3 | Results and discussion

In this work we aim to study the effect of chain flexibility on the dynamic exchange of surfactants between micelles and the bulk solution. To this end, we studied the behavior of the L44 triblock copolymer in water at 37 °C by using SCMF calculations. This particular block copolymer was selected as it is a relatively short Pluronic ($EO_{10}PO_{23}EO_{10}$), but still long enough to allow for different flexibilities to be introduced. Three degrees of surfactant chain flexibility have been chosen. The different flexibilities are obtained by adjusting the stiffness of the surfactant chain through the number of monomers in each Kuhn segment in the hydrophilic *head* l_k^{H} and the hydrophobic *tail* l_k^{T} blocks (see

Table 3.1). Only in the *Semiflexible* case does the surfactant correspond to a realistic experimental system, namely the L44 Pluronic surfactant. In the other two cases, *Flexible* and *Rigid*, the resulting chain has not been chosen to represent any given known experimental system.

Before we can study the dynamics of our systems, we need to estimate their equilibrium properties. On applying the equilibrium SCMF simulation technique already described, it is possible to calculate the standard chemical potentials of chains in micelles containing N chains, μ_N^0, as compared to those in the bulk solution, μ_1^0 (127). Figure 3.3 depicts the resulting standard chemical potential difference $(\mu_N^0 - \mu_1^0)/k_\mathrm{B}T$ as a function of the number of surfactants in the micelle. In all three cases the systems prefer to self-assemble into micelles rather than form a homogeneous solution, as evidenced by the appearance of a minimum value in our SCMF results where the preferred micelles are expected to appear. Further details of these calculations can be found in Appendix B. In Table 3.1 the minimum of the standard chemical potential difference, as a function of the aggregation number N, is given together with the corresponding aggregation number and CMC estimated by $\log \mathrm{CMC} = \min((\mu_N^0 - \mu_1^0)/k_\mathrm{B}T)$.

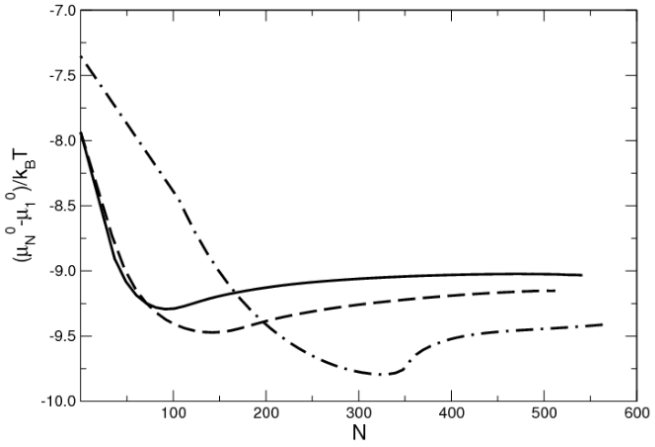

Figure 3.3: Standard chemical potential difference, $(\mu_N^0 - \mu_1^0)/k_\mathrm{B}T$, versus the aggregation number, N. Solid, dashed and dot-dashed lines indicate the *Flexible*, *Semiflexible*, and *Rigid* cases, respectively.

As expected, the aggregation number of the minimum free energy of the micelles depends on the flexibility of the chain, with larger micelles being preferred for stiffer chains. In particular, for the *Flexible* surfactant the preferred micelle has an aggregation number of 91, the *Semiflexible* surfactant is significantly larger containing 145 chains, and the *Rigid* case is much larger, with 320 surfactants. In Figure 3.4 schematic repre-

Case Study	$l_k^{EO}(\sigma)$	$l_k^{PO}(\sigma)$	N	$\min((\mu_N^0 - \mu_1^0)/k_BT)$	CMC (mol/L)
Flexible	2	2	91	-9.2	$5.1 \cdot 10^{-3}$
Semiflexible	3	4	145	-9.4	$4.0 \cdot 10^{-3}$
Rigid	10	20	320	-9.7	$3.3 \cdot 10^{-3}$

Table 3.1: Equilibrium properties of L44 triblock copolymers ($EO_{10}PO_{23}EO_{10}$) in water at 37°C from SCMF calculations: l_k^{EO} and l_k^{PO} are the size of the Kuhn segments of the hydrophilic (EO) and hydrophobic (PO) blocks, aggregation number (N), minimum chemical potential differences, and Critical Micelle Concentration.

sentations of the equilibrium micelles are given for the three different case studies of chain flexibilities. These diagrams plot the most probable conformations of the chains corresponding to the free energy minimum for each case study.

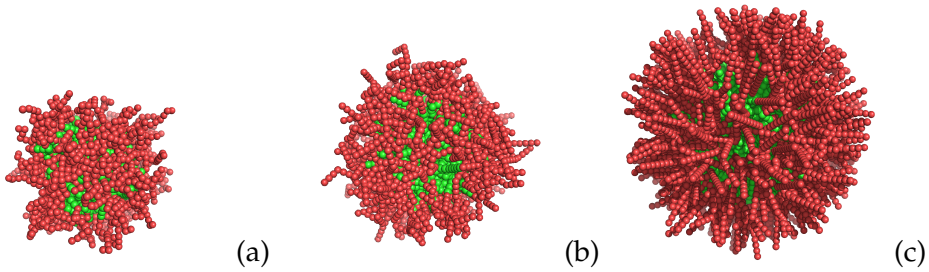

Figure 3.4: Schematic diagram of typical micelle configurations for the three case studies: (a) *Flexible* $N = 91$, (b) *Semiflexible* $N = 145$, and (c) *Rigid* $N = 320$. The EO monomers are shaded red and the more hydrophobic PO monomers green.

For the dynamic simulations, we consequently decided to use 91 surfactants for the *Flexible* surfactant and 145 for the *Semiflexible* case, in line with the preferred micelle size for these systems. However, we chose an aggregation size of 150 for the *Rigid* surfactant, instead of the preferred micelle size, in order to reduce the computational time needed for a system with such a large micelle. This can be achieved by a suitable choice of the number of available surfactants within the simulation box. The size of the micelle is not expected to have a strong effect on the micelle dynamics.

To study the dynamic equilibrium exchange of the micelle chains with the bulk solution we used a correlation function, $F(t)$, similar to the one used in the experimental TR-SANS studies (116; 128; 129) namely,

$$F(t) = \frac{f(t)}{f(0)} \tag{3.11}$$

The chains which are inside the micelle are labelled at time $t = 0$ and keep this label throughout the simulation. This leads to the initial number of labeled chains inside the

micelle, $f(0)$. During the simulation, the number of labelled chains inside the micelle, $f(t)$, is tracked as a function of time. The micelle is in thermal equilibrium during the whole process, namely, no variation in the average fields is produced, due to the fact that new chains from the bulk replace the ones which exit the micelle, but the former may not be tagged. By initially tagging the chains inside the micelle we create a virtual non-equilibrium state which causes the subsequent mixing process between tagged and untagged chains until an eventual equilibrium between the tagged molecules in the bulk and within the micelle. Therefore, the final equilibrium distribution of tagged chains inside the micelle is not zero. The time span of our simulations is shorter than the one required to reach such a new equilibrium. The results of the evolution of the labeled surfactant chains over time for each case of flexibility can be seen in Figure 3.5 in a linear-log plot, which helps to highlight the presence of the logarithmic decay as a straight line.

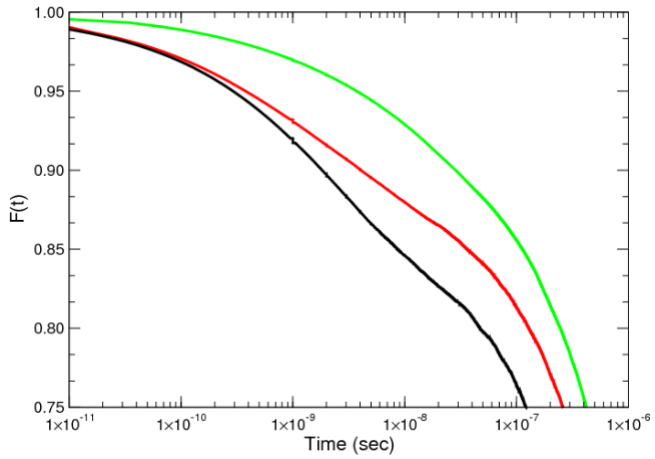

Figure 3.5: Dynamic equilibrium exchange correlation function, $F(t)$, as a function of time for a linear-log plot for the three case studies. From left to right: *Flexible* in black, *Semiflexible* in red, and *Rigid* in green.

As previously mentioned in the Model details section, in order to connect our findings with experimental data we need to convert the simulation cycles, t_{cyc}, into physical time. This was performed by using eqs (3.9) and (3.10), and the main results of the estimated simulation diffusion coefficients. The resulting conversion of the simulation cycles into time in seconds can be found in Table 3.2.

In the cases studied in this work we can detect up to three regimes depending on the chain flexibility, see Figure 3.5. In all there is an initial regime at short times ($t < 10^{-10}$ s), which corresponds to a very fast exit of the chains that are ready to leave at

Case Study	D_{SCMF} ($\sigma^2/cycle$)	Physical time, t_{cycle} ($t_{cyc}s/cycle$)
Flexible	$0.5 \cdot 10^{-3}$	$2.6 \cdot 10^{-13}$
Semiflexible	$1.3 \cdot 10^{-3}$	$7.0 \cdot 10^{-13}$
Rigid	$58.8 \cdot 10^{-3}$	$17.4 \cdot 10^{-13}$

Table 3.2: Diffusion coefficient from SCMF simulations and physical time for each chain flexibility.

$t = 0$ due to their appropriate instantaneous chain conformation. This regime may be followed by an *intermediate logarithmic regime* with a width of about two orders of magnitude ($10^{-10} < t < 10^{-8}$ s). A final regime can also be identified for $t > 10^{-7}$ s which shows an exponential decay. Later in this article we will discuss in more detail this final exponential relaxation behavior with respect to the Halperin and Alexander model for block copolymers, and the possible existence of an intermediate exponential regime followed by a terminal exponential decay.

On inspection of Figure 3.5 we find that an intermediate logarithmic regime appears for the *Flexible* and *Semiflexible* surfactants and takes on the form of a characteristic straight section in the linear-log plots. Such a straight line section is indicative of a logarithmic decay, $F(t) \sim -\log(t)$ which emerges for the cases where the surfactants are sufficiently flexible, and is absent for the more rigid chain. The signature of a logarithmic decay has been observed by several authors in experiments (94; 116), as well as from our previous simulation studies (75; 82). As already mentioned, the main thesis of the experimental groups is to attribute the appearance of this peculiar logarithmic regime to the polydispersity of the available polymer samples. However, our previous and present simulation results give a similar logarithmic behaviour using a purely monodisperse distribution of chain length. Therefore, as we have already argued (75; 82), this logarithmic trend needs to be considered as being caused by some intrinsic property of the micellar system, rather than only to the polydispersity of the samples. Polydispersity will play some role, but obviously it cannot explain the simulation results performed with strictly monodisperse samples. The present analysis thus focuses on the impact of the rigidity of the hydrophobic block in the form of such intermediate decay, which, as our analyzes reveal, must be the key element to understand the apparently disparate interpretation of the experimental results. Interestingly, in the case of the *Rigid* block copolymers, no intermediate logarithmic regime is observed. The representation of the simulated data in a log-log plot (not shown) does not change this interpretation of the data.

To emphasize the form of the terminal regime, we have plotted our simulation re-

sults using a log-linear plot in Figure 3.6. If an exponential regime is attained, the curves should be straight lines in this plot which we expect to occur after around $t \sim 10{-}7$ s. In the cases of the *Rigid* and *Semiflexible* chains it was possible to begin to enter this regime, however, in the case of the *Flexible* chain, it was not possible to simulate sufficiently long times.

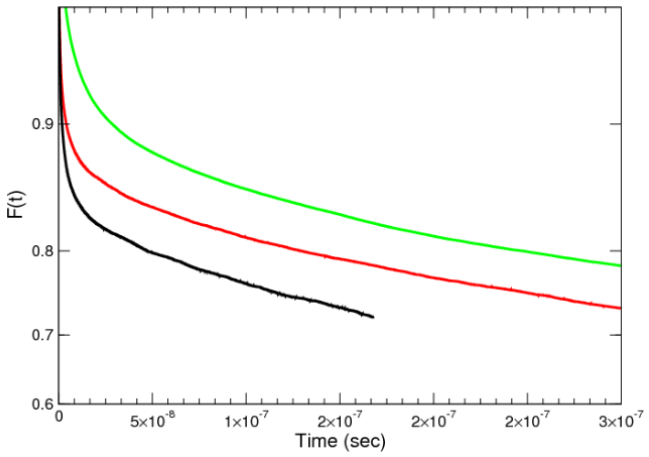

Figure 3.6: Dynamic equilibrium exchange correlation function, $F(t)$, as a function of time using a log-linear plot for the three case studies. From left to right: *Flexible* in black, *Semiflexible* in red, and *Rigid* in green.

The appearance of a logarithmic decay thus requires the surfactant chains to have a sufficient degeneracy of the energy states in the micelle core together with a preferred conformation on exit, which does not exist for the most rigid chain. This degeneracy is a result of the different conformations of the hydrophobic block segment in the core and so must require a sufficient number of hydrophobic monomers. On inspection of Figure 3.5, we find that the extension of this logarithmic regime is significantly larger for the *Flexible* chain and appears over almost three orders of magnitude. In the case of the *Semiflexible* chains this regime is reduced to being observed over closer to two orders of magnitude, although it is difficult to be categoric due to the nature of the data available. What is clear is that for the *Rigid* chains this regime is not present. Our results thus indicate that the 2 hydrophobic Kuhn segments of the *Rigid* chains are not enough to produce the effect, but the 6 Kuhn segments of the *semiflexible* chains is already sufficient.

If we test this view by comparing with the experimental studies where only an exponential decay was observed, we find that only n-alkyl ethers: $C_n - PEO_5$ and $C_n - PEO_{10} - C_n$, with n = 18, 22, 24, 28, 30 were used, as already mentioned in the introduction. The re-

sulting Kuhn hydrophobic blocks of these polymers range from about 2 to almost 4 segments. According to the simulation results from this work, these surfactants may not be long enough to allow for a clear logarithmic regime and would explain why none was observed. Clearly, it would be instructive to perform experiments for monodisperse surfactants with larger hydrophobic block lengths to see if this logarithmic behavior then appears. It should be noted that the first regime, where a rapid rearrangement of the surfactant occurs due to the initial labelling of surfactants, does not appear in the experimental results.

To better understand the behavior of the block copolymers, we examined any changes in the chain conformations on leaving the micelle. In particular, we calculated the radius of gyration of the central hydrophobic block as a function of the radial distance of the center of mass of these PO blocks with respect to the center of the micelle.

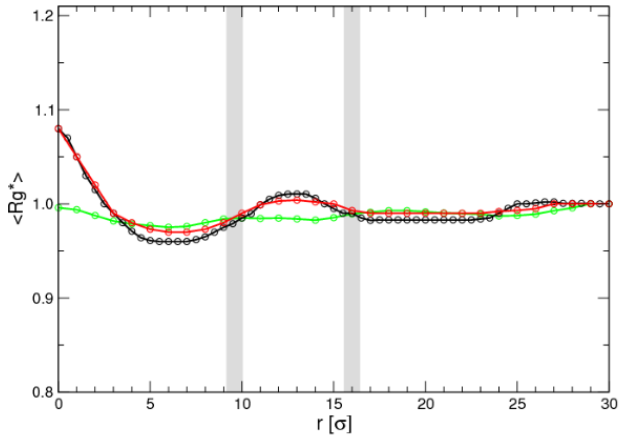

Figure 3.7: Radius of gyration of the PO block relative to the bulk solution value (Rg*) with respect to the distance from the micelle center for each case study: *Flexible* in black, *Semiflexible* in red, and *Rigid* in green. The blue dashed lines represent the interfaces between the core of the micelle and corona (left) and between the corona and bulk solution (right), while the thickness corresponds to the differences between the three case studies.

Specifically, according to Figure 3.7, there is a significant change in R_g for the *Flexible* and *Semiflexible* chains when moving from the centre of the micelle to the threshold of the corona, while the *Rigid* chain does not show any significant change. This fact supports the opinion that there are preferred conformations on exit for the systems that are flexible enough as to produce some sort of hairpin structure with a crumpled hydrophobic core, as this last figure suggests.

On crossing the micelle corona, all chains display a slight swelling which is much

slighter than the collapse for the *Flexible* and *Semiflexible* chains, and similar for the *Rigid* chains. On leaving the corona, the chains attain the bulk solution value, which may mean a slight swelling or collapse depending on the chain flexibility.

In addition, we calculated the average angle between the two hydrophilic blocks as a function of distance from the micelle centre for each case of flexibility. Here we define two vectors from the center of mass of the PO block to the centers of mass of the two EO blocks and calculate the resulting angle. A completely stretched chain will have an angle of 180° and will be reduced as it approaches a hairpin conformation. As can be seen in Figure 3.8, in all cases the angle between the PO and EO blocks decreases as the surfactants approach the EO-PO interface and then increases until the surfactants reach the corona-water interface, where they leave the micelle and enter the bulk solution. It is also remarkable that as the flexibility of the surfactants decreases, the changes in the angle between the EO-PO blocks became smaller, which arises from the fact that the conformations are more limited as the surfactant is more rigid. Again, Figure 3.8 confirms that the chain flexibility favors the formation of hairpin conformations that are more likely to leave the micelle than more stretched ones. As we argued in Ref. (82), crumpled conformations offer less contact between the hydrophobic monomers and hydrophilic corona monomers or bulk fluid, thus minimizing the energy barrier to be overcome to escape the micelle. Therefore, chain flexibility is the crucial feature underlying the non-exponential decay in the intermediate logarithmic regime.

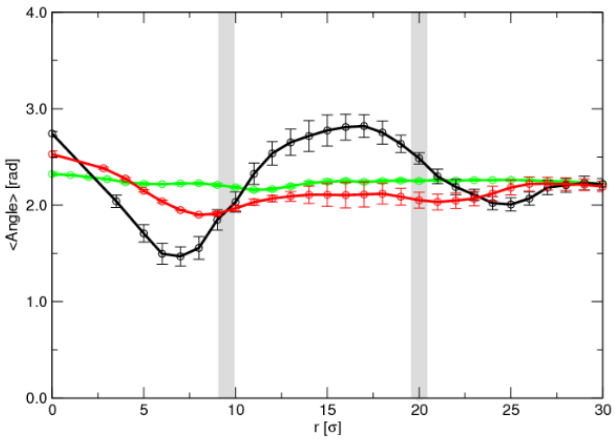

Figure 3.8: Average angle between the PO and EO blocks as a function of distance from the micelle center for each case study: *Flexible* in black, *Semiflexible* in red, and *Rigid* in green. The blue dashed lines represent the interfaces between the core of the micelle and corona (left) and between the corona and bulk solution (right), while the thickness corresponds to the differences between the three case studies.

TR-SANS and fluorescence spectroscopy experiments for diblock and triblock copolymer systems support the idea that the chains are either collapsed (94; 117; 130) or stretched (93; 128; 129; 130) when leaving the micelle. However, from our calculations, we do not observe neither completely collapsed nor stretched conformations, when leaving the micelle. In Figure 3.9 we show a sketch of the micelle escape process for the three chain rigidities studied in this article.

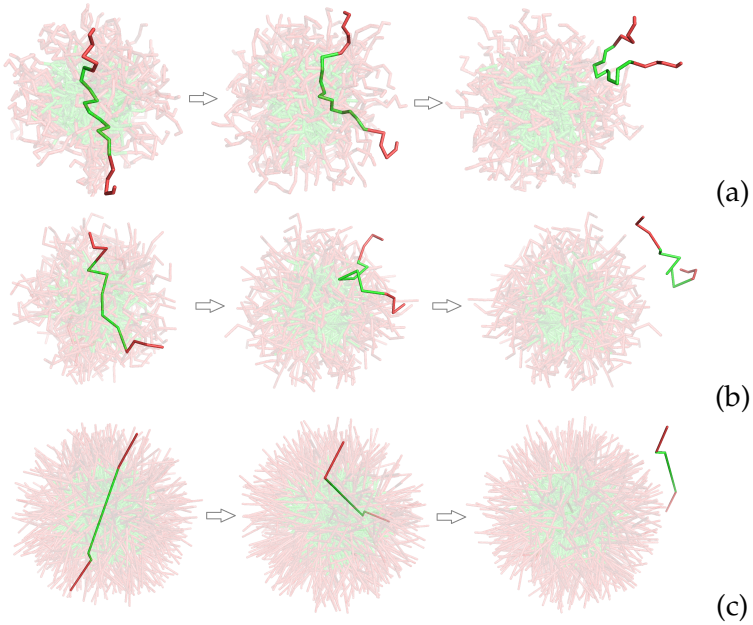

Figure 3.9: Schematic diagrams of the most likely surfactant configurations for three different distances from the micelle center (in the core, passing through the corona, and reaching the bulk) for the three case studies: (a) *Flexible*, (b) *Semiflexible* and (c) *Rigid*. The EO monomers are shaded red and the more hydrophobic PO monomers green.

To better understand the simulation results and to be able to compare with the available experimental data, we decided to try to fit the correlation function with an appropriate mathematical expression able to reproduce the main features of the dynamic process. The Eyring equation was a natural starting point since it already provides a logarithmic dependence, however, since the final regime has its own kinetics, for this system we require a modified version of the Eyring equation which includes a third parameter, namely,

$$\frac{dF(t)}{dt} + k_1\left(e^{\frac{F(t)}{\epsilon}} - 1\right) + k_2\left(1 - e^{-\frac{F(t)}{\epsilon}}\right) = 0 \tag{3.12}$$

where k_1 represents the characteristic kinetic constant for the initial and intermediate

regimes, k_2 is indicative of the kinetic constant in the final exponential regime, and ϵ is a crossover value of the correlation function. These constants need to be fitted by using either the simulation data from the correlation function, $F(t)$, or experimental data for the same quantity. Note that this modified Eyring equation has an additional third term with a constant k_2 which gives three different regimes, as required. This differential equation can be analytically solved, yielding,

$$F(t) = -\epsilon \ln \left(\frac{1 - k\, e^{-\frac{k_1+k_2}{\epsilon} t}}{\frac{k_2}{k_1}\, k\, e^{-\frac{k_1+k_2}{\epsilon} t} + 1} \right) \tag{3.13}$$

where

$$k \equiv \frac{e^{1/\epsilon} - 1}{e^{1/\epsilon} + \frac{k_2}{k_1}} \tag{3.14}$$

However, the exact closed form does not reveal the subtleties of the different regimes, which are better discerned through a simple asymptotic analysis shown later on in this section. On fitting eq (3.12) to our correlation function simulation data for the different case studies, we find that in all cases it is possible to obtain a good fit with an accuracy of 98-99%. In Table 3.3 we show the fitted parameters ϵ, k_1, and k_2 of the modified Eyring equation (eq 3.13) used in this study. As can be observed, ϵ is approximately constant with a value of about $\sim 2 \times 10^{-2}$, as is k_2, which has values between $4 - 7 \times 10^5 s^{-1}$. However, k_1 changes several orders of magnitude between $10^{-8} - 10^{-14} s^{-1}$ on going from the flexible to the rigid chain.

Case Study	ϵ ($\sigma^2/cycle$)	$k_1(s^{-1})$ ($t_{cyc}s/cycle$)	$k_2(s^{-1})$
Flexible	$2.6 \cdot 10^{-2}$	$1.0 \cdot 10^{-8}$	$6.8 \cdot 10^5$
Semiflexible	$2.0 \cdot 10^{-2}$	$1.0 \cdot 10^{-13}$	$4.1 \cdot 10^5$
Rigid	$1.9 \cdot 10^{-2}$	$1.0 \cdot 10^{-14}$	$4.3 \cdot 10^5$

Table 3.3: Results from fitting the modified Eyring equation to the correlation function for each chain flexibility.

Since several experimental results of correlation functions for block copolymers are available in the literature, we decided to also fit the parameters of the modified Eyring equation using the experimental data. Table 3.4 summarizes the estimated parameters associated with fitting eq. (3.13) with previous experimental data (116; 128; 129). We found that in all cases the accuracy was good, about 95-99%.

The experimental data implemented for the fitting were based on TR-SANS experiments. Specifically, *Set 1* are from the equilibrium exchange kinetics of starlike

Table 3.4: Results from fitting the modified Eyring equation to the correlation function from previous studies based on TR-SANS experiments.

Set 1[a]	ϵ	$k_1(s^{-1})$	$k_2(s^{-1})$
PEP1-PEO20 47 °C	$7.2 \cdot 10^{-2}$	$4.1 \cdot 10^{-10}$	$2.4 \cdot 10^{-9}$
PEP1-PEO20 55 °C	$7.9 \cdot 10^{-2}$	$3.6 \cdot 10^{-9}$	$9.4 \cdot 10^{-10}$
PEP1-PEO20 60 °C	$8.2 \cdot 10^{-2}$	$1.2 \cdot 10^{-8}$	$4.8 \cdot 10^{-10}$
PEP1-PEO20 65 °C	$10.1 \cdot 10^{-2}$	$1.2 \cdot 10^{-7}$	$4.4 \cdot 10^{-10}$
Set 2[b]	ϵ	$k_1(s^{-1})$	$k_2(s^{-1})$
1% vol PEP-PS-PEP	$8.2 \cdot 10^{-2}$	$1.3 \cdot 10^{-2}$	0.7
6% vol PEP-PS-PEP	$8.4 \cdot 10^{-2}$	$3.4 \cdot 10^{-3}$	$3.3 \cdot 10^{-4}$
Set 3[c]	ϵ	$k_1(s^{-1})$	$k_2(s^{-1})$
PS-PEP-1	$9.1 \cdot 10^{-2}$	$1.8 \cdot 10^{-5}$	$3.8 \cdot 10^{-4}$
PS-PEP-2	$9.4 \cdot 10^{-2}$	$7.2 \cdot 10^{-9}$	$4.3 \cdot 10^{-8}$

[a]Lund et al. (116) for poly(ethylene-propylene)- poly(ethylene oxide) ($PEP_1 - PEO_{20}$ the numbers represent the molecular weight in kg/mol) diblock copolymers.
[b]Lu et al. (128) for poly(styrene)-poly(ethylene propylene)-poly(styrene) (PEP-PS-PEP).
[c]Choi et al. (129) for poly(styrene)-poly(ethylene propylene) (PS-PEP) diblock copolymers with different hydrophobic (PS) lengths ($\langle N_{\mathrm{PS}} \rangle = 255$ for PS-PEP-1 and $\langle N_{\mathrm{PS}} \rangle = 412$ for PS-PEP-2).

poly(ethylene-propylene)- poly(ethylene oxide) ($PEP_1 - PEO_{20}$) micelles in a 25% dimethylformamide (DMF)-water solvent mixture, at $\phi = 1\%$, for different temperatures (47°C, 55°C, 60°C, 65°C) (116). *Set 2* are from the kinetic analysis of poly(ethylene propylene)-poly(styrene)-poly(ethylene propylene) (PEP-PS-PEP) triblock micelles at two different concentrations (1 vol % PEP-PS-PEP, 6 vol % PEP-PS-PEP) (128). Finally, *Set 3* are from the micelle exchange dynamics of two poly(styrene-b-ethylene-alt-propylene) copolymers, PS-PEP-1 and PS-PEP-2, in squalane with different hydrophobic (PS) repeat units, $< N_{PS} >= 255$ and $< N_{PS} >= 412$ respectively (129).

According to the estimated parameters, we observe that ϵ remains approximately constant in all cases, with values of the order of magnitude of 10^{-2}. However, we observe significant changes for k_1 and k_2. Specifically, k_1 has values between $10^{-10} - 10^{-5} s^{-1}$, except for the cases of 1% vol PEP-PS-PEP, 6% vol PEP-PS-PEP in which it takes values of $10^{-2} s^{-1}$ and $10^{-3} s^{-1}$, respectively. Finally, with respect to the k_2 parameter, we observe that it also has a wide range of values between $10^{-10} s^{-1}$ and $1 s^{-1}$. However, the relevant parameter for the dynamics is the ratio of these two kinetic constants, which we have denoted as $\gamma \equiv k_1/k_2$. Two different dynamic classes can be identified depending on whether this value is larger or smaller than 1. In particular, the simulation results belong to the class of $\gamma < 1$ where, in fact γ is negligibly small (see Table 3.3). The following experimental results also belong to this same class: case 1 of

Set 1 (*cf.* Table 3.4) with a value of $\gamma \sim 10^{-1}$, case 1 of *Set 2* with $\gamma \sim 10^{-2}$, and the two cases of *Set 3*, whose values are $\gamma \sim 10^{-1}$. The rest of the experimental cases correspond to the dynamic class where $\gamma > 1$, with values of $\gamma \sim 10 - 10^3$.

These experimental values are for block copolymers different from the Pluronic modelled in this paper, and are in addition in different solvents and temperatures. Nevertheless, we can attempt to compare some of the main features. In particular, it is interesting to note that the ϵ parameter from our simulations has the same order of magnitude to the experiments with only small variations. In addition, the k_1 parameters estimated from our simulation are also within the range of values of the experiments. Contrarily, the values of the k_2 parameters are orders of magnitudes higher than any of the ones from the experiments. This is probably due to a lack of sufficient data in the terminal regime with an exponential decay in the experiments, doubtlessly because the experimental block copolymers, solvents, and temperatures were chosen to highlight the intermediate logarithmic regime. Consequently, the k_2 parameters, obtained on fitting to the experimental data, should be taken with caution as their lack of precision can be responsible for the appearance of these low values. With the information gathered about the values of the parameters, we can return to eq. (3.12) and analyze its properties. In the first place, let us introduce a new variable $y \equiv \exp(F/\epsilon)$ and rewrite eq. (3.12) as

$$\epsilon \frac{dy}{dt} = -k_1 y(y-1) - k_2(y-1) \tag{3.15}$$

Since $F(0) = 1$ and $\epsilon \sim 10^{-2}$, the initial value of the variable y is very large. To analyze the equation in the initial stages, we introduce a rescaling of the variable, $y = e^{1/\epsilon}\tilde{y}$, so that $\tilde{y} \sim 1$. Hence, the resulting equation reads

$$\frac{\epsilon}{k_2}\frac{d\tilde{y}}{dt} = -\frac{k_1}{k_2}e^{1/\epsilon}\,\tilde{y}(\tilde{y} - e^{-1/\epsilon}) - (\tilde{y} - e^{-1/\epsilon}) \tag{3.16}$$

According to this form, we can assume that $\tilde{y} \gg e^{-1/\epsilon}$. Introducing a scaling of the two variables, $t = at^*$ and $\tilde{y} = by^*$, eq. (3.16) can be reduced to a parameter-free form for y^* and t^* by choosing

$$a = \frac{\epsilon}{k_2} \tag{3.17}$$

$$b = \frac{k_2}{k_1}e^{-1/\epsilon} = \frac{1}{\gamma}e^{-1/\epsilon} \tag{3.18}$$

which yields the dimensionless form

$$\frac{dy^*}{dt^*} \simeq -y^{*2} - y^* \tag{3.19}$$

The important aspect of this scaling of variables is that it allows us to place all the experimental data under one single master curve, which strongly supports the existence of an underlying universal behavior. Thus, taking t^* as the independent variable, using the parameters given in Table 3.4 in eq. (3.17) for each experimental set, and setting $y^* = \frac{k_1}{k_2}\exp(F/\epsilon)$ as the dependent variable, we obtain the master curve given in Fig. 3.10.

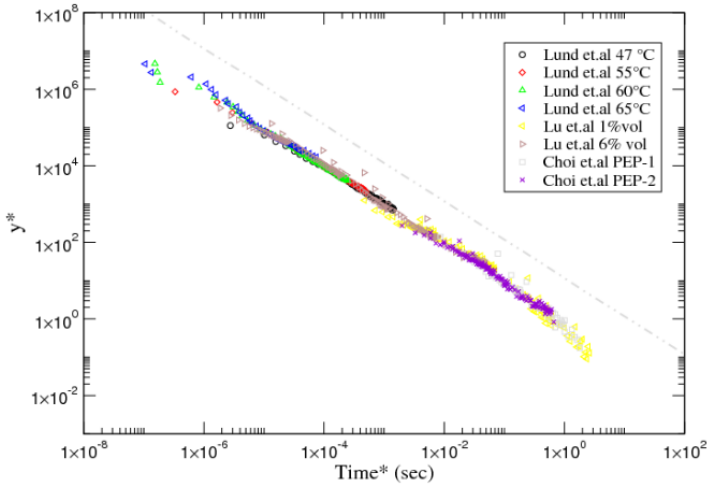

Figure 3.10: Log-log plot of the experimental data of the references given in Table 3.4 with the scaled variables. An additional grey dot-dashed line of slope 1 indicative of a logarithmic decay is included above the data sets. Notice that the scaling is able to also capture the crossover towards the exponential regime, which should appear in the region $t^* \gg 1$.

This figure shows that the logarithmic behavior spans over 6 decades, involving up to 8 data sets of two different groups. To make apparent the logarithmic behavior, let us consider the region in which $y^* \gg 1$ and, therefore,

$$\frac{dy^*}{dt^*} \simeq -y^{*2} \tag{3.20}$$

The solution of this equation is of the form

$$y^*(t^*) = \frac{\gamma e^{1/\epsilon}}{1+\gamma e^{1/\epsilon} t^*} \sim \frac{1}{t^*} \tag{3.21}$$

where the last expression is valid for $t^* \gg e^{-1/\epsilon}/\gamma$. This asymptotic behavior can be identified as a slope of -1 in a log-log plot of y^* vs. t^* (see the grey dot-dashed line in Fig. 3.10). In terms of the original variables, one finds

$$F(t) \sim 1 - \epsilon \ln\left(1 + \frac{k_1}{\epsilon} e^{1/\epsilon} t\right) \sim 1 - \epsilon \ln\left(\frac{k_1}{\epsilon} e^{1/\epsilon} t\right) \tag{3.22}$$

Therefore, the logarithmic behavior is established after an initial time $\tau_1 \equiv \frac{\epsilon}{k_1} e^{-1/\epsilon}$, in the region $t > \tau_1$, where τ_1 is also a characteristic time-scale of the decay. Notice that the time scale of the logarithmic decay is governed by the kinetic constant k_1 together with the crossover parameter ϵ. The crossover towards the next regime depends on whether the parameter γ is smaller or larger than 1 and is, therefore, system-dependent.

Let us start with the case $\gamma > 1$, which we will refer to as *type a* dynamics. In this case, the regime that appears after the logarithmic decay is determined by the point at which $\tilde{y} \sim e^{-1/\epsilon} > e^{-1/\epsilon}/\gamma$ (equivalently, $y^* \sim \gamma > 1$), namely, one enters the exponential terminal regime before the second term on the right-hand side of eq. (3.19) is important. The dynamics of such a terminal regime is obtained by assuming that $y^* - \gamma$ is very small and, therefore,

$$\begin{aligned} \frac{dy^*}{dt^*} &= -y^*(y^* - \gamma) - (y^* - \gamma) \\ &\simeq -\gamma(y^* - \gamma) - (y^* - \gamma) = -(1+\gamma)(y^* - \gamma) \end{aligned} \tag{3.23}$$

which yields

$$y^* \simeq \gamma\left(1 - e^{-(1+\gamma)t^*}\right) + Ce^{-(1+\gamma)t^*} \tag{3.24}$$

When expressed in terms of the natural variables, one finds that, effectively, the decay is exponential,

$$\frac{F(t^*)}{\epsilon} \sim e^{-(1+\gamma)t^*} \sim e^{-\left(\frac{k_1+k_2}{\epsilon}\right)t} \tag{3.25}$$

The characteristic time-scale of the exponential decay is $\tau_2 = \frac{\epsilon}{k_1+k_2}$. Thus, since $1/\tau_1 \gg 1/\tau_2$, we can asymptotically match the two solutions by assuming $C \simeq C(t/\tau_1)$ and equate the limits $t/\tau_1 \to \infty$ with $t/\tau_2 \to 0$, yielding

$$y^* \simeq \gamma\left(1 - e^{-(1+\gamma)t^*}\right) + \left[\frac{\gamma e^{1/\epsilon}}{1 + \gamma e^{1/\epsilon} t^*}\right] e^{-(1+\gamma)t^*} \tag{3.26}$$

Type b dynamics with $\gamma < 1$ is characterized by the fact that the second term in eq. (3.19) is important when $y^* \sim 1 > \gamma$. This implies that an additional regime spans from the logarithmic decay to the terminal exponential decay for $1 > y^* > \gamma$. The simplicity of our model allows us to calculate the solution of eq. (3.19) exactly, i.e.

$$y^*(t^*) \simeq \frac{\gamma e^{1/\epsilon} e^{-t^*}}{1 + \gamma e^{1/\epsilon}(1 - e^{-t^*})} \tag{3.27}$$

Obviously, the logarithmic decay previously derived from eq. (3.21) is recovered here in the limit $t^* \ll 1$. It is interesting to note that this second intermediate regime, when it exists, is also universal. Therefore, the break from universality is produced through the transition to the terminal exponential regime.

The matching of the outer and inner solutions requires that eq. (3.24) be rewritten as

$$y^* \simeq \gamma \left(1 - e^{-(1+\gamma)\, t^*}\right) + C'(t^*) e^{-\gamma\, t^*} \tag{3.28}$$

where, compared to the previous case, $C'(t^*) = C(t^*) e^{-t^*}$. Thus, in a similar way to the one needed to reach eq. (3.26), we obtain

$$y^* \simeq \gamma \left(1 - e^{-(1+\gamma)\, t^*}\right) + \left[\frac{\gamma e^{1/\epsilon}\, e^{-t^*}}{1 + \gamma e^{1/\epsilon}\, (1 - e^{-t^*})}\right] e^{-\gamma\, t^*} \tag{3.29}$$

The analysis of these asymptotic behaviors in comparison with the simulated and experimental data give rise to the following conjectures. First, the simulation results seem to lie far from the terminal exponential regime and the deviation from the logarithmic behavior shows instead the transition towards the second intermediate regime. Due to the fact that γ is virtually negligible for the three cases, and in view of eq. (3.29), we can consider that the terminal regime is virtually unattainable and that the observable terminal regime in Fig. 3.11 is the second intermediate regime, which also behaves exponentially for $t^* \sim 1$. Effectively, from eq. (3.29),

$$y^*_{sim} \simeq \gamma \left(1 - e^{-t^*}\right) + \left[\frac{\gamma e^{1/\epsilon}\, e^{-t^*}}{1 + \gamma e^{1/\epsilon}\, (1 - e^{-t^*})}\right] \rightarrow \gamma \left(1 - e^{-t^*}\right) + e^{-t^*} \tag{3.30}$$

Second, all the experimental data corresponding to $\gamma > 1$ seem to lie entirely inside the

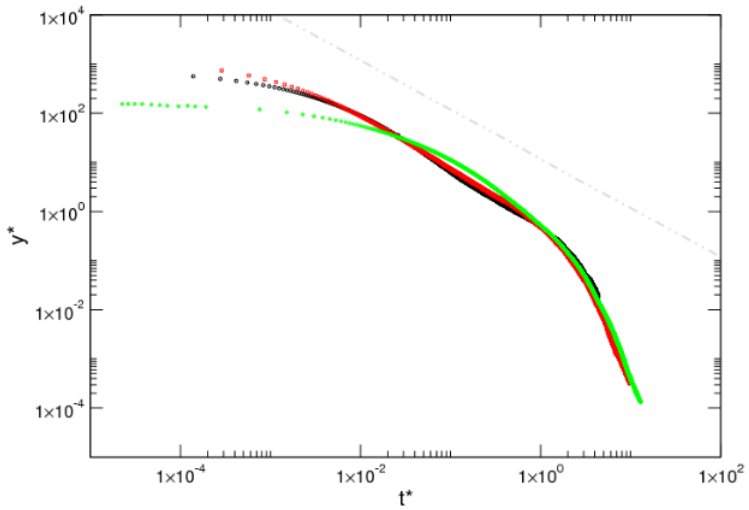

Figure 3.11: Simulation data represented with the scaling form in a log-log plot for each case study: *Flexible* in black, *Semiflexible* in red, and *Rigid* in green. An additional grey dot-dashed line of slope 1 indicative of a logarithmic decay is included above the data sets.

logarithmic region. Therefore, our estimate of the kinetic constant k_2 for these sets is not reliable as there is a lack of data in the required non-logarithmic region. Finally, see Fig. 3.10, three sets display deviations from the logarithmic decay at around $t^* \sim 1$ (system 1 Set 2; systems 1 and 2 Set 3) . These three cases correspond to $\gamma < 1$ and hence we can conclude that they show the onset of the second intermediate regime and that the estimate of k_2 is meaningful.

In view of these observations, we can conjecture that the experimental situations where we found $\gamma > 1$ were due to the lack of significant data outside the logarithmic decay. If we admit that the only relevant situation is thus $\gamma < 1$, then, the exponential decays detected are due to the asymptotic behavior of the second intermediate regime. Thus, the experimental curves as well as the simulation data could be well fitted with a mathematical expression of the form of (3.30), which in ordinary variables reads

$$y = e^{F(t)/\epsilon} \simeq \left(1 - e^{-\frac{k_2}{\epsilon}t}\right) + \left[\frac{e^{1/\epsilon}\, e^{-\frac{k_2}{\epsilon}t}}{1 + \frac{k_1}{k_2} e^{1/\epsilon}\left(1 - e^{-\frac{k_2}{\epsilon}t}\right)}\right] \tag{3.31}$$

Furthermore, see Fig. 3.11, we observe that both the *Flexible* and *Semiflexible* chains show a rather wide logarithmic behavior of about two decades. Moreover, their behavior in scaled variables is rather coincident, enforcing our claim that the observed decay is universal, provided the polymers have a similar physical nature. Interestingly, the *Rigid* chain does not show any trace of a logarithmic decay. In fact, no scaling of the data was found that was able to give the same master curve decay shown by the first two cases. This fact strongly suggests that the mechanism leading to the intermediate regimes is absent if the chain lacks sufficient conformational degrees of freedom. Therefore, we can also conjecture that the internal chain flexibility and number of Kuhn segments is the key element to understand the nature of the exotic intermediate regimes and that its entropic nature is in the basis of the observed universal behavior.

3.4 | Conclusions

In this paper, we have analyzed the relaxation kinetics of copolymeric micellar systems at short and intermediate times. We have carried out simulations of Pluronic surfactants in water at 37°C as a function of the chain flexibility. The L44 triblock copolymer was chosen and given three different degrees of flexibility, two of which are hypothetical and do not correspond to any molecule. The surfactants were described using a coarse-grain model in an implicit solvent of water which correctly reproduces the CMC. The dynamic simulations start with an equilibrated micelle in which the surfactants are labelled, after

which we follow the kinetics of the exchange of labelled single surfactants between the micelle and the bulk.

On plotting the corresponding correlation function, three well defined regimes were observed. In the first regime at very short times the surfactants are expelled without conformational changes, while the third regime seems to correspond to a cross-over towards the terminal Halperin and Alexander exponential decay, which must exist well beyond the limit of our simulation data. The second regime only appears for the two case studies with higher chain flexibility and not for the *Rigid* case. This intermediate regime corresponds to a characteristic logarithmic relaxation. In our previous works we used our simulation data to justify that this particular logarithmic decay arises from a degeneracy of energy states of the hydrophobic block in the micelle core, which becomes broken on entering the corona. Here, we provide qualitative proof that this process could control the initial stages, but that the explanation for longer times (the intermediate regime) requires the existence of a preferred conformation -hairpin for the triblock copolymers used in this study- on exit. Such a preferred conformation is characterized by a rather crumpled hydrophobic core, which gives the lowest energy barrier to escape across the hydrophilic corona. Thus, after the initial stages of the process, chains have to diffuse in conformational space to reach such a preferred hairpin conformation on exit. The different conformations are separated by entropic barriers that should be overcome before exiting, which induces the variety of free-energy barrier heights responsible for the non-exponential decay rate. It is consistent with this interpretation that a sufficient number of degenerate conformational states needs to occur in order for this second regime to appear. This number requires a minimum number of Kuhn segments in the hydrophobic block. In our model 6 Kuhn segments was enough, but 2 was insufficient.

This second regime with a logarithmic relaxation has also been seen in several experimental studies using TR-SANS and it is the interpretation of the cause of this second logarithmic regime that this article is particularly concerned with. In some experimental works this peculiar logarithmic relaxation is attributed to the polydispersity of the block copolymer samples. The justification is that the escape of chains is governed by energetic barriers in the corona, whose height vary depending on the chain length. However, in one of our previous works we indicated that the logarithmic behavior required a rather particular form of polydispersity (82). Here we show that such a logarithmic behavior is rather universal for many different systems, and that it is also present in our monodisperse simulations. Therefore, as we also argued in this last reference, it should be rooted in the physical nature of the system. The argument based on the polydispersity gained further weight due to the fact that in some monodisperse systems, namely

poly(ethylene oxide) polymers (PEO) with n-alkyl ethers, the logarithmic behavior was not identified. It should be noted, however, that in these cases the hydrophobic block was limited to at most $n = 30$ monomers which is about 4 Kuhn segments. In the simulation studies 6 Kuhn segments were sufficient for the logarithmic regime to appear, however 2 segments were not enough. Therefore, this suggests that the chains used in these works did not have the required flexibility for displaying the discussed mechanism leading to the non-exponential intermediate regime. Consequently, our conclusion is that the hydrophobic blocks of the copolymers used in the experiments are not sufficiently long for the required degeneracy of the energy states to appear. Polydispersity is doubtlessly an important factor in the chain kinetics, but our simulations indicate that the logarithmic regime can already be obtained without it if the hydrophobic block of the polymer is able to sample a sufficient number of degenerate configurational states in the micelle core.

Another important element in the understanding of surfactant dynamics is with regards to any conformational changes on leaving the core. As in our previous studies, although we do find a slight collapse of the hydrophobic block and a certain folding of the chain, this is a subtle effect and not a complete collapse or a full stretching of the chain as sometimes assumed in other works.

The proposed modified version of Eyring's equation has allowed us to fit both our data, as well as the experimental ones available in the literature, onto a general master curve. An analysis of the experimental data reveals that they collapse onto a master curve in which only the logarithmic decay and the onset of the crossover toward the next regime is observed. While the logarithmic decay requires one kinetic constant k_1, the crossover is governed by a second constant k_2, which cannot be reliably determined in the sets where the end of the logarithmic decay has not been reached. For the cases where we obtained a reliable determination of k_2, this constant was significantly larger than k_1. The same is observed from the fit of the simulation data to the modified Eyring´s equation. All in all, casting these varied data under this model has allowed us to propose that this crossover regime is in fact also universal. This regime is previous to the final true Halperin and Alexander exponential decay, which lies far beyond the limit of the reported and simulated data. Finally, from an asymptotic analysis, we have proposed a curve that must phenomenologically describe the short time dynamics of this type of micellar systems (eq. (3.31)), which reproduces the three observable regimes of the displayed data. A question still remains to be answered regarding the interpretation of the exponential decays observed in experimental data with respect to the Halperin and Alexander model. For example, poly(ethylene oxide) polymers (PEO) with n-alkyl ethers where only an exponential decay is found, which we have argued may be due to

the presence of too rigid polymers without the necessary configurational states. Such an exponential decay could be the second intermediate regime predicted by the modified Eyring´s equation, rather than the Halperin and Alexander relaxation (75), but further experimental data and analysis is required to confirm this statement.

Finally, we like to mention some of the limitations of our methodology. Although we exactly model the intra chain interactions by explicit single chain conformations, the mean-field nature of the inter chain interactions does not allow us to include the correlated behavior of several chains. For example, within SCMF theory it is not possible to model hindrances to the chain motion due to entanglements with other chains, which may play some role in the dynamic behavior of the system. However, in view of the shortness of the chains considered in this work, we expect that their influence is not significant since the distance between entanglements may in fact be larger than the chain length. A more important limitation is that the use of an implicit solvent effectively limits the application of our model to the temperature of the experimental data used to fit the interaction parameters, in this case 37°C. However, temperature dependent model parameters could be developed by fitting to experimental data at other temperatures.

4

Thermodynamic Equilibrium Properties of Mixed Micelles using Coarse-Grain Mean Field Simulations

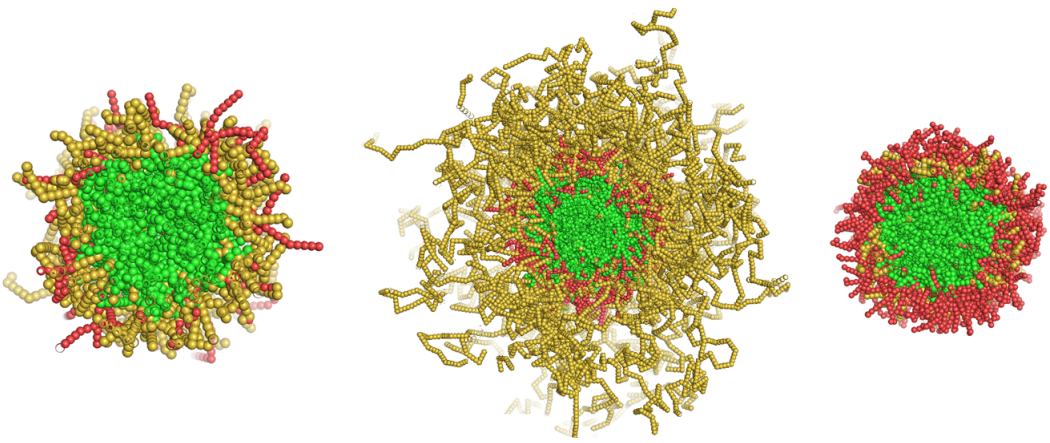

4.1 | Introduction

Block copolymers surfactants are known for their amphiphilic nature, because they consist of two or more different types of polymer blocks that can have both hydrophobic (oil-like) and hydrophilic (water-like) properties. The hydrophobic blocks tend to avoid contact with the water molecules, while the hydrophilic blocks tend to be attracted to water (4). When the concentration of these copolymers exceeds a certain level, known as the critical micelle concentration (CMC), they begin to form small aggregates like micelles or larger structures such as vesicles, bilayers, and liposomes (19). Micelles in particular, are very small aggregates, typically with a size of 10–100 nm, consisting of a hydrophobic core and a hydrophilic corona (131). This unique structure makes the micelles highly suitable for various biopharmaceutical and industrial applications (5; 7; 14; 30; 132; 133). In the cleaning industry, micelles are utilized as cleaning agents due to their ability to dissolve and remove dirt (134) in the food industry they are used for oil and protein extraction (30), while in wastewater treatment they have the ability to isolate and remove low concentration contaminants and toxic substances (135; 136). In the last few decades, micelles have gained significant importance in biopharmaceutical and medical applications, serving as vehicles for targeted drug delivery systems for both diagnostic and therapeutic purposes (137; 138; 139; 140; 141; 142; 143; 144; 145; 146). These systems are designed to prevent drug degradation, increase the bioavailability of drugs, and maximize the amount of drugs delivered to the targeted area of interest, while minimizing any harm to neighboring healthy tissues. The hydrophobic core of the micelles is ideal for encapsulating hydrophobic drugs, while the hydrophilic corona acts as a stabilizer, preventing the drug from dissolving into water. Furthermore, micelles can be formed by block copolymers that are non-toxic and biocompatible, making them suitable for use in the human body (131).

Nonionic block copolymers, characterized by the absence of an electrical charge in their hydrophobic heads, are of particular interest among the various block copolymers available. They are less expensive to manufacture and more environmentally friendly materials (10; 147). One particularly interesting class includes blocks of PolyEthylene Oxide (PEO) and PolyPropylene Oxide (PPO). These nonionic block copolymers can be found in a range of molecular weights and PEO/PPO composition ratios. Triblock PEO/PPO copolymers are termed poloxamers but are also known by their trade name of Pluronics®. They have one central hydrophilic PPO block surrounded by two hydrophobic PEO blocks. When dissolved in water, they are able to form various types of micelles, such as spherical, cylindrical, or lamellar, depending mainly on the ratio between the hydrophobic and hydrophilic blocks (148). Due to their small size, micelles

formed by triblock copolymers have an improved ability to target specific areas, have a longer circulation time in the body, and can be easily produced for effective drug delivery (149). These types of block copolymers have been used in several drug delivery system studies and the most of them focus on the investigation of the encapsulation efficiency (EE) and loading content (LC) of the micelles in order to determine the effectiveness of drug encapsulation as well as the release timing. For example, Han et al. (150) have shown that paclitaxel (PTX)-loaded polymeric micelles formed by Pluronic P123 block copolymers can effectively increase the bloodstream residence time of the drug and change the way the drug is distributed in the body, thus improving its targeting capability. Additionally, Kabanov's team has extensively studied the use of Pluronic micelles as drug delivery systems for gene therapy and cancer treatment. Their research focuses on overcoming resistance mechanisms of the drugs to the tumors and improving the effectiveness of treatment (149; 151; 152; 153; 154). Nevertheless, these surfactants have a high threshold for forming micelles and tend to be less stable. One way to address this issue is to dissolve multiple types of surfactants in the solution, resulting in the formation of mixed micelles.

Contrary to single-component micelles, mixed micelles made up of different types of block copolymers have demonstrated greater potential in terms of their drug loading capacity, lower critical micelle concentration (CMC) values, kinetic stability, better control over the release timing, improved cellular targeting, and enhanced bioavailability (155). For example, Akbar et al.'s (156) studies on the encapsulation of curcumin in micelles made of single component and in mixed micelles have shown that the formation of mixed polymeric micelles increases the stability and solubility of curcumin, when compared to micelles made of a single component. This may lead to an improvement in the bioavailability and efficacy of the drug.

A significant amount of research has been dedicated to examining the thermodynamic properties of mixed micelle systems in equilibrium, with much of the focus being on determining the critical micelle concentration (CMC), the aggregation number (AN) and the size distribution of the aggregates. CMC can be determined by a variety of methods including surface tension measurements (157; 158; 159; 160), chromatography (161; 162), light scattering (163; 164; 165), small angle neutron scattering (SANS) etc. (166). Furthermore, the size and structure of the micelles can be determined by techniques such as dynamic light scattering (167) and transmission electron microscopy (162). Drug encapsulation efficiency (EE) and loading content (LC) of the micelles were evaluated by high-performance liquid chromatography (161; 162), while drug-polymer interaction, can be investigated through Fourier-transform infrared spectroscopy (156).

Additionally, computer simulations can be used to investigate the formation of mixed

micelle systems, as they are a valuable tool to save time, compare with experimental data and gain a deeper understanding of the behavior of these systems. Atomistic and coarse-grained models can be employed to study the formation of polymeric micelles, including Monte Carlo simulations, Molecular dynamics, Brownian dynamics, Dissipative Particle Dynamics (DPD) etc. However, atomistic simulations are typically be limited to only relatively short time scales. To overcome this limitation, coarse-grained simulation models are often used. For example, Dissipative Particle Dynamics (DPD) which is a stochastic method that takes into account random forces acting on each particle, has been extensively used to study mixed micelles (168; 169; 170; 171; 172; 173; 174). For instance, Prhashanna et al (172) conducted a study on four binary mixtures of Pluronics in aqueous solution. They observed that both pure and mixed micelles coexist in all cases. However, the fraction of shorter Pluronics involved in mixed micelles was found to be lower in the F127/L64 system compared to other systems studied, due to L64's higher CMC and shorter block length. When the two Pluronics have similar concentrations, the proportion of mixed micelles can be increased. Additionally, the shorter chains were discovered to be situated closer to the center of the micelle. According to Kacar et. al studies (171), on the ibuprofen encapsulation of micelles made of L64 surfactant pluronics, the hydrophobic part of the micelles, mainly contains the drug molecules, but a small amount is also present in the hydrophilic corona. The micelle size as well as the number of L64 chains decrease as ibuprofen is incorporated. In addition, his analysis of radial distribution functions reveals that drug-free micelles have a higher concentration of water beads, while drug-containing micelles have a more compact arrangement of beads in both the hydrophobic and hydrophilic regions.

Recently, simulation methods based on Mean field theories, such as the self-consistent field (SCF) and Single Chain Mean Field (SCMF), have gained attention for their ability to predict the properties of surfactant systems (1; 81; 126; 175; 176; 177; 178). These methods have proven to be effective for studies of micellar self-assembly because they simplify the many-body problem to a one-body one, greatly reducing computational time.

In our study, we use the Single Chain Mean field theory for binary systems to investigate the equilibrium thermodynamic properties of mixed micelles consisting of two different kinds of poloxamers (Pluronics®).

4.2 | Single-Chain Mean-Field theory

The SCMF theory simplifies the analysis of complex systems consisting of many interacting molecules by reducing the problem to the study of a single representative central chain with a set of conformations $\{\alpha\}$. This central chain interacts with the surrounding molecules through a mean field approximation, which is used to determine the most likely conformations of the molecule based on the probabilities of individual conformations. The properties of the representative molecule are determined by solving a set of nonlinear equations, which take into account the probabilities of individual conformations and the mean field. These equations, defined by the self-consistent closure of the model, allow for the calculation of all equilibrium properties when solved. The methodology for SCMF simulation has already been fully detailed in previous publications (1; 81; 175; 176).

In this study, the SCMF theory is applied in a modified version that accounts for the existence of a second surfactant in the system. The objective is to determine the thermodynamic equilibrium properties of the mixed micelle system and compare them with the properties of single-component micelles from previous studies as well as experimental and theoretical works.

4.2.1 | Single-Chain Mean-Field Theory for Binary Systems

his theory considers two single central chains with sets of conformations $\{\alpha\}$, $\{\beta\}$ respectively representing the two different kinds of surfactants, in order to study their interactions with the system (solvent and other surfactants). Specifically, these interactions refer to the a) Intramolecular interactions, which are determined precisely, and to the b) Intermolecular interactions with the solvent and the remaining surfactant chains. The intermolecular interactions are calculated through the averages of the molecular fields, and they are determined by the probability distribution functions of the chains conformations, P[α], P[β] respectively and the distribution of the solvent molecules, through the minimization of the aggregate's total free energy.

$$F = \langle E \rangle - T\langle S \rangle. \tag{4.1}$$

This theory assumes that the entire available space is occupied by surfactants of species A, surfactants of species B and solvent molecules. This can be expressed in terms of the incompressibility condition

$$\phi_s(\mathbf{r}) + N_A\langle \phi(\mathbf{r}, \alpha) \rangle + N_B\langle \phi(\mathbf{r}, \beta) \rangle = 1, \tag{4.2}$$

where $\phi_s(\mathbf{r})$ represents the volume fraction of solvent molecules, and $\langle\phi(\mathbf{r},\alpha)\rangle$, $\langle\phi(\mathbf{r},\beta)\rangle$ represent the volume fractions of surfactants A and B, respectively.

The internal energy (eq. (4.3)) is calculated taking into account the intramolecular interactions and the intramolecular interactions of the chain with the solvent and the remaining chain molecules, which are given in terms of the solvent concentration ($c_s(\mathbf{r})$) and the average chains concentrations $\langle c(\mathbf{r})\rangle_A = \int d\alpha P[\alpha] c(\alpha,\mathbf{r})$, $\langle c(\mathbf{r})\rangle_B = \int d\beta P[\beta] c(\beta,\mathbf{r})$ together with their corresponding available volume.

$$< E >= N_A \int d\alpha P[\alpha](U_{intra}(\alpha) + U_{inter}(\alpha)) + N_B \int d\beta P[\beta](U_{intra}(\beta) + U_{inter}(\beta)). \tag{4.3}$$

The entropy is computed as the sum of the conformational entropy of chains A and B, and the translational entropy of the solvent molecules.

$$< S >= -k_B \left[(N_A \int d\alpha P(\alpha) lnP(\alpha) + N_B \int d\beta P(\beta) lnP(\beta) + \int d\mathbf{r} c_s(\mathbf{r}) ln\phi_s(\mathbf{r}) \right]. \tag{4.4}$$

By minimizing the free energy subject to P[α], P[β], and $c_s(\mathbf{r})$ and by considering the Lagrange multipliers $\pi(\mathbf{r})$, we can calculate any thermodynamic property of the system.

$$P(\alpha) = \frac{1}{Q_A} e^{\frac{-H(\alpha)}{kT}}, \tag{4.5}$$

$$P(\beta) = \frac{1}{Q_B} e^{\frac{-H(\beta)}{kT}}, \tag{4.6}$$

$$\pi(\mathbf{r}) = -\frac{kT}{v_s} log\phi_s(\mathbf{r}). \tag{4.7}$$

The Hamiltonians, $H(\alpha)$ and $H(\beta)$, of the system are dependent on the coarse-grained model used. In this case, they can be formulated as follows.

$$\begin{aligned} H[\alpha] = U_{\text{intra}}(\alpha) &+ (N_A - 1)\epsilon_{\text{EO,PO}} \int d\mathbf{r} \left(\Phi_{\text{EO}}(\alpha,\mathbf{r})\langle c_{\text{PO}}(\mathbf{r})\rangle + \Phi_{\text{PO}}(\alpha,\mathbf{r})\langle c_{\text{EO}}(\mathbf{r})\rangle\right) \\ &+ \epsilon_{\text{EO},s} \int d\mathbf{r}\, \Phi_{\text{EO}}(\alpha,\mathbf{r}) c_{\text{s}}(\mathbf{r}) + \epsilon_{\text{PO},s} \int d\mathbf{r}\, \Phi_{\text{PO}}(\alpha,\mathbf{r}) c_{\text{s}}(\mathbf{r}) \\ &+ k_{\text{B}}T \int d\mathbf{r} \left(\frac{\log \phi_{\text{s}}(\mathbf{r})}{v_{\text{s}}} \left[\phi_{\text{EO}}(\alpha,\mathbf{r}) + \phi_{\text{PO}}(\alpha,\mathbf{r})\right] \right), \end{aligned} \tag{4.8}$$

and

$$H[\beta] = U_{\text{intra}}(\beta) + (N_B - 1)\epsilon_{\text{EO,PO}} \int d\mathbf{r}\, (\Phi_{\text{EO}}(\beta, \mathbf{r})\langle c_{\text{PO}}(\mathbf{r})\rangle + \Phi_{\text{PO}}(\beta, \mathbf{r})\langle c_{\text{EO}}(\mathbf{r})\rangle) + \epsilon_{\text{EO},s} \int d\mathbf{r}\, \Phi_{\text{EO}}(\beta, \mathbf{r}) c_{\text{s}}(\mathbf{r}) + \epsilon_{\text{PO},s} \int d\mathbf{r}\, \Phi_{\text{PO}}(\beta, \mathbf{r}) c_{\text{s}}(\mathbf{r}) + k_{\text{B}}T \int d\mathbf{r} \left(\frac{\log \phi_{\text{s}}(\mathbf{r})}{v_{\text{s}}} \left[\phi_{\text{EO}}(\beta, \mathbf{r}) + \phi_{\text{PO}}(\beta, \mathbf{r})\right] \right). \quad (4.9)$$

In order to connect the microscopic and macroscopic equilibrium quantities, we have extended the mass action model used in a previous work (1; 81; 176), by including a third component. The key point in this model is to consider the chemical potentials and the concentrations of the free and the aggregated surfactant (Figure 4.1). Namely,

$$\mu_1 = \mu_1^0 + kTlogX_1, \quad (4.10)$$

Where μ_1 is the chemical potential, μ_1^0 the standard chemical potential and X_1 the concentration, in mole fraction, of the surfactants in the bulk solution.

For surfactants in aggregates of size N, the chemical potential takes the following form

$$\mu_N = \mu_N^0 + \frac{kT}{N} \log \frac{X_N}{N}, \quad (4.11)$$

where μ_N^0 is the standard chemical potential and X_N is the concentration, in mole fraction, of surfactant in micelles of size N.

If we take into account a second type of surfactant in the system, according to the thermodynamic equilibrium

$$\begin{aligned} \mu_1^A &= \mu_{N_A+N_B}^A, \\ \mu_1^B &= \mu_{N_A+N_B}^B, \end{aligned} \quad (4.12)$$

where μ_1^A, μ_1^B, $\mu_{N_A+N_B}^A$ and $\mu_{N_A+N_B}^B$ are the chemical potentials of A and B free and aggregated surfactants, respectively, and they are given by

$$\begin{aligned} \mu_1^A &= \mu_1^{0,A} + KTlnX_1^A, \\ \mu_1^B &= \mu_1^{0,B} + KTlnX_1^B, \end{aligned} \quad (4.13)$$

$$\begin{aligned} \mu_{N_A+N_B}^A &= \mu_{N_A+N_B}^{0,A} + \frac{kT}{N_A+N_B} \log \frac{X_{N_A+N_B}}{N_A+N_B}, \\ \mu_{N_A+N_B}^B &= \mu_{N_A+N_B}^{0,B} + \frac{kT}{N_A+N_B} \log \frac{X_{N_A+N_B}}{N_A+N_B}. \end{aligned} \quad (4.14)$$

The combination of eqs. (4.12), (4.13) and (4.14) yields

$$X_{N_A+N_B} = (X_1^A)^{N_A} \cdot (X_1^B)^{N_B} e^{-\frac{1}{KT}\left[N_A(\Delta\mu^{0,A})+N_B(\Delta\mu^{0,B})\right]}. \tag{4.15}$$

Eq. (4.15) represents the mass action model (MAM) for a binary system. Using this equation, we can determine the CMC (critical micelle concentration) and the mixed micelle size distribution based on the chemical potential differences displayed in the exponential term $e^{-\frac{1}{KT}\left[N_A(\Delta\mu^{0,A})+N_B(\Delta\mu^{0,B})\right]}$.

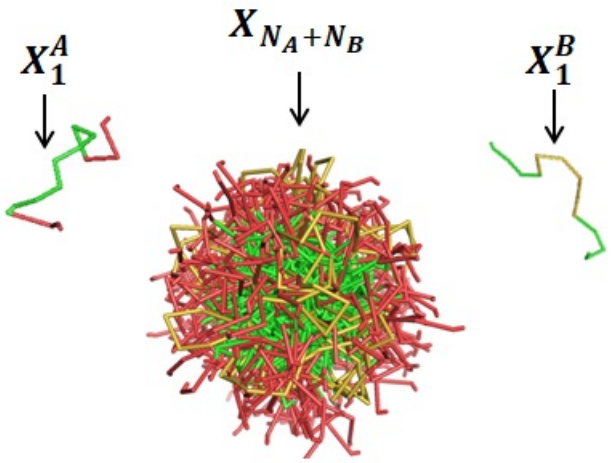

Figure 4.1: Schematic illustration of a mixed micelle consisting of A and B surfactant chains and free surfactants of species A and B in the solvent. The PO block for both chains is indicated by the color green whereas the EO block of chain A is in red and for chain B in yellow (please note that B is a reverse poloxamer).

The CMC can be determined by plotting the free surfactant concentrations of the sum of A (X_1^A) and B (X_1^B) against the total concentration of surfactants in the system, X_T, which is given by $\left((N_A + N_B)\left(\sum_{N_A}\sum_{N_B} X_{N_A+N_B}\right)\right)$, at a fixed ration of the total concentration of A $\left(X_A^T = \sum_{N_A} N_A(X_{N_A+X_B})\right)$ and B $\left(X_B^T = \sum_{N_B} N_B(X_{N_A+X_B})\right)$ surfactants in the system, represented by $R = X_B^T/X_A^T$. This ratio is held at a fixed value by manipulating the free surfactant A and B concentrations, where this careful manipulation of the free surfactant concentrations allows for the consistent and predictable behavior of the system.

From this plot, the CMC is defined as the point at which the concentration of free surfactants reaches saturation and only increases slowly. This means that any additional surfactant in the system will tend to join the micellar aggregates rather than remain free

in the bulk solution. This approach is taken because it enables us to compare the results with those obtained from experiments carried out previously.

To do so, the chemical potential differences need to be estimated. The chemical potential is related to the partition function according to the general form given by

$$Q = N\, e^{-\mu/kT}, \tag{4.16}$$

while the partition functions within the SCMF are given by

$$\begin{aligned} Q_A &= \int d\alpha e^{-H[\alpha]/kT}, \\ Q_B &= \int d\beta^{-H[\beta]/kT}, \end{aligned} \tag{4.17}$$

where $H[\alpha]$ and $H[\beta]$ are the Hamiltonians given by the eqs. (4.8), (4.9), respectively.

Since the aggregate is fixed by the mean-fields in the center of the simulation cell, whereas the free surfactants can appear anywhere in the cell, the translational contribution in the chemical potential has to be included only for the aggregate and the volume of the system appears in the final expression. Thus, combining the eqs. (4.16),(4.17) the differences in the chemical potentials of free and aggregated surfactants $\Delta\mu^{0,A}$, $\Delta\mu^{0,B}$, can be derived by

$$\begin{aligned} e^{-\left(\mu^{0,A}_{N_A+N_B}-\mu^{0,A}_1\right)} &= \frac{V}{N_A+N_B}\frac{\int d\alpha\cdot e^{-\frac{H^A_{N_A}[\alpha]}{KT}}}{\int d\alpha\cdot e^{-\frac{H^A_1[\alpha]}{KT}}}, \\ e^{-\left(\mu^{0,B}_{N_A+N_B}-\mu^{0,B}_1\right)} &= \frac{V}{N_A+N_B}\frac{\int d\beta\cdot e^{-\frac{H^B_{N_B}[\beta])}{KT}}}{\int d\beta\cdot e^{-\frac{H^B_1[\beta]}{KT}}}. \end{aligned} \tag{4.18}$$

4.2.2 | Coarse-grain Model

In this study we use coarse grain modeling to investigate the thermodynamic equilibrium properties for various mixed micelle systems. The initial step in SCMFT calculations is to establish a coarse-grained model of the molecule and its interactions with the mean-fields. To accomplish this, a series of coarse-grained models for Pluronics of varying lengths in water at a constant temperature of 37^oC were used. These models are linear chains made up of two types of beads with the same diameter σ. These beads represent the hydrophilic PEO group (CH_2CH_2O) and hydrophobic PPO group

$(CH_9CH_3)CH_2O)$ respectively. Figure 4.2a, illustrates a coarse-grained model of L44 surfactant, which has the form $PEO_{10} - PPO_{23} - PEO_{10}$ and contains 43 consecutive beads. Another example is the reversed Pluronic, represented by 10R5, which has the form $PPO_{11} - PEO_{16} - PPO_{11}$ and contains 38 consecutive beads, as shown in Figure 4.2b. The flexibility of the chain was taken into account by defining rigid segments of the Kuhn length, between which complete flexibility is allowed.

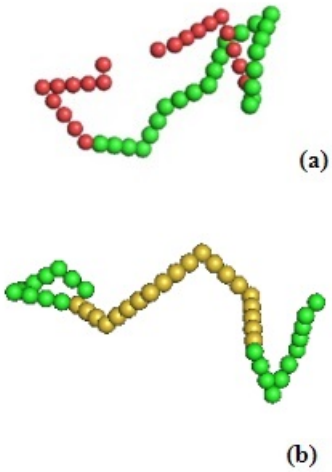

Figure 4.2: Coarse-Grained model for (a) Pluronic L44 $(PEO_{10} - PPO_{23} - PEO_{10})$ and (b) Reversed Pluronic 10R5 $(PPO_{11} - PEO_{16} - PPO_{11})$. Red beads represent the hydrophilic PEO group, and the green beads represent the hydrophobic PPO groups.

In this study, we aim to investigate the binary combination of various types of surfactants in water at 37^0C and to calculate properties related to the formation of mixed micelles, such as CMC, aggregation number, and size distribution. The selection of surfactants was based on their widespread usage and research in recent years in drug delivery systems, as well as the differences in the length of their hydrophobic blocks and their structural differences (Table 4.1). Specifically, the systems under study are the L64-F127, L64-L44 and L44-10R5. Specifically, the systems under study are the L64-F127, L64-L44 and L44-10R5. The first has two blocks which are very different in the length of both the hydrophobic PPO block and the hydrophilic PEO block, whereas in the second the two are relatively similar. The third system is characterized by the reverse nature of the exterior PPO block in the reverse pluronic 5R10 compared to the standard pluronics where the PPO block is central.

Polymer	MW	EO Blocks	PO Blocks	Total Blocks
10R5	1950	16	22	38
L44	2200	20	23	43
L64	2900	26	30	56
F127	12600	200	65	265

Table 4.1: Physical properties of triblock copolymers under study.

4.3 | Results and Discussion

4.3.1 | Standard Chemical Potential Calculations

Calculations of the free energy can give us a deeper understanding of mixed micelle formation. The minimization of the free energy drives the self-assembly of surfactant molecules into aggregates that provide the system with maximum stability when the concentration of surfactant in the solution is sufficiently high. The standard chemical potential differences defined in the last section are the key element in these free energies and any minimum provides information about the thermodynamic stability and aggregation number of the associated micelles. Namely, a lower chemical potential indicates a more stable system, which is generally associated with larger, more tightly packed micelles. On the other hand, a higher chemical potential corresponds to a less stable system, which is generally associated with smaller, less tightly packed micelles (179). A 3D plot can be used to visualize the standard chemical potential difference as a function of the aggregation numbers NA and NB, for each type of surfactant, allowing for identification of the most favorable surfactant aggregate numbers for any given mixed micelle system. However, this is only an approximation, as the entropic contributions also play a role, and the most likely aggregates may not be at the minimum although they are expected in general to be close. Figures 4.3, 4.4, 4.5, illustrate the minimum points of the standard chemical potential difference, with respect to the standard chemical potential of A and B (Figures (a), (b) respectively). Additionally, density maps can be used to provide a more detailed view of where the minimum points are located.

In the first system being studied (Figure 4.3), namely L44-L64, the minimum of the standard chemical potential differences of both surfactants suggests that the optimal mixed micelle will be composed of both L44 and L64 surfactants. With respect to the minimum L44 (Figure 4.3a) the optimal micelle would have approximately 45 L44 and 110 L64 surfactants, while for the L64 minimum (Figure 4.3b), the micelle would mainly consist of 155 L64 surfactant chains and a minor portion of 25 L44 surfactants. The depths of the minimums are quite similar, with L64 standard chemical potential differ-

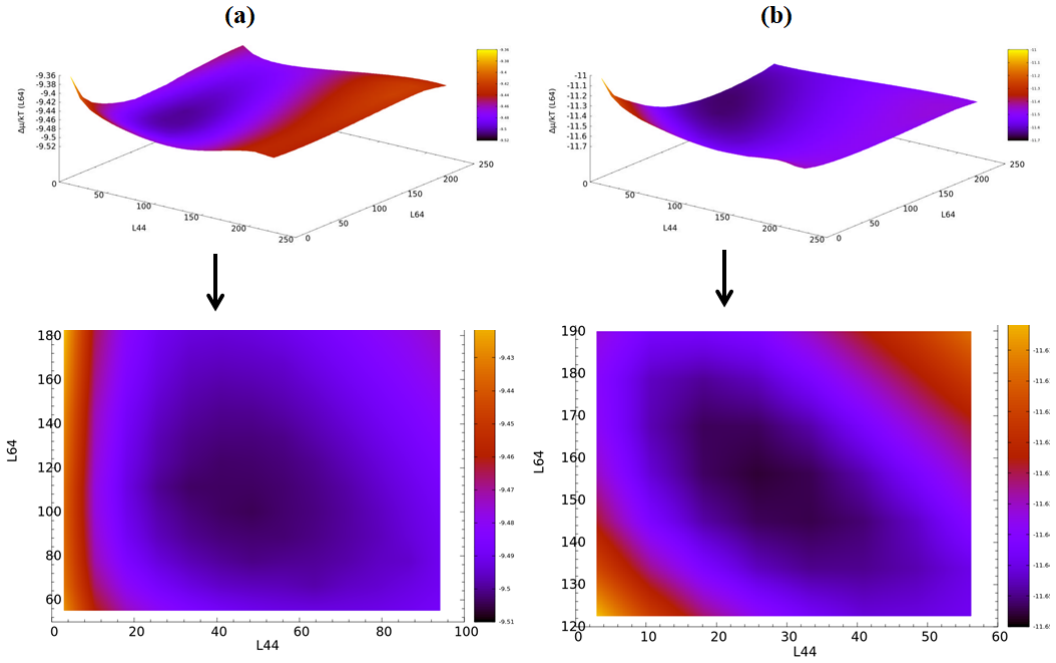

Figure 4.3: Above, a 3D visualization of the standard chemical potential differences of (a) L44 and (b) L64, surfactants compared to the micellar aggregation numbers. Below, a density map provides a closer view of the region where the minimum is located.

ence being slightly more negative, which is in line with the minimum standard chemical potential differences of pure L44 and L64 surfactants.

As demonstrated in Figure 4.4a, the preferred micelle aggregation number for the L64-F127 mixed surfactant system with respect to the standard chemical potential of L64 is $N_{L64} = 180$ and $N_{F127} = 20$, whereas based on the standard chemical potential of F127 (Figure 4.4b), it is $N_{L64} = 195$ and $N_{F127} = 10$. Unlike the L44-L64 system, the two minima are quite comparable in terms of aggregation numbers, with L64 being significantly larger than F127, and close to the aggregation number of pure L64 micelles, which is equal to 187 (1). However, the minimum standard chemical potential difference is significantly lower for the F127 surfactants compared to that of L64 surfactants, indicating that F127 surfactants can be expected to initially form micelles, which will then incorporate L64 surfactants later, finally resulting in a mixed L64-F127 micelle.

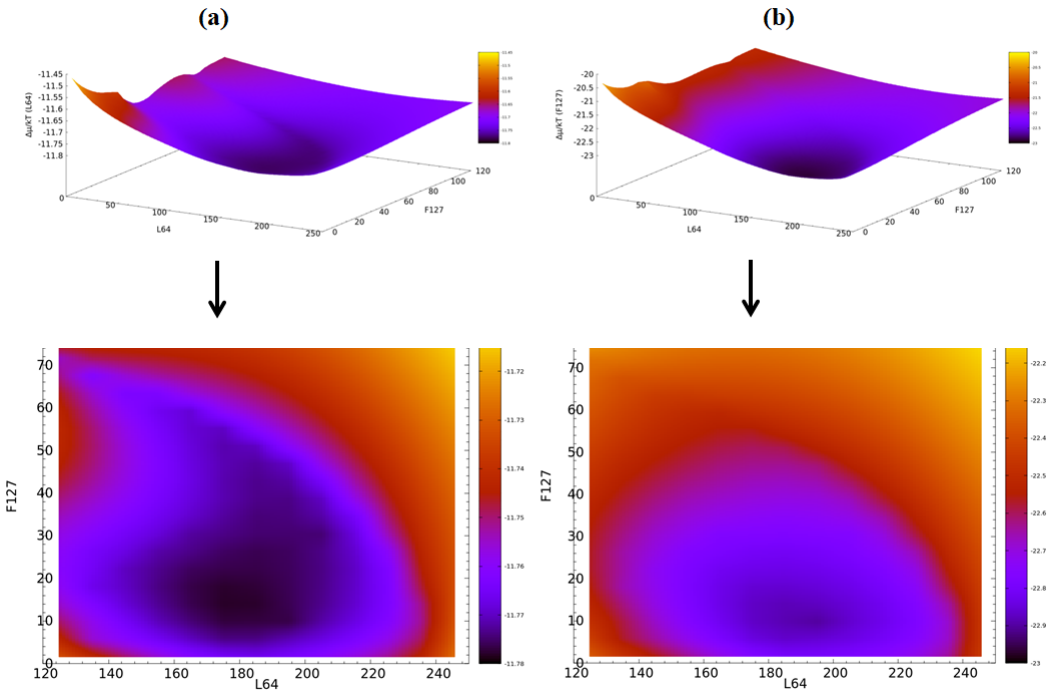

Figure 4.4: Above, a 3D visualization of the standard chemical potential differences of (a) L64 and (b) F127 surfactants compared to their aggregation numbers. Below, a density map provides a closer view of the region where the minimum is located.

Unlike the previous two cases, the minimum is not well defined and extends approximately linearly with the number of the two types of surfactants, indicating that the optimal mixed micelle will consist of both surfactants L44 and 10R5 as illustrated in Figure 4.5. However, it is noted that the minimum value is approximately the same for both surfactant cases, suggesting an equal likelihood of forming aggregates for both surfactants.

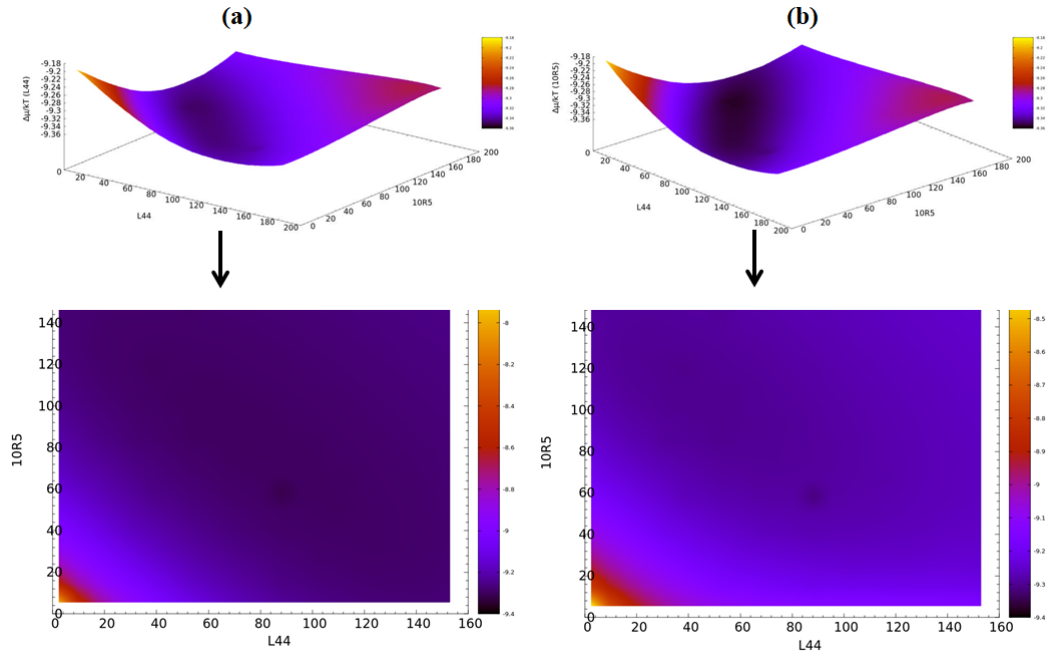

Figure 4.5: Above, a 3D visualization of the standard chemical potential differences of (a) L64 and (b) 10R5 surfactants compared to their aggregation numbers. Below, a density map provides a closer view of the region where the minimum is located.

4.3.2 | Volume Fraction Calculations

Once we have obtained the size of the aggregates at the minimum of the standard chemical potential, the analysis of the aggregates volume fraction profiles can provide valuable information about the structure of these micelles (Figure 4.6). Namely, the distribution of the heads and tails of both surfactants of the mixture and the solvent molecules as a function of the distance from the core of the micelle. The distance from the core of the micelles, r, is measured in units of σ, which as noted in the model details section is approximately equal to 0.5nm. Consequently, the volume fraction profiles can provide an estimate of the size of the resulting aggregates. The volume fraction profile's aggregation numbers were chosen in proximity to the standard chemical potential minimums observed in the previous plots (Figures 4.3, 4.4, 4.5). Specifically, for the L44-L64, L64-F127, and L44-10R5 systems, aggregation numbers of $N_{L44} = 20$ and $N_{L64} = 150$, $N_{L64} = 180$ and $N_{F127} = 20$, $N_{L44} = 90$ and $N_{10R5} = 80$ were selected, respectively.

As can be seen from Figure 4.6a for the L44-L64 binary mixture, at small distances from the micelle core center the tail volume fractions are close to a maximum value of 0.6 and 0.15 for L44 and L64, respectively, while the head volume fraction is close to

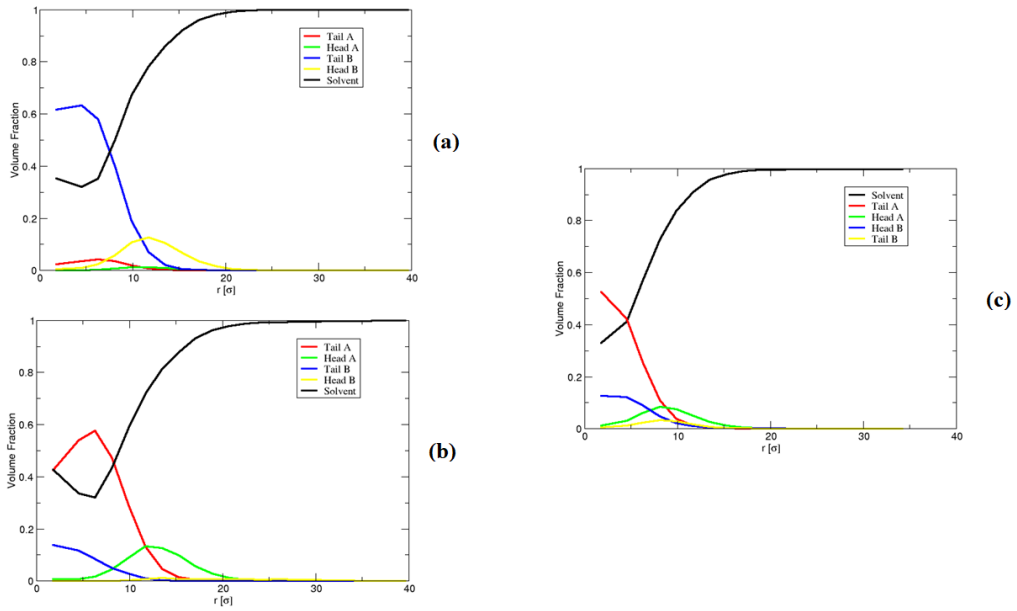

Figure 4.6: Aggregate volume fraction profiles (distribution of tails and heads of A and B surfactants and solvent molecules) versus the distance from the micellar core. (a) L44(A)-L64(B) for $N_{L44} = 20$ and $N_{L64} = 150$, (b) L64(A)-F127(B), for $N_{L64} = 180$ and $N_{F127} = 20$, (c) L44(A)-10R5(B), for $N_{L44} = 90$ and $N_{10R5} = 80$.

zero for both surfactants, and the solvent values are close to 0.38. This indicates that there is a high presence of tails in the core, but a low one of the head blocks. At medium distances the tail volume fractions of L44 and L64 decrease, while the head A and B and solvent volume fractions increase. This indicates the limit of the core and the beginning of the corona. At larger distances, head and tail volume fractions of both surfactants fall to their bulk value while the solvent volume fraction reaches its highest value close to 1, indicating that at large distances from the center, mostly solvent molecules are present with only a minimal concentration of surfactants in water.

A similar behavior is observed for the L64-F127 binary mixture (Figure 4.6b), but with a slightly lower presence of surfactant A (L64) tails in the center of the micelle with a total volume fraction equal to 0.4 that increases with the distance from the center until reaching a value of about 0.6, then begins to decrease following the pattern seen in the previous system. This can be explained by the relatively large size of these micelles which makes it difficult for the shorter L64 copolymers to be able to access the central core volumes unless they assume unfavorably stretched configurations.

For the L44-10R5 binary mixture, we observe a high head volume fraction of the reverse surfactant in the center together with a high concentration of L44 tails while

at intermediate distances 10R5 tail and L44 head concentrations are high. Beyond the core of the micelle, the head and tail volume fractions of both surfactants approach zero. (Figure 4.6c). This observation aligns with the previous systems and confirms the hydrophobicity of the micelle core and the hydrophilicity of its corona.

Concerning the size of the resulting micelles, the core diameter of the micelles can be identified as the intersection between the distribution of heads and tails, while the micelle diameter is estimated at the point where the head distribution is close to zero. It is observed that the mixed micelles composed of different surfactants species differ in their core and overall sizes indicating that each system possesses a distinct structure that may render it appropriate for specific applications. The L64-F127 mixed micelle forms the largest micelle since it has a large core size of about 26σ (13nm) and an overall size of 40σ (20nm). This may result in the solubilization of larger hydrophobic molecules, as well as increased stability due to the larger corona size. The L44-L64 mixed micelle on the other hand, has a slightly smaller core size of 24σ (12nm) and an overall size of 36σ (18nm). Finally, the L44-10R5 micelle has a core size of approximately 16σ (8nm), which is even smaller than that of the L44-L64 mixed micelle, and the overall size is at around 28σ (14nm). This may result in a similar solubilization capacity as the L44-L64 mixed micelle, but due to their overall small size they could be advantageous for transporting drugs to locations with tight access, such as the brain.

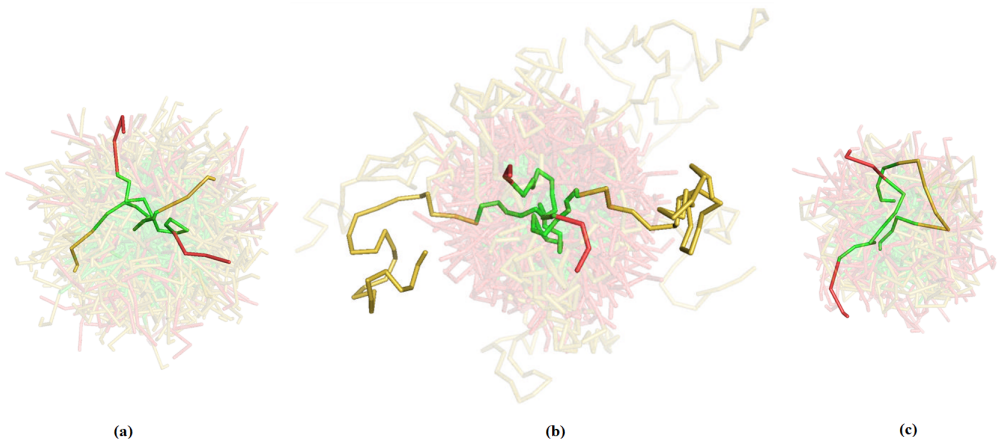

Figure 4.7: Schematic illustration of the minimum chemical potential aggregate with the most probable surfactant conformations (highlighted) (a) L44(green-red) and L64(green-yellow), (b) L64(green-red) and F127(green-yellow), (c) L44(green-red) and 10R5(green-yellow).

Figure 4.7a, 4.7b, 4.7c, present schematic illustrations of micelles composed of L44-L64, L64-F127 and L44-10R5, respectively, while they correspond to the same aggrega-

tion numbers that were employed in the volume fraction profiles. These illustrations are constructed by utilizing the most likely configurations of the block copolymer surfactants (highlighted) and the following most likely configurations until the aggregation number of the most likely aggregate size is reached(shaded).

In Figure 4.8, the cross-section of mixed micelles consisting of different surfactant types is presented. Specifically, Figures 4.8a, 4.8b, and 4.8c correspond to mixed micelles made of L44-L64, L64-F127, and L44-10R5, respectively. The distinct colors in the figures represent the variation in hydrophobicity of the surfactant blocks, with green indicating a hydrophobic character and yellow and red representing a hydrophilic character. The cross-sections reveal the internal organization of the mixed micelles, with the hydrophobic blocks of both surfactants forming a core surrounded by a shell of the hydrophilic blocks.

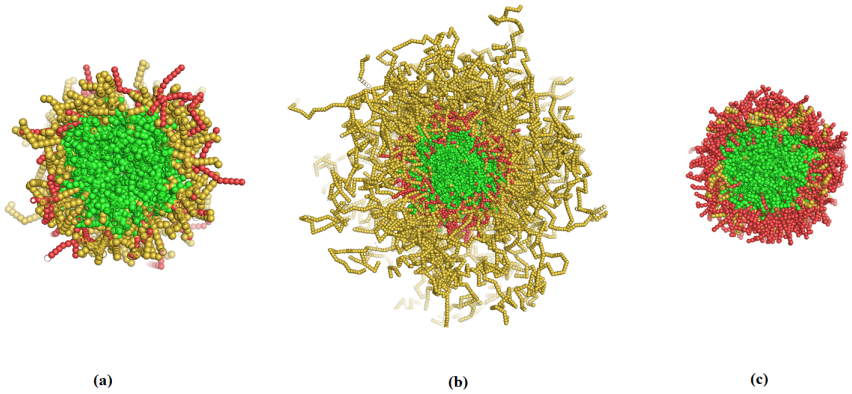

Figure 4.8: Cross-sectional view of large mixed micelles comprising various surfactant combinations, including (a) L44-L64 composed of $N_{L44} = 150$ and $N_{L64} = 200$, (b) L64-F127 composed of $N_{L64} = 200$ and $N_{F127} = 150$, and (c) L44-10R5 composed of $N_{L44} = 200$ and $N_{10R5} = 200$. The distinct colors represent the different surfactant block hydrophilicities. Green represents the hydrophobic blocks, red and yellow represents the hydrophilic blocks.

4.3.3 | CMC Calculations

As mentioned in the methodology section, the CMC is defined as the saturation point at which the concentration of the free surfactants no longer significantly increases with the increase of the total surfactant concentration of the system. At this saturation point, micelles start to form and the additional surfactants in the system prefer to aggregate rather than remain free in the bulk solution. The point of saturation is identified as the total concentration of free surfactants A and B, where the line of unit slope passing through the origin $(x = y)$ diverges from the line representing the concentration of free surfactant chains $(X_1^A + X_1^B)$ against the total surfactant concentration in the system (X_T) at a fixed ratio of the total concentration of A and B surfactants in the system, R_c (Figure 30).

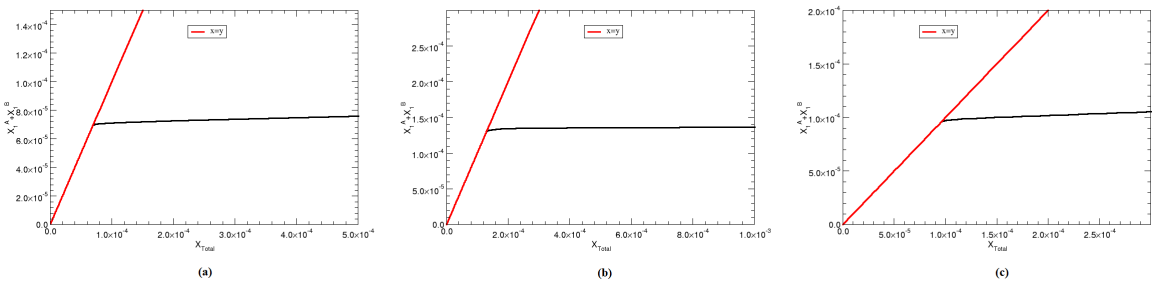

Figure 4.9: Concentrations of free surfactants (X1A+X1B) with the total concentration of surfactants for different rations of total L44 and 10R5 surfactants.

Pluronics	CMC_{Sim} (Mole fraction)	CMC_{Sim} (mol/L)	CMC_{Exp} (mol/L)
L44	$7.7 \cdot 10^{-5}$	$4.0 \cdot 10^{-3}$	$3.6 \cdot 10^{-3}$
10R5	-	-	-
L64	$6.5 \cdot 10^{-6}$	$3.7 \cdot 10^{-4}$	$4.8 \cdot 10^{-4}$
F127	$2.1 \cdot 10^{-9}$	$1.3 \cdot 10^{-7}$	$2.8 \cdot 10^{-7}$

Table 4.2: CMC calculations for pure Pluronics (1), compared with experimental data (2).

The ratios under examination differed between the systems and were chosen with respect to a critical value given by the ratio between the CMCs of the pure B and A micelles $(Rc = CMC_B/CMC_A)$. For each system, three different ratios, denoted as R_1, R_2, and R_3, were examined to be in the vicinity of the critical ratio. Namely, for the L44-L64 system, the critical ratio is $R_c = 8 \cdot 10^{-2}$ and the ratios selected were $R_1 = 1 \cdot 10^{-3}$,

$R_2 = 1.0$, and $R_3 = 10.0$. For the L64-F127 system, $R_c = 3 \cdot 10^{-4}$, and the selected ratios were $R_1 = 1 \cdot 10^{-6}$, $R_2 = 1 \cdot 10^{-4}$, and $R_3 = 1 \cdot 10^{-2}$. And for the L44-10R5 system where it is not possible to define an R_c ratio since there is no CMC found for the pure system of the reverse pluronic, the ratios studied were $R_1 = 1 \cdot 10^{-2}$, $R_2 = 1.0$, and $R_3 = 5.0$. Pure and mixed micelles CMCs can be seen in Tables 4.2, 4.3 respectively, together with the experimental values when available.

Mixture	CMC_{Sim} (Mole fraction)	CMC_{Sim} (mol/L)	CMC_{Exp} (mol/L)
L44-L64			
$R_1 = 1 \cdot 10^{-3}$	$7.3 \cdot 10^{-5}$	$3.9 \cdot 10^{-3}$	-
$R_2 = 1.0$	$7.1 \cdot 10^{-5}$	$3.8 \cdot 10^{-3}$	-
$R_3 = 10.0$	$7.8 \cdot 10^{-6}$	$4.3 \cdot 10^{-4}$	-
L64-F127			
$R_1 = 1 \cdot 10^{-6}$	$7.8 \cdot 10^{-6}$	$4.3 \cdot 10^{-4}$	-
$R_2 = 1 \cdot 10^{-4}$	$5.0 \cdot 10^{-6}$	$2.7 \cdot 10^{-4}$	-
$R_3 = 1 \cdot 10^{-2}$	$3.0 \cdot 10^{-8}$	$1.7 \cdot 10^{-6}$	-
L44-10R5			
$R_1 = 1 \cdot 10^{-2}$	$7.1 \cdot 10^{-5}$	$3.0 \cdot 10^{-3}$	-
$R_2 = 1.0$	$1.4 \cdot 10^{-4}$	$7.5 \cdot 10^{-3}$	$5.0 \cdot 10^{-2*}$
$R_3 = 5.0$	$9.6 \cdot 10^{-5}$	$5.2 \cdot 10^{-3}$	-

Table 4.3: CMC calculations for mixed Pluronics for three different ratios, compared with experimental values (3), when available.

4.3.4 | Size Distribution Calculations

In order to gain further insight, we calculated the size distribution of the mixed micelles on changing the ratios of the total concentrations of surfactants of species A and B. This allows us to understand how variations in the relative concentrations of the two surfactant species affect the micelle formation and size distribution. By analyzing these results in combination with the information obtained from the 3D chemical potential difference maps, we can gain a more complete understanding of the mechanisms of mixed micelle formation and the role of surfactant interactions in these systems. This approach can help us to compare the SCMF simulation results with the experimental

data, when available, and to identify the optimal ratio of surfactant species for achieving a desired micelle size and structure.

The size distribution calculations of the mixed micelles were determined using the equation derived from the mass action model presented earlier in the introduction, Eq. 4.15. This equation takes into account the standard chemical potential differences of surfactants A and B, as well as their free concentrations within the system. The selected free surfactant concentrations X_1^B and X_1^A were based on the critical micelle concentration (CMC) calculations, so to study how the micelle size distribution changes at concentrations below, equal to, and above the CMC. Figures 4.10, 4.11, and 4.12 show the size distribution of the mixed micelles in three dimensions for the different ratios of R for the L44-L64, L64-F127 and L44-10R5 systems respectively, for concentrations of free surfactants below and above the CMC. The peaks in the plot correspond to the preferred aggregation numbers depending on the total concentration of the free surfactants A and B in the system. Aggregation Numbers of pure and mixed micelles can be seen in Tables 4.4, 4.5.

Table 4.4: Aggregation Number calculations for pure Pluronics, compared with experimental data.

Pluronics	CMC_{Sim} (Mole fraction)	CMC_{Sim} (mol/L)
L44	145[a]	-
10R5	-	-
L64	187[b]	37[c]
F127	120[b]	145[d]

[a] Pure equilibrium L44 results are shown in Appendix B (Table B.1. [b] Simulation results taken from (1). Experimental results taken from [c] (180) [d] (166).

As can be seen in Figure 4.10c, for higher concentrations of L64 surfactants in the system ($R_3 = 10$), only micelles composed of this type of surfactant are formed with an aggregation number close to the one for pure L64 micelles. The mixed micelles grow in size on increasing the total surfactant concentration in an analogue way to micellar systems with only one surfactant. For equal concentrations ($R_2 = 1$) of free L64 and L44 surfactants, L64 aggregates originally form while above the CMC mixed micelles containing both L64 and L44 surfactants appear. At higher L44 surfactant concentrations ($R = 1 \cdot 10^{-3}$), aggregates made of L64 form at first, but as the concentration of both surfactants increases, aggregates composed mostly of L44 with a small amount of L64 form. It is also observed, for concentrations very close to the CMC the coexistence of two different types of micelles, a mixed micelle composed of L44 and L64 surfactant chains and an almost pure L44 micelle. Once the concentration surpasses the critical

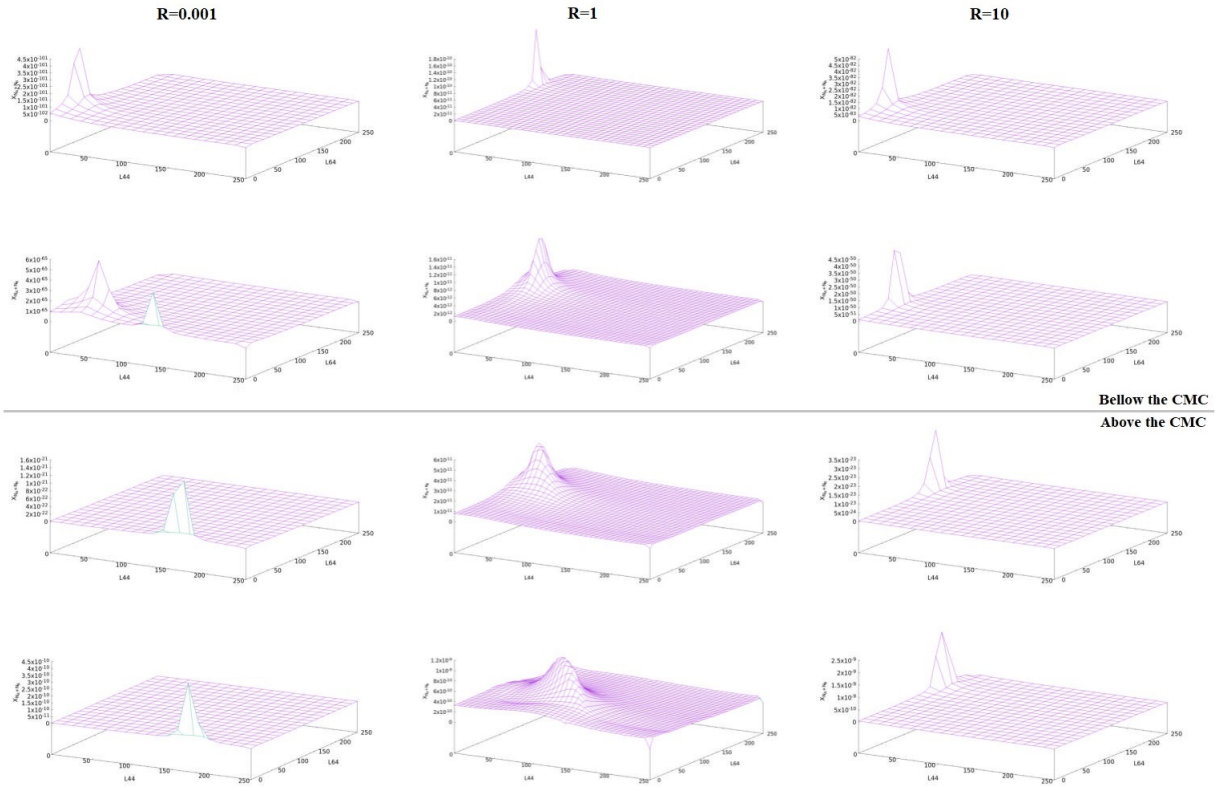

Figure 4.10: Aggregate size distribution plots with varying ratios, R, of total L44 and L64 surfactants below and above the CMC.

micelle concentration, only micelles consisting mainly of L44 surfactants appear with an aggregation number slightly larger than micelles made of pure L44 surfactants (Table 4.5).

Figure 4.11 displays size distribution plots for the L64-F127 binary system. At low F127 concentrations ($R_1 = 1 \cdot 10^{-6}$), micelles appear to be nearly pure L64, and an increase in the concentration of free surfactants leads to the formation of larger aggregates. Similar behavior is observed for a ration close to the critical ratio ($R_2 = 1 \cdot 10^{-4}$), but in this case the aggregates are almost pure with a small F127 surfactant contribution. When the ratio is even larger ($R_3 = 1 \cdot 10^{-2}$), mixed aggregates containing both surfactants are present, with a higher aggregation number for F127. However, when the concentration exceeds the CMC, L64 micelles with fewer F127 chains are formed. At higher F127 concentrations ($R_3 = 1$), mixed micelles mainly composed of L64 block copolymers exist, with only a small proportion of the more soluble F127 chains. This pattern aligns with previous experimental findings, where the analysis of micelle size, temperature dependence of scattering intensity, and heating indicated that F127 chains

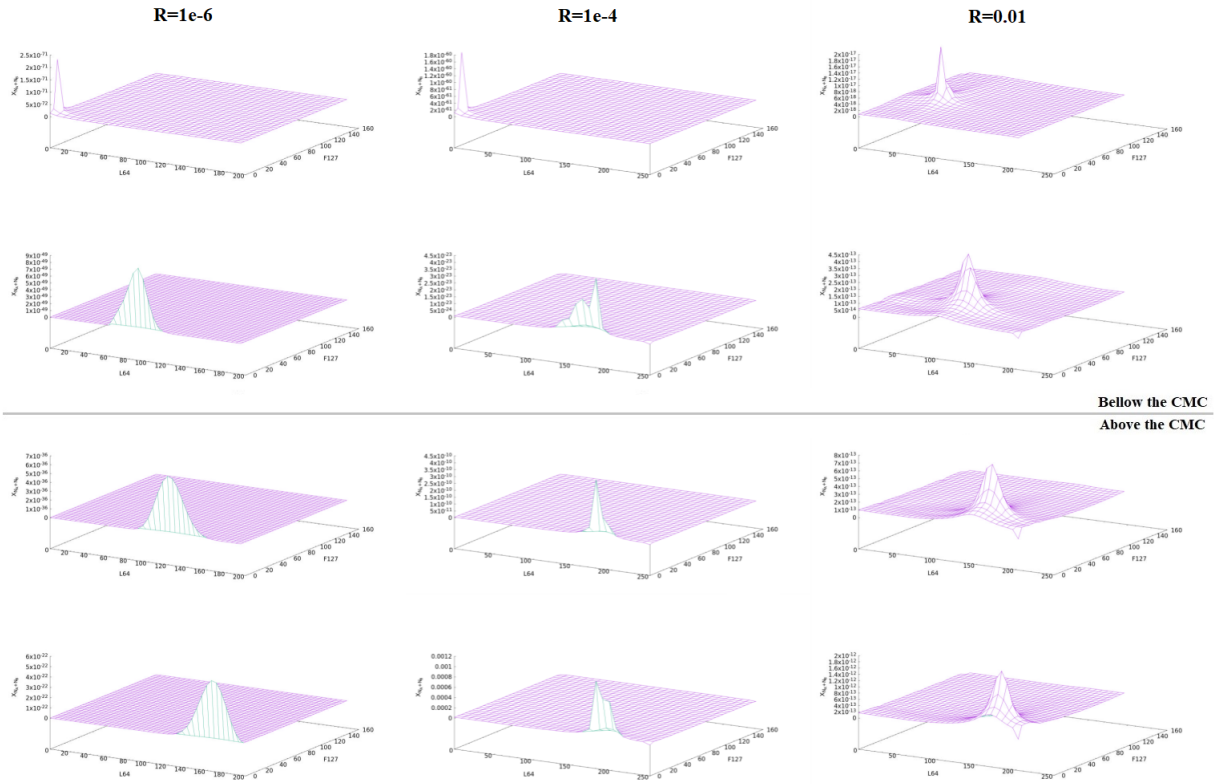

Figure 4.11: Aggregate size distribution plots with varying ratios R of L64 and F127 surfactants below and above the CMC.

formed micelles first, followed by the incorporation of L64 into existing F127 micelles at elevated temperatures (181).

Finally, the results for the L44-10R5 system are given in Figure 4.12. It can be observed that when the concentration of free L44 surfactants is higher than 10R5 free surfactant concentration, $R_1 = 1 \cdot 10^{-2}$, L44 aggregates are formed with only a minor amount of the reverse surfactant present. This behavior is reminiscent of pure L44 micellar systems. However, when $R_2 = 1$, micelles made of both surfactants are formed, as can be expected from an inspection of the standard chemical potential differences plot, Figure 4.5. When the concentration of 10R5 surfactants is high $(R_3 = 10)$, micelles composed of reverse pluronics are mostly formed with only a small contribution from L44 surfactants. This is particularly noteworthy as our previous SCMF calculations for pure surfactant systems showed that systems with only 10R5 surfactants do not form micelles. This result is in line with previous experiment studies, where the formation of mixed micelles consisting of both L44 and 10R5 surfactants was observed at 37°C, but no micellization was seen for 10R5 surfactants alone (3).

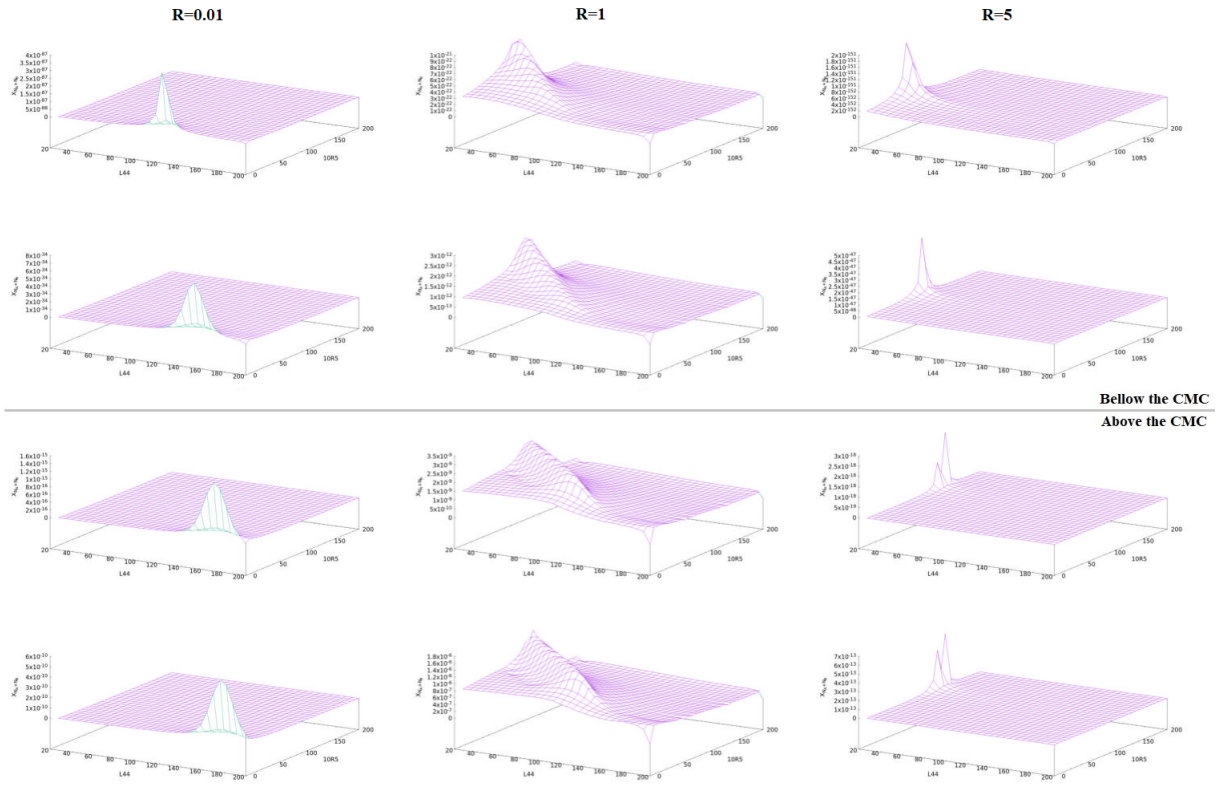

Figure 4.12: Aggregate size distribution plots with varying ratios R of L44 and 10R5 surfactants below and above the CMC.

In agreement with previous experiments (182; 183), it is observed that when L44 is added to L64 pure pluronic micelles to form a L64-L44 binary mixture, the CMC of the mixed micelles exhibits, an intermediate value between that of the pure L64 and L44 micelles. Similarly, in L64-F127 binary mixtures, the addition of F127 surfactants reduces the CMC of the pure L64 pluronic micelles, with the CMC of the mixed micelles exhibiting a value between that of the pure micelles. Finally, for the L44-10R5 system micelles are found unlike pure 10R5 systems and a CMC of 0.0052 mol/L is found when R=5. (Table 4.3)

In the article by Borovinskii et al. (184), five regimes were defined for a copolymer solution in which two types of polymer chains, A-B and C-B, are present. In their study, they use diblock copolymers where the C and A blocks are hydrophobic and only different in terms of length, N, of the block where the C block is longer than the A block (NC>NA). The head block, B, is identical for both polymers and much longer than the tail blocks (NB»NA). In our work we use triblock copolymers with different head and tail block lengths to model the commercially available pluronics used experimentally.

Binary Mixture	N_A	N_B	Total Aggregation Number
L44-L64			
$R_1 = 1 \cdot 10^{-3}$	170	2	172
$R_2 = 1.0$	25	120	145
$R_3 = 10.0$	2	150	152
L64-F127			
$R_1 = 1 \cdot 10^{-6}$	140	2	142
$R_2 = 1 \cdot 10^{-4}$	170	20	190
$R_3 = 1 \cdot 10^{-2}$	20	40	60
L44-10R5			
$R_1 = 1 \cdot 10^{-2}$	180	2	182
$R_2 = 1.0$	100	20	120
$R_3 = 5.0$	20	140	160

Table 4.5: The most probable aggregate size, denoted as the aggregation number, for each ratio of every binary mixture.

The different regimes are found on changing the concentrations of the two types of chain and their lengths. Regime I is characterized by low polymer volume fractions and all the chains are dissolved in solution (unimers) with no aggregates forming. Regime II is characterized by the formation of "pure" micelles of the C-B chains and the presence of unimers of short A-B chains. In Regime III, short A-B chains are included in the mixed micelles. Regime IV is characterized by the coexistence of comicelles and micelles of only short A-B chains. Regime V is characterized by the formation of comicelles of approximately equal size and composition of the two types of chains. In line with the findings of Borovinskii et al (184), our analysis supports the concept of the formation of micelles as concentration increases and the identification of distinct regimes of behavior. Specifically, we observed regimes I, II, III, IV and V where at initial stages only free surfactants are observed and as the concentration increases, micelles composed of shorter surfactants were predominant. Subsequently, shorter chains aggregated to form mixed micelles consisting of both A and B surfactants. Finally, in some cases (L44-L64, R=0.01), the coexistence of comicelles and micelles is observed.

4.4 | Conclusions

The SCMF theory, developed her for binary mixtures, was applied to examine the equilibrium properties of two distinct surfactants, A and B, in water at a temperature of 37^0C. The selection of the surfactant pairs was made carefully to take into account, not only the difference in length between the blocks of surfactants A and B (such as in the case of L44-L64 or L64-F127), but also the reversibility of the block structures (as demonstrated in the L44-10R5 mixture). The availability of experimental data was also a key factor in the selection of the binary systems.

The standard chemical potential differences play a crucial role in determining the thermodynamic stability of mixed micelles in surfactant systems and provide an approximation of the expected most favorable aggregation number. Micelle volume fraction profiles are also an important aspect in the development of various applications such as drug delivery systems, because they provide information about the size and shape of the aggregate. In our analysis, assuming a spherical geometry, volume fraction profiles showed that micelles of specific aggregation number contain a hydrophobic core surrounded by a hydrophilic corona while differing in sizes depending on the mixed system under study. Depending on specific applications, it may be necessary to be able to control the size of both core and corona. In our case, it is possible to see the trivial result that longer block lengths make larger cores and coronas, but also affect the stability of the associated micelles. If both size and stability need to be tuned, then mixed micelles may be required.

The critical micelle concentration (CMC), aggregation number, and size distributions were calculated by adjusting the ratio between the total concentration of surfactants A and B in the system. The ratios under study were selected based on a critical ratio defined by the CMCs of the individual pure A and B surfactants, with the goal of comparing with existing experimental data. Our findings reveal that the formation of micelles depends greatly on this ratio, meaning that either pure micelles of surfactant A or B, or mixed micelles composed of both species can be formed, depending on the concentration of total A and B surfactants. Namely, if this ratio exceeds the critical ratio, then almost pure micelles of one of the surfactant type form, while for ratios near the critical, mixed micelles composed of both species appear. However, in the case of L64-F127, L64 micelles seem to be more likely to form, even with a large amount of F127 surfactants in the system. It is also noted that the CMC of the mixed micelles for all the systems under study, was observed to be lower than that of the shorter surfactant and lies between the CMCs of the pure A and B surfactants. The results were compared to available experimental data and showed good agreement, which further supports the validity of the

findings.

In conclusion, this study highlights the importance of considering mixed surfactant systems in the development of many applications such as drug delivery systems. The SCMF theory provides a useful tool for examining the quantitative behavior of these systems and understanding how they can be optimized for maximum efficacy. The future study of the dynamic behavior of mixed micelles will be a crucial step in advancing the field of drug delivery, by providing insights into drug release rate, playing a key role in the development of more effective and safe drug delivery systems.

5

Conclusions & Future work

5.1 | Conclusions

The advancements in biomedicine and nanotechnology have opened up an array of new possibilities, one of which is the creation of nanostructures with unique properties. These fields have made remarkable strides, leading to innovative solutions and breakthroughs that are changing the way we live and perceive the world around us. The design of nanostructures has specifically revolutionized the way we think about materials and their characteristics, offering tremendous potential for a wide range of applications in areas such as healthcare, energy, and electronics. In order to bring these advancements to life, it is crucial to have predictive tools that can assess the ability of molecules in forming nanoscale superstructures and functionalities without relying on time-consuming and costly empirical research. This thesis focuses on exploring and controlling the mechanisms behind the formation and dynamic behavior of both pure micelles as well as the equilibrium behavior of mixed micelles of specific size and shape. Micelles form when surfactants aggregate under certain conditions, self-assembling into systems that are widely used across many industries.

Molecular simulation offers a quick and efficient way to explore complex molecular systems and can serve as a roadmap for essential experimental validation. Despite the extensive research that has been conducted in this field, utilizing both experimental and simulation techniques, there remain certain limitations that hinder a comprehensive understanding of the systems being studied. This thesis aims to address these limitations and offer another approach to explore these systems, proposing the usage of a combination of Monte Carlo molecular simulation and Single-Chain Mean Field Theory. In addition, a novel approach to studying the equilibrium properties of mixed micelles through Single-Chain Mean-Field for binary systems has been introduced. The study of mixed micelles is of great importance, as they have been found to be excellent candidates for various biopharmaceutical applications, such as drug delivery systems for therapeutic and diagnostic purposes. Despite this potential, there is a lack of research on mixed micelles, making further investigation in this area a priority.

This thesis is divided in two parts, the first part explores the dynamic behavior of micelles by the combination of the Monte Carlo simulations and the SCMF theory, with the introduction of the time correlation functions to study the Exit Dynamics of Block Copolymers from Micelles at Short and Long Time Scales. Results show that the exit of poloxamer copolymers from equilibrated micelles has revealed up to four distinct regimes, each with its own characteristic behavior. An initial fast reorganization, followed by a logarithmic intermediate regime, an exponential intermediate regime, and a final exponential decay, are all observed and analyzed using dynamic Single-Chain

Mean-Field theory simulations. Despite the commonly held belief that the logarithmic response is due to the polydispersity of the polymer samples, the simulations show that it can also arise from a degeneracy of energy states of the hydrophobic block in the micelle core, provided there are a sufficient number of conformational states available. This insight allows for a modified Eyring equation to be proposed, which is capable of reproducing the observed dynamic behavior and unifying results from different sources and systems. The results suggest that the short-time dynamic response of these systems has an entropic origin rather than being influenced by polydispersity, as previously believed.

The second section of this thesis delves into the examination of the equilibrium behavior of mixed micelles that are formed when the concentration of two different types of surfactants A and B surpass the Critical Micellar Concentration (CMC) in water at 37^0C, utilizing the Single-Chain Mean-Field method for binary systems. The study involves the evaluation of three pairs of surfactants by adjusting the ratio of the total concentration of A and B surfactants to three different values near a *critical* ratio defined by the ratio between the Critical Micellar Concentrations (CMCs) of pure A and B surfactants. Our research reveals that the formation of micelles is greatly influenced by this ratio, meaning that either pure micelles composed of surfactant A or B, or mixed micelles that contain both species, can be formed based on the concentration of total A and B surfactants and the ratio between them. Furthermore, the CMC of the mixed micelles was found to be lower than that of the shorter surfactant and falls between the CMCs of the pure A and B surfactants. The results were compared with existing experimental data, and a good match was observed, further validating the findings.

The Single-Chain Mean Field (SCMF) theory is a powerful tool for exploring the equilibrium and dynamic properties of pure and mixed micelles. This theoretical framework provides a simplified approach to understanding the interactions between individual surfactant chains within the micelle system. The level of details provided by this theory can give a clear connection between the molecular properties of a single surfactant chain and the properties of the final micelle solution through mean fields approximations, saving a large amount of computational time. The SCMF theory has been shown to be highly effective in modeling micelles, making it an essential tool for advancing our understanding of these systems and their potential applications in various industries, particularly in the field of biopharmaceuticals. However, while SCMF is a useful tool, it is limited by its mean-field approximation and does not account for all the complex interactions that occur in these systems. Specifically, the implicit solvent model used in the simulations is relatively simple and does not accurately include, for instance, the effects of temperature in water. However, this is common to most, if not all,

coarse grain models. As a result, the simulations may not accurately reflect the behavior of the system under more realistic conditions. To overcome these limitations, it would be valuable to develop a model that takes into account an explicit solvent. This would allow for a more comprehensive understanding of the behavior of block copolymers in micelles and help to advance the field of biomedicine and nanotechnology.

5.2 | Future Work

In the future, there are several exciting areas of research that could be explored in the field of pure and mixed micelles. One of the most interesting areas is the study of micelles under different conditions such as variations in temperature, pH, and solvents. This would provide a deeper understanding of how changes in the external environment affect the behavior of mixed micelles and could lead to the development of new applications for these systems. Another important area of future work is to investigate the dynamic behavior of mixed micelles. This could involve studies on the kinetics of micellization and the relationship between the aggregation number, size, and stability of mixed micelles. Understanding how these systems change over time will provide important information about the release of drugs. In the field of drug delivery, controlling the release rate of drugs is a critical aspect in ensuring efficacy and reducing side effects. By studying the dynamic behavior of mixed micelles, researchers will be able to determine how the release rate can be optimized for maximum efficacy. A third area of future work is to examine the equilibrium and dynamic properties of micelles made up of a pair of surfactants with different flexibilities. This could involve investigating the influence of the flexibility of the surfactant molecules on the stability and behavior of mixed micelles and could result in the development of new methods for controlling the size and shape of these systems. Another promising area of future research is to replace one of the surfactants with a hydrophobic drug molecule such as ibuprofen. This would allow researchers to study the encapsulation and release of drugs using micelles, which could have important implications for drug delivery applications. Finally, another way that could further increase the understanding of mixed micelles is by exploring the interaction between surfactants and drug molecules in a water-based system. By including three components in their experiments, two types of surfactants and a drug molecule, they would be able to examine the effects of these interactions on the stability and behavior of mixed micelles, which can then be compared with the characteristics of pure micelles as drug delivery vehicles. In conclusion, there is a wealth of exciting opportunities for future research in the field of pure and mixed micelles. From exploring the

effects of different conditions on mixed micelles to investigating the behavior of these systems with different types of surfactants and drugs, there is much to be discovered and many new applications to be developed.

UNIVERSITAT ROVIRA I VIRGILI
UNRAVELING THE DYNAMICS AND EQUILIBRIUM BEHAVIOR OF PURE AND MIXED MICELLES: INSIGHTS FROM MICROSCOPIC COARSE-GRAIN MODELING
Maria Pantelidou

A

Incompressibility Condition Calculations

In a system consisting of N surfactant chains surrounded by water molecules, the incompressibility condition is introduced as the assumption that the available volume is occupied either by solvent or surfactant chains. The system is arranged with concentric spherical shells of molecular fields, each with a radius "r" where the densities of surfactants and solvent are uniform within each shell but can change between different shells. The volume of "layer r", defined by two concentric spheres with radii r and $r + dr$ (Figure A.1), is occupied entirely by both surfactants and solvent molecules due to the incompressibility condition. This can be expressed through

$$\phi_s(\mathbf{r}) + \langle \phi(\mathbf{r}) \rangle_N = 1, \tag{A.1}$$

where $\phi_s(\mathbf{r})$ is the solvent volume fraction at $\mathbf{r}$. In the second term of the above equation, the brackets represent the ensemble average of the chain volume fraction $\phi(\mathbf{r})$.

The ensemble averages can be correlated to the probability distribution, $P[\alpha_1, \ldots, \alpha_N]$, of the N chains where α_i represents the conformation of surfactant i, and the total volume fraction, $\phi(\alpha_1, \ldots, \alpha_N; \mathbf{r})$, of the chains at layer r

$$\phi_s(\mathbf{r}) + \sum_{\{\alpha_1,\ldots,\alpha_N\}} P[\alpha_1, \ldots, \alpha_N] \phi(\alpha_1, \ldots, \alpha_N; \mathbf{r}) = 1. \tag{A.2}$$

The sum in the equation is computed over all the available configurations of the N chains.

Considering that all the N chains are identical, eq.(A.2) can be substituted by a single-chain average, and derived by

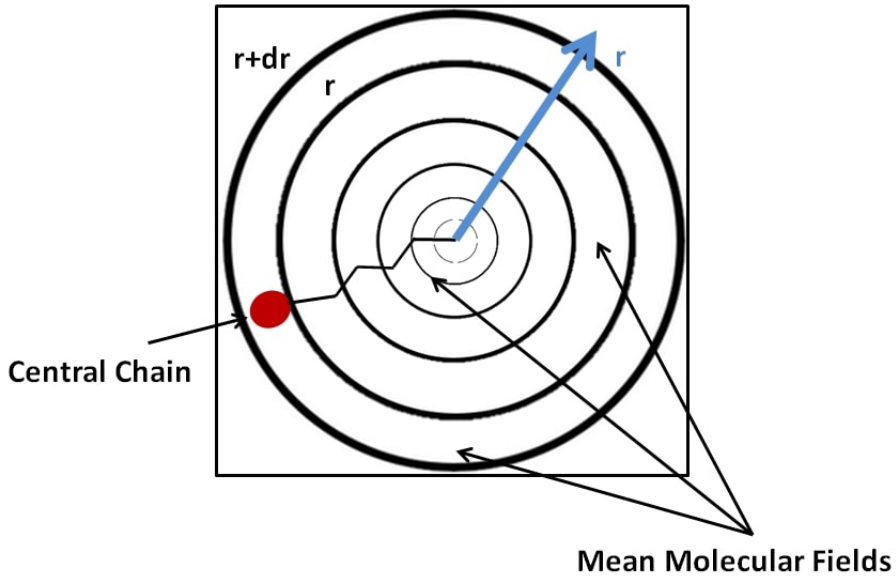

Figure A.1: Schematic of the SCMF with a central chain and the mean molecular fields as concentric spherical layers. Each layer has a radius r and thickness dr, within which the densities of the surfactants and solvent are assumed to be uniform.

$$\phi_s(\mathbf{r}) + N \sum_{\alpha} P[\alpha]\phi(\alpha, \mathbf{r}) = 1, \tag{A.3}$$

where $P[\alpha]$ is the probability of finding a chain in conformation α. The second term of the above equation can be written as the average over all the possible conformations of a single surfactant chain, as follows

$$\phi_s(\mathbf{r}) + N\langle\phi(\mathbf{r})\rangle = 1, \tag{A.4}$$

B

Effect of flexibility on the equilibrium micellization behavior

The flexibility of the surfactant chain is measured by the introduction of the Kuhn segment length l_k, which is a measure of the stiffness of the polymer chain (125). More specifically, a real polymer chain can be modeled as a collection of N Kuhn segments, each with a Kuhn length l_k. Each segment is a freely jointed segment and can be randomly oriented in any direction. In other words, the polymer chain is described by a random walk with a contour length, L, given by

$$L = N \cdot l_k \tag{B.1}$$

In this work, the L44 surfactant chain stiffness has been included by changing the size of the Kuhn segments to model hypothetical chains not based on any real system. For example, for a high flexibility surfactant chain, we have used a Kuhn length of 2 consecutive monomers in the case of "*PO*" and 2 consecutive monomers in the case of "*EO*" blocks. On the other hand, for a highly rigid chain we have used Kuhn lengths of 10 consecutive monomers for the hydrophobic block and 23 consecutive monomers for the hydrophilic one.

The preferred Aggregation Number is obtained when the total free energy is minimized. For each case of flexibility we obtained the preferred aggregation number through the minimum free energy of the system, which is related approximately to the minimum of the Standard Chemical Potential difference. To do so, we plotted the Standard Chemical Potential differences, obtained by the SCMF theory, versus the Aggregation Number of the micelle when excluding the surfactants in the bulk (N_c) (Figure B.1).

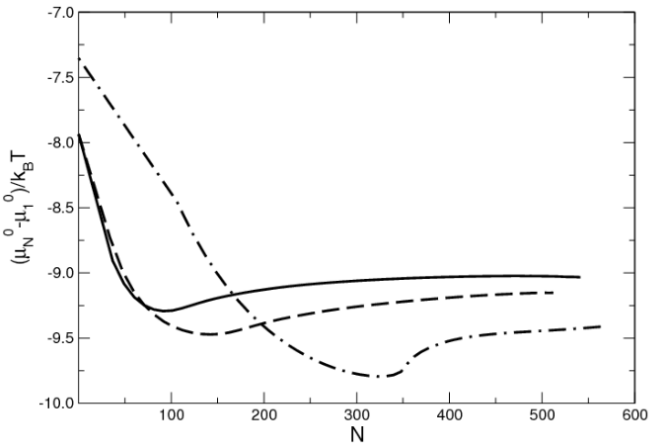

Figure B.1: Standard chemical potential difference, $(\mu_N^0 - \mu_1^0)/k_BT$, versus the aggregation number, N. Solid, dashed and dot-dashed lines indicate the *Flexible*, *Semiflexible*, and *Rigid* cases, respectively.

Regarding the Critical Micelle Concentration (CMC), in order to make comparisons with experiments, it is defined as the saturation point at which the concentration of free surfactants in the bulk solution (X_1^A) no longer increases with an increase in the total surfactant concentration (X_T). This point is depicted through a plot shown in Figure 2.3 which illustrates the relationship between the free surfactant concentration and the total surfactant concentration. The CMC, represented in volume fraction, can be obtained from this plot, and it can be converted to mol/L by the following equation

$$CMC_{mol/L} = \frac{1}{V_M + V_s\left(\frac{1}{CMC_X} - 1\right)}, \tag{B.2}$$

Where V_s and V_M are the molar volume of the solvent (water=0.018 L/mol) and the molar volume of the surfactant (L44=2.2 L/mol), respectively (185).

Results can be found in **Table B.1** and show that at a constant temperature T, the CMC value is lower for stiffer chains, while the Aggregation Number is higher. Contrariwise, when the surfactant chain is flexible, the CMC value is higher, and the Aggregation Number is lower. We can observe the preferred distribution of the different species (head, tail, solvent) by plotting the volume fraction profiles of micelles versus the distance from the micellar center, for each stiffness case (Figure B.2).

Generally, in all flexibility cases, at small distances from the micellar center, the tail distribution function is close to a maximum value of 0.6 while the head is close to zero and the solvent values are close to 0.4. At medium distances, the tail distribution function decreases, while the head and solvent increases. At larger distances, the head as

Case Study	$l_k^{EO}(\sigma)$	$l_k^{PO}(\sigma)$	N	$\min((\mu_N^0 - \mu_1^0)/k_BT)$	CMC (mol/L)
Flexible	2	2	91	-9.2	$5.1 \cdot 10^{-3}$
Semiflexible	3	4	145	-9.4	$4.0 \cdot 10^{-3}$
Rigid	10	20	320	-9.7	$3.3 \cdot 10^{-3}$

Table B.1: Equilibrium properties of L44 triblock copolymers ($EO_{10}PO_{23}EO_{10}$) in water at 37°C from SCMF calculations: l_k^{EO} and l_k^{PO} are the size of the Kuhn segments of the hydrophilic (EO) and hydrophobic (PO) blocks, aggregation number (N), minimum chemical potential differences, and Critical Micelle Concentration.

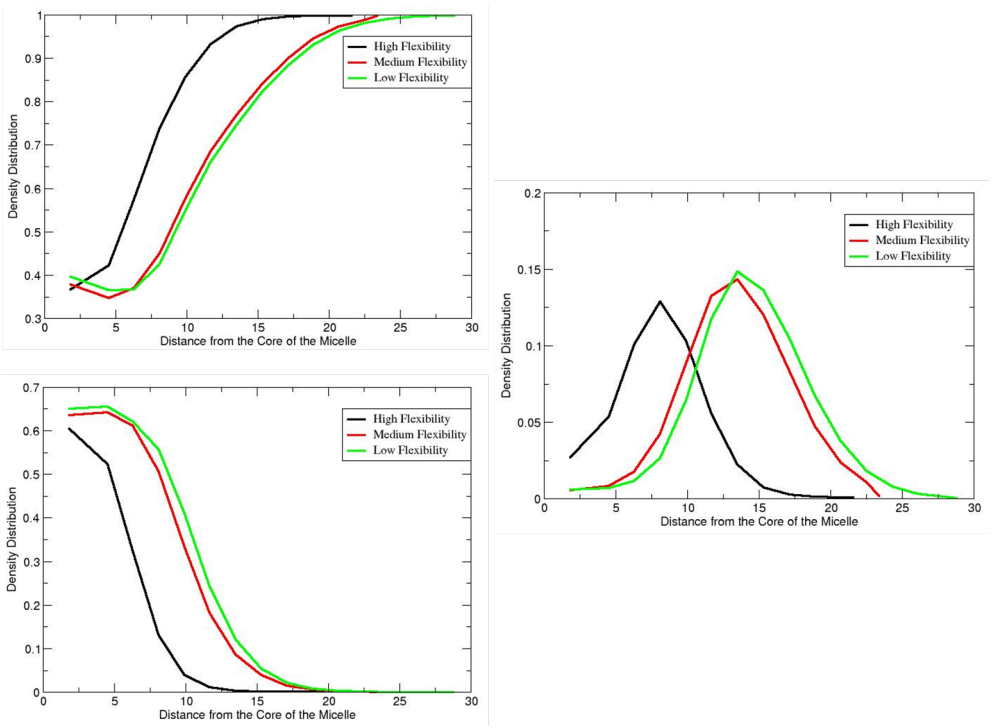

Figure B.2: Volume Fraction Profiles (distribution of tails (a), heads (b) and solvent (c) molecules) versus the distance from the micellar core, r [σ], for each case of chain flexibility.

well the tail concentrations drop to their bulk value, while the solvent concentration reaches a maximum value close to 1, which means that finally at large distances from the center, mainly solvent molecules are present with only a small concentration of the bulk concentration of the surfactant in water. Independently, for each case of chain flexibility, we obtained that at small distances from the micellar core, the tails are more crowded and much greater for the stiffer surfactant chains than for the high flexibility one. This

observation leads to the explanation of the larger aggregation number for the stiffer surfactant chains. With respect to the solvent distribution function, we can observe (Figure B.2c) that, the saturate value of almost 1, where almost only the solvent molecules are present, is reached faster from aggregates formed by flexible chains. Consequently, the size of the micelle is larger, when it is composed of stiffer surfactant chains. Figure B.3, presents a schematic diagram of the micelles formed by our surfactant chains of 20 head units and 23 tail units with different chain flexibilities corresponding to the minimum of the free energy: high, medium and low flexibilities, respectively. These micelles are merely schematic and are constructed by using the most probable configurations of the single chain, representing the surfactants in the equilibrium state. As we can see, in the first case, where the micelle consists of high flexibility surfactant chains, the aggregate is significantly smaller than the micelles composed of more rigid chains. This happens because, the higher surfactant stiffness forces the micellar core to be bigger, as the tails are unable to collapse as much as the more flexible case.

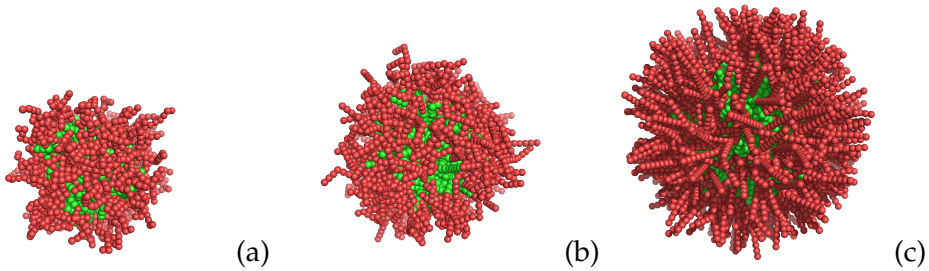

Figure B.3: Schematic diagram of typical micelle configurations for the three case studies: (a) *Flexible* $N = 91$, (b) *Semiflexible* $N = 145$, and (c) *Rigid* $N = 320$. The EO monomers are shaded red and the more hydrophobic PO monomers green.

References

[1] Fabian A Garcia Daza, Alexander J Colville, and Allan D Mackie. Mean-field coarse-grained model for poly (ethylene oxide)-poly (propylene oxide)-poly (ethylene oxide) triblock copolymer systems. *Langmuir*, 31(12):3596–3604, 2015.

[2] Elena Batrakova, Shengmin Lee, Shu Li, Annie Venne, Valery Alakhov, and Alexander Kabanov. Fundamental relationships between the composition of pluronic block copolymers and their hypersensitization effect in mdr cancer cells. *Pharmaceutical research*, 16:1373–1379, 1999.

[3] Bappaditya Naskar, Soumen Ghosh, and Satya P Moulik. Solution behavior of normal and reverse triblock copolymers (pluronic l44 and 10r5) individually and in binary mixture. *Langmuir*, 28(18):7134–7146, 2012.

[4] Guang-Guo Ying. Fate, behavior and effects of surfactants and their degradation products in the environment. *Environment international*, 32(3):417–431, 2006.

[5] Laurier L Schramm. *Surfactants: fundamentals and applications in the petroleum industry*. Cambridge university press, 2000.

[6] JJ Lewis. An introduction to surfactants. In *Preservation of Surfactant Formulations*, pages 53–82. Springer, 1995.

[7] Paschalis Alexandridis. Amphiphilic copolymers and their applications. *Current Opinion in Colloid & Interface Science*, 1(4):490–501, 1996.

[8] Ajay Singh, Jonathan D Van Hamme, and Owen P Ward. Surfactants in microbiology and biotechnology: Part 2. application aspects. *Biotechnology advances*, 25(1):99–121, 2007.

[9] Babak Babajanzadeh, Saied Sherizadeh, and Hasan Ranji. Detergents and surfactants: a brief review. *Open Access Journal of Science*, 3(3):94–99, 2019.

[10] Gannu P Kumar and Pogaku Rajeshwarrao. Nonionic surfactant vesicular systems for effective drug delivery—an overview. *Acta pharmaceutica sinica B*, 1(4):208–219, 2011.

[11] Ewa Olkowska, Zaneta Polkowska, and Jacek Namiesnik. Analytics of surfactants in the environment: problems and challenges. *Chemical reviews*, 111(9):5667–5700, 2011.

[12] DN Rubingh and T Jones. Mechanism of detergency in systems containing cationic and nonionic surfactants. *Industrial & Engineering Chemistry Product Research and Development*, 21(2):176–182, 1982.

[13] Santanu Paria. Surfactant-enhanced remediation of organic contaminated soil and water. *Advances in colloid and interface science*, 138(1):24–58, 2008.

[14] Ratan Sarkar, Aniruddha Pal, Atanu Rakshit, and Bidyut Saha. Properties and applications of amphoteric surfactant: A concise review. *Journal of Surfactants and Detergents*, 24(5):709–730, 2021.

[15] MR Porter and MR Porter. Use of surfactant theory. *Handbook of surfactants*, pages 24–48, 1991.

[16] Lutz Maibaum, Aaron R Dinner, and David Chandler. Micelle formation and the hydrophobic effect. *The Journal of Physical Chemistry B*, 108(21):6778–6781, 2004.

[17] David Chandler. Interfaces and the driving force of hydrophobic assembly. *Nature*, 437(7059):640–647, 2005.

[18] Jacob N Israelachvili. *Intermolecular and surface forces*. Academic press, 2011.

[19] Krister Holmberg, Bo Jönsson, Bengt Kronberg, Björn Lindman, et al. *Polymers in aqueous solution*. Wiley-Blackwell New York, 2002.

[20] Maria Velinova, Durba Sengupta, Alia V Tadjer, and Siewert-Jan Marrink. Sphere-to-rod transitions of nonionic surfactant micelles in aqueous solution modeled by molecular dynamics simulations. *Langmuir*, 27(23):14071–14077, 2011.

[21] Vladimir P Torchilin. Structure and design of polymeric surfactant-based drug delivery systems. *Journal of controlled release*, 73(2-3):137–172, 2001.

[22] Walter C Presto and Walter Preston. Some correlating principles of detergent action. *The Journal of Physical Chemistry*, 52(1):84–97, 1948.

[23] Dilek Keskin and Aysen Tezcaner. Micelles as delivery system for cancer treatment. *Current Pharmaceutical Design*, 23(35):5230–5241, 2017.

[24] Younsoo Bae, Nobuhiro Nishiyama, Shigeto Fukushima, Hiroyuki Koyama, Matsumura Yasuhiro, and Kazunori Kataoka. Preparation and biological characterization of polymeric micelle drug carriers with intracellular ph-triggered drug release property: tumor permeability, controlled subcellular drug distribution, and enhanced in vivo antitumor efficacy. *Bioconjugate chemistry*, 16(1):122–130, 2005.

[25] Nathalie Bailly, Mark Thomas, and Bert Klumperman. Poly (n-vinylpyrrolidone)-block-poly (vinyl acetate) as a drug delivery vehicle for hydrophobic drugs. *Biomacromolecules*, 13(12):4109–4117, 2012.

[26] Amalina Bte Ebrahim Attia, Zhan Yuin Ong, James L Hedrick, Phin Peng Lee, Pui Lai Rachel Ee, Paula T Hammond, and Yi-Yan Yang. Mixed micelles self-assembled from block copolymers for drug delivery. *Current Opinion in Colloid & Interface Science*, 16(3):182–194, 2011.

[27] Louise Hespel, Arlette El Asmar, Gaëlle Morandi, Laurence Lecamp, Luc Picton, and Fabrice Burel. Synthesis of dual-sensitive core cross-linked mixed micelles through thiol–ene addition and subsequent drug release behavior. *Macromolecular Chemistry and Physics*, 218(15):1700016, 2017.

[28] Tao Liu, Yinfeng Qian, Xianglong Hu, Zhishen Ge, and Shiyong Liu. Mixed polymeric micelles as multifunctional scaffold for combined magnetic resonance imaging contrast enhancement and targeted chemotherapeutic drug delivery. *Journal of Materials Chemistry*, 22(11):5020–5030, 2012.

[29] Rafeeq Tanbour, Ana M Martins, William G Pitt, and Ghaleb A Husseini. Drug delivery systems based on polymeric micelles and ultrasound: a review. *Current Pharmaceutical Design*, 22(19):2796–2807, 2016.

[30] Xiaohong Sun and Nandika Bandara. Applications of reverse micelles technique in food science: A comprehensive review. *Trends in Food Science & Technology*, 91:106–115, 2019.

[31] A Flamberg and R Pecora. Dynamic light scattering study of micelles in a high ionic strength solution. *The Journal of Physical Chemistry*, 88(14):3026–3033, 1984.

[32] Karin Schillen, Wyn Brown, and Robert M Johnsen. Micellar sphere-to-rod transition in an aqueous triblock copolymer system. a dynamic light scattering study of translational and rotational diffusion. *Macromolecules*, 27(17):4825–4832, 1994.

[33] HB Bohidar and M Behboudnia. Characterization of reverse micelles by dynamic light scattering. *Colloids and Surfaces A: Physicochemical and Engineering Aspects*, 178(1-3):313–323, 2001.

[34] Robert A Day, Brian H Robinson, Julian HR Clarke, and Jane V Doherty. Characterisation of water-containing reversed micelles by viscosity and dynamic light scattering methods. *Journal of the Chemical Society, Faraday Transactions 1: Physical Chemistry in Condensed Phases*, 75:132–139, 1979.

[35] F Reiss-Husson and Vittorio Luzzati. Small-angle x-ray scattering study of the structure of soap and detergent micelles. *Journal of Colloid and Interface Science*, 21(5):534–546, 1966.

[36] Bengt Svens and Bjorn Rosenholm. An investigation of the size and structure of the micelles in sodium octanoate solutions by small-angle x-ray scattering. *Journal of Colloid and Interface Science*, 44(3):495–504, 1973.

[37] Fr Reiss-Husson and Vittorio Luzzati. The structure of the micellar solutions of some amphiphilic compounds in pure water as determined by absolute small-angle x-ray scattering techniques. *The Journal of physical chemistry*, 68(12):3504–3511, 1964.

[38] Grethe Vestergaard Jensen, Reidar Lund, Jérémie Gummel, Theyencheri Narayanan, and Jan Skov Pedersen. Monitoring the transition from spherical to polymer-like surfactant micelles using small-angle x-ray scattering. *Angewandte Chemie*, 126(43):11708–11712, 2014.

[39] Jan Lipfert, Linda Columbus, Vincent B Chu, Scott A Lesley, and Sebastian Doniach. Size and shape of detergent micelles determined by small-angle x-ray scattering. *The journal of physical chemistry B*, 111(43):12427–12438, 2007.

[40] Saim M Emin, Pavletta S Denkova, Karolina I Papazova, Ceco D Dushkin, and Eiki Adachi. Study of reverse micelles of di-isobutylphenoxyethoxyethyldimethylbenzylammonium methacrylate in benzene by nuclear magnetic resonance spectroscopy. *Journal of colloid and interface science*, 305(1):133–141, 2007.

[41] Tuck C Wong. Micellar systems: Nuclear magnetic resonance spectroscopy. *Encyclopedia of surface and colloid science*, 5:3742, 2006.

[42] Jamil K Salem, Issa M El-Nahhal, and Safy F Salama. Determination of the critical micelle concentration by absorbance and fluorescence techniques using fluorescein probe. *Chemical Physics Letters*, 730:445–450, 2019.

[43] Mandeep Singh Bakshi, Kulbir Singh, and Jasmeet Singh. Characterization of mixed micelles of cationic twin tail surfactants with phospholipids using fluorescence spectroscopy. *Journal of colloid and interface science*, 297(1):284–291, 2006.

[44] Soma De, Vinod K Aswal, Prem S Goyal, and Santanu Bhattacharya. Characterization of new gemini surfactant micelles with phosphate headgroups by sans and fluorescence spectroscopy. *Chemical physics letters*, 303(3-4):295–303, 1999.

[45] Sven Falke and Christian Betzel. Dynamic light scattering (dls). In *Radiation in Bioanalysis*, pages 173–193. Springer, 2019.

[46] Gabriel A Rothbauer, Elisabeth A Rutter, Chelsea Reuter-Seng, Simon Vera, Eugene J Billiot, Yayin Fang, Fereshteh H Billiot, and Kevin F Morris. Nuclear magnetic resonance investigation of the effect of ph on micelle formation by the amino acid-based surfactant undecyl l-phenylalaninate. *Journal of surfactants and detergents*, 21(1):139–153, 2018.

[47] Viswanathan V Krishnan. Molecular thermodynamics using nuclear magnetic resonance (nmr) spectroscopy. *Inventions*, 4(1):13, 2019.

[48] S Karaborni, K Esselink, PAJ Hilbers, B Smit, Jl Karthauser, NM Van Os, and R Zana. Simulating the self-assembly of gemini (dimeric) surfactants. *Science*, 266(5183):254–256, 1994.

[49] John C Shelley and Mee Y Shelley. Computer simulation of surfactant solutions. *Current opinion in colloid & interface science*, 5(1-2):101–110, 2000.

[50] Pradip Kr Ghorai and Sharon C Glotzer. Molecular dynamics simulation study of self-assembled monolayers of alkanethiol surfactants on spherical gold nanoparticles. *The Journal of Physical Chemistry C*, 111(43):15857–15862, 2007.

[51] RG Larson. Monte carlo simulation of microstructural transitions in surfactant systems. *The Journal of chemical physics*, 96(11):7904–7918, 1992.

[52] RG Larson, LE Scriven, and HT Davis. Monte carlo simulation of model amphiphile-oil–water systems. *The Journal of chemical physics*, 83(5):2411–2420, 1985.

[53] RG Larson. Monte carlo simulations of the phase behavior of surfactant solutions. *Journal de physique II*, 6(10):1441–1463, 1996.

[54] S Karaborni, NM Van Os, K Esselink, and PAJ Hilbers. Molecular dynamics simulations of oil solubilization in surfactant solutions. *Langmuir*, 9(5):1175–1178, 1993.

[55] K Esselink, PAJ Hilbers, NM Van Os, B Smit, and S Karaborni. Molecular dynamics simulations of model oil/water/surfactant systems. *Colloids and Surfaces A: Physicochemical and Engineering Aspects*, 91:155–167, 1994.

[56] Ashish V Sangwai and Radhakrishna Sureshkumar. Coarse-grained molecular dynamics simulations of the sphere to rod transition in surfactant micelles. *Langmuir*, 27(11):6628–6638, 2011.

[57] J-B Maillet, V Lachet, and Peter V Coveney. Large scale molecular dynamics simulation of self-assembly processes in short and long chain cationic surfactants. *Physical Chemistry Chemical Physics*, 1(23):5277–5290, 1999.

[58] T Zehl, M Wahab, H-J Mögel, and P Schiller. Monte carlo simulations of self-assembled surfactant aggregates. *Langmuir*, 22(6):2523–2527, 2006.

[59] T Zehl, M Wahab, P Schiller, and H-J Mogel. Monte carlo simulation of surfactant adsorption on hydrophilic surfaces. *Langmuir*, 25(4):2090–2100, 2009.

[60] Christopher M Wijmans and Per Linse. Surfactant self-assembly at a hydrophilic surface. a monte carlo simulation study. *The Journal of Physical Chemistry*, 100(30):12583–12591, 1996.

[61] Prabal K Maiti and Debashish Chowdhury. Micellar aggregates of gemini surfactants: Monte carlo simulation of a microscopic model. *EPL (Europhysics Letters)*, 41(2):183, 1998.

[62] Martin Lısal, Carol K Hall, Keith E Gubbins, and Athanassios Z Panagiotopoulos. Self-assembly of surfactants in a supercritical solvent from lattice monte carlo simulations. *The Journal of chemical physics*, 116(3):1171–1184, 2002.

[63] Daniel W Cheong and Athanassios Z Panagiotopoulos. Monte carlo simulations of micellization in model ionic surfactants: Application to sodium dodecyl sulfate. *Langmuir*, 22(9):4076–4083, 2006.

[64] RG Larson. Monte carlo lattice simulation of amphiphilic systems in two and three dimensions. *The Journal of chemical physics*, 89(3):1642–1650, 1988.

[65] RG Larson. Self-assembly of surfactant liquid crystalline phases by monte carlo simulation. *The Journal of chemical physics*, 91(4):2479–2488, 1989.

[66] Radek Erban. From molecular dynamics to brownian dynamics. *Proceedings of the Royal Society A: Mathematical, Physical and Engineering Sciences*, 470(2167):20140036, 2014.

[67] WF Van Gunsteren and HJC Berendsen. Algorithms for brownian dynamics. *Molecular Physics*, 45(3):637–647, 1982.

[68] Jim C Chen and Albert S Kim. Brownian dynamics, molecular dynamics, and monte carlo modeling of colloidal systems. *Advances in colloid and interface science*, 112(1-3):159–173, 2004.

[69] Robert D Groot and Timothy J Madden. Dynamic simulation of diblock copolymer microphase separation. *The Journal of chemical physics*, 108(20):8713–8724, 1998.

[70] Pep Espanol and Patrick Warren. Statistical mechanics of dissipative particle dynamics. *EPL (Europhysics Letters)*, 30(4):191, 1995.

[71] JMVA Koelman and PJ Hoogerbrugge. Dynamic simulations of hard-sphere suspensions under steady shear. *EPL (Europhysics Letters)*, 21(3):363, 1993.

[72] PJ Hoogerbrugge and JMVA Koelman. Simulating microscopic hydrodynamic phenomena with dissipative particle dynamics. *EPL (Europhysics Letters)*, 19(3):155, 1992.

[73] Robert D Groot and Patrick B Warren. Dissipative particle dynamics: Bridging the gap between atomistic and mesoscopic simulation. *The Journal of chemical physics*, 107(11):4423–4435, 1997.

[74] Kolattukudy P Santo and Alexander V Neimark. Dissipative particle dynamics simulations in colloid and interface science: a review. *Advances in colloid and interface science*, 298:102545, 2021.

[75] Fabian A Garcia Daza, Josep Bonet Avalos, and Allan D Mackie. Simulation analysis of the kinetic exchange of copolymer surfactants in micelles. *Langmuir*, 33(27):6794–6803, 2017.

[76] Nadezhda P Shusharina, Per Linse, and Alexei R Khokhlov. Lattice mean-field modeling of charged polymeric micelles. *Macromolecules*, 33(22):8488–8496, 2000.

[77] Zaid A Al-Anber, Josep Bonet Avalos, and Allan D Mackie. Prediction of the critical micelle concentration in a lattice model for amphiphiles using a single-chain mean-field theory. *The Journal of chemical physics*, 122(10):104910, 2005.

[78] MP Pepin and MD Whitmore. Monte carlo and mean field study of diblock copolymer micelles. *Macromolecules*, 33(23):8644–8653, 2000.

[79] Nadezhda P Shusharina, Per Linse, and Alexei R Khokhlov. Micelles of diblock copolymers with charged and neutral blocks: Scaling and mean-field lattice approaches. *Macromolecules*, 33(10):3892–3901, 2000.

[80] Patricia N Hurter, Jan MHM Scheutjens, and T Alan Hatton. Molecular modeling of micelle formation and solubilization in block copolymer micelles. 1. a self-consistent mean-field lattice theory. *Macromolecules*, 26(21):5592–5601, 1993.

[81] Fabián A García Daza, Alexander J Colville, and Allan D Mackie. Chain architecture and micellization: A mean-field coarse-grained model for poly (ethylene oxide) alkyl ether surfactants. *The Journal of Chemical Physics*, 142(11):114902, 2015.

[82] Fabián A García Daza, Josep Bonet Avalos, and Allan D Mackie. Logarithmic exchange kinetics in monodisperse copolymeric micelles. *Physical Review Letters*, 118(24):248001, 2017.

[83] I Szleifer, A Ben-Shaul, and WM Gelbart. Chain organization and thermodynamics in micelles and bilayers. ii. model calculations. *The Journal of chemical physics*, 83(7):3612–3620, 1985.

[84] I Szleifer, A Ben-Shaul, and WM Gelbart. Chain statistics in micelles and bilayers: effects of surface roughness and internal energy. *The Journal of chemical physics*, 85(9):5345–5358, 1986.

[85] A Ben-Shaul, I Szleifer, and WM Gelbart. Chain organization and thermodynamics in micelles and bilayers. i. theory. *The Journal of chemical physics*, 83(7):3597–3611, 1985.

[86] Sergey Pogodin and Vladimir A Baulin. Coarse-grained models of phospholipid membranes within the single chain mean field theory. *Soft Matter*, 6(10):2216–2226, 2010.

[87] Sergey Pogodin and Vladimir A Baulin. Equilibrium insertion of nanoscale objects into phospholipid bilayers. *Current Nanoscience*, 7(5):721–726, 2011.

[88] Josep Bonet Avalos, Allan D Mackie, and Silvia Díez-Orrite. Comparison of the importance sampling single chain mean field theory with monte carlo simulation and self-consistent field calculations for polymer adsorption onto a flat wall. *Macromolecules*, 37(3):1143–1151, 2004.

[89] Yingli Niu, Xiangyu Bu, and Xinghua Zhang. Single chain mean-field theory study on responsive behavior of semiflexible polymer brush. *Materials*, 14(4):778, 2021.

[90] Joseph Mauk Smith, Hendrick C Van Ness, Michael M Abbott, and Mark Thomas Swihart. *Introduction to chemical engineering thermodynamics*. McGraw-Hill Singapore, 1949.

[91] John M Prausnitz and Rudiger N Lichtenthaler. Eg d. azevedo, 1999.

[92] Bruno Linder. *Thermodynamics and introductory statistical mechanics*. John Wiley & Sons, 2004.

[93] David Schaeffel, Andreas Kreyes, Yi Zhao, Katharina Landfester, Hans-Jurgen Butt, Daniel Crespy, and Kaloian Koynov. Molecular exchange kinetics of diblock copolymer micelles monitored by fluorescence correlation spectroscopy. *ACS Macro Letters*, 3(5):428–432, 2014.

[94] Reidar Lund, Lutz Willner, Dieter Richter, and Elena E Dormidontova. Equilibrium chain exchange kinetics of diblock copolymer micelles: Tuning and logarithmic relaxation. *Macromolecules*, 39(13):4566–4575, 2006.

[95] David Roylance and Su Su Wang. Penetration mechanics of textile structures: Influence of non-linear viscoelastic relaxation. *Polymer Engineering & Science*, 18(14):1068–1072, 1978.

[96] Jens Fritsch, S Hiermaier, and G Strobl. Characterizing and modeling the non-linear viscoelastic tensile deformation of a glass fiber reinforced polypropylene. *Composites science and technology*, 69(14):2460–2466, 2009.

[97] Per Linse. Micellization of poly (ethylene oxide)-poly (propylene oxide) block copolymers in aqueous solution. *Macromolecules*, 26(17):4437–4449, 1993.

[98] A Halperin and S Alexander. Polymeric micelles: their relaxation kinetics. *Macromolecules*, 22(5):2403–2412, 1989.

[99] EAG Aniansson and S N_ Wall. Kinetics of step-wise micelle association. *The Journal of Physical Chemistry*, 78(10):1024–1030, 1974.

[100] E. A. G. Aniansson and S. N. Wall. Kinetics of step-wise micelle association. correction and improvement. *The Journal of Physical Chemistry*, 79(8):857–858, 1975.

[101] Alexander Patist, SG Oh, R Leung, and DO Shah. Kinetics of micellization: its significance to technological processes. *Colloids and Surfaces A: Physicochemical and Engineering Aspects*, 176(1):3–16, 2001.

[102] James A. Swinehart. Relaxation kinetics: An experiment for physical chemistry. *Journal of Chemical Education*, 44(9):524, 1967.

[103] Gordon C Kresheck, Eugene Hamori, Gary Davenport, and Harold A Scheraga. Determination of the dissociation rate of dodecylpyridinium iodide micelles by a temperature-jump technique1a, b. *Journal of the American Chemical Society*, 88(2):246–253, 1966.

[104] EAG Aniansson, SN Wall, M Almgren, H Hoffmann, I Kielmann, W Ulbricht, R Zana, J Lang, and C Tondre. Theory of the kinetics of micellar equilibria and quantitative interpretation of chemical relaxation studies of micellar solutions of ionic surfactants. *The Journal of Physical Chemistry*, 80(9):905–922, 1976.

[105] T Telgmann and U Kaatze. On the kinetics of the formation of small micelles. 1. broadband ultrasonic absorption spectrometry. *The Journal of Physical Chemistry B*, 101(39):7758–7765, 1997.

[106] Y Rharbi. Fusion and fragmentation dynamics at equilibrium in triblock copolymer micelles. *Macromolecules*, 45(24):9823–9826, 2012.

[107] G Landazuri, VVA Fernandez, JFA Soltero, and Y Rharbi. Length of the core forming block effect on fusion and fission dynamics at equilibrium in peo–ppo–peo triblock copolymer micelles in the spherical regime. *Macromolecules*, 54(5):2494–2505, 2021.

[108] Alexander Patist, James R Kanicky, Pavan K Shukla, and Dinesh O Shah. Importance of micellar kinetics in relation to technological processes. *Journal of colloid and interface science*, 245(1):1–15, 2002.

[109] Joshua A Mysona, Alon V McCormick, and David C Morse. Mechanism of micelle birth and death. *Physical review letters*, 123(3):038003, 2019.

[110] Joshua A Mysona, Alon V McCormick, and David C Morse. Simulation of diblock copolymer surfactants. ii. micelle kinetics. *Physical Review E*, 100(1):012603, 2019.

[111] EA G_ Aniansson and SN Wall. Kinetics of step-wise micelle association. correction and improvement. *The Journal of Physical Chemistry*, 79(8):857–858, 1975.

[112] Yongmei Wang, Charles M Kausch, Moonseok Chun, Roderic P Quirk, and Wayne L Mattice. Exchange of chains between micelles of labeled polystyrene-block-poly (oxyethylene) as monitored by nonradiative singlet energy transfer. *Macromolecules*, 28(4):904–911, 1995.

[113] En Wang, Jie Lu, Frank S Bates, and Timothy P Lodge. Effect of corona block length on the structure and chain exchange kinetics of block copolymer micelles. *Macromolecules*, 51(10):3563–3571, 2018.

[114] Thomas Zinn, Lutz Willner, Vitaliy Pipich, Dieter Richter, and Reidar Lund. Effect of core crystallization and conformational entropy on the molecular exchange kinetics of polymeric micelles. *ACS Macro Letters*, 4(6):651–655, 2015.

[115] Thomas Zinn, Lutz Willner, Reidar Lund, Vitaliy Pipich, and Dieter Richter. Equilibrium exchange kinetics in n-alkyl–peo polymeric micelles: single exponential relaxation and chain length dependence. *Soft Matter*, 8(3):623–626, 2012.

[116] Reidar Lund, Lutz Willner, Jörg Stellbrink, Peter Lindner, and Dieter Richter. Logarithmic chain-exchange kinetics of diblock copolymer micelles. *Physical review letters*, 96(6):068302, 2006.

[117] Reidar Lund, Lutz Willner, Jörg Stellbrink, Peter Lindner, and Dieter Richter. Erratum: Logarithmic chain-exchange kinetics of diblock copolymer micelles [phys. rev. lett. 96, 068302 (2006)]. *Phys. Rev. Lett.*, 104:049902, Jan 2010.

[118] Türkan Haliloglu, Ivet Bahar, Burak Erman, and Wayne L Mattice. Mechanisms of the exchange of diblock copolymers between micelles at dynamic equilibrium. *Macromolecules*, 29(13):4764–4771, 1996.

[119] Zhenlong Li and Elena E Dormidontova. Kinetics of diblock copolymer micellization by dissipative particle dynamics. *Macromolecules*, 43(7):3521–3531, 2010.

[120] Zhenlong Li and Elena E Dormidontova. Equilibrium chain exchange kinetics in block copolymer micelle solutions by dissipative particle dynamics simulations. *Soft Matter*, 7(9):4179–4188, 2011.

[121] Ammu Prhashanna and Elena E Dormidontova. Micelle self-assembly and chain exchange kinetics of tadpole block copolymers with a cyclic corona block. *Macromolecules*, 53(3):982–991, 2020.

[122] BAC Van Vlimmeren, NM Maurits, AV Zvelindovsky, GJA Sevink, and JGEM Fraaije. Simulation of 3d mesoscale structure formation in concentrated aqueous solution of the triblock polymer surfactants (ethylene oxide) 13 (propylene oxide) 30 (ethylene oxide) 13 and (propylene oxide) 19 (ethylene oxide) 33 (propylene oxide) 19. application of dynamic mean-field density functional theory. *Macromolecules*, 32(3):646–656, 1999.

[123] Josep Bonet Avalos, Allan D Mackie, and Silvia Díez-Orrite. Development of an importance sampling single chain mean field theory for polymer adsorption onto a flat wall. *Macromolecules*, 37(3):1124–1133, 2004.

[124] Inge Bos, Marga Timmerman, and Joris Sprakel. Fret-based determination of the exchange dynamics of complex coacervate core micelles. *Macromolecules*, 54(1):398–411, 2020.

[125] Shaul M Aharoni. On entanglements of flexible and rodlike polymers. *Macromolecules*, 16(11):1722–1728, 1983.

[126] Allan D Mackie, Athanassios Z Panagiotopoulos, and Igal Szleifer. Aggregation behavior of a lattice model for amphiphiles. *Langmuir*, 13(19):5022–5031, 1997.

[127] Zaid A Al-Anber, Josep Bonet Avalos, and Allan D Mackie. Prediction of the critical micelle concentration in a lattice model for amphiphiles using a single-chain mean-field theory. *The Journal of chemical physics*, 122(10):104910, 2005.

[128] Jie Lu, Frank S Bates, and Timothy P Lodge. Remarkable effect of molecular architecture on chain exchange in triblock copolymer micelles. *Macromolecules*, 48(8):2667–2676, 2015.

[129] Soo-Hyung Choi, Timothy P Lodge, and Frank S Bates. Mechanism of molecular exchange in diblock copolymer micelles: hypersensitivity to core chain length. *Physical review letters*, 104(4):047802, 2010.

[130] Reidar Lund, Lutz Willner, Vitaliy Pipich, Isabelle Grillo, Peter Lindner, Juan Colmenero, and Dieter Richter. Equilibrium chain exchange kinetics of diblock copolymer micelles: Effect of morphology. *Macromolecules*, 44(15):6145–6154, 2011.

[131] SR Croy and GS Kwon. Polymeric micelles for drug delivery. *Current pharmaceutical design*, 12(36):4669–4684, 2006.

[132] Bjorn Lindman, Paschalis Alexandridis, et al. *Amphiphilic block copolymers*. Elsevier, 2000.

[133] Laurier L Schramm, Elaine N Stasiuk, and D Gerrard Marangoni. 2 surfactants and their applications. *Annual Reports Section" C"(Physical Chemistry)*, 99:3–48, 2003.

[134] Shmaryahu Ezrahi, Eran Tuval, Abraham Aserin, and Nissim Garti. Daily applications of systems with wormlike micelles. In *Giant Micelles*, pages 515–544. CRC Press, 2007.

[135] Mileena Moreno, Luciana P Mazur, Silvio Edegar Weschenfelder, Renata J Regis, Rodrigo AF de Souza, Belisa A Marinho, Adriano da Silva, Selene MA Guelli U de Souza, and Antônio Augusto U de Souza. Water and wastewater treatment by micellar enhanced ultrafiltration–a critical review. *Journal of Water Process Engineering*, 46:102574, 2022.

[136] Afzal Shah, Suniya Shahzad, Azeema Munir, Mallikarjuna N Nadagouda, Gul Shahzada Khan, Dilawar Farhan Shams, Dionysios D Dionysiou, and Usman Ali Rana. Micelles as soil and water decontamination agents. *Chemical reviews*, 116(10):6042–6074, 2016.

[137] Zhong-Gao Gao, Heidi D Fain, and Natalya Rapoport. Controlled and targeted tumor chemotherapy by micellar-encapsulated drug and ultrasound. *Journal of Controlled Release*, 102(1):203–222, 2005.

[138] Guang Hui Gao, Yi Li, and Doo Sung Lee. Environmental ph-sensitive polymeric micelles for cancer diagnosis and targeted therapy. *Journal of Controlled Release*, 169(3):180–184, 2013.

[139] Vladimir S Trubetskoy. Polymeric micelles as carriers of diagnostic agents. *Advanced drug delivery reviews*, 37(1-3):81–88, 1999.

[140] Jaskiran Kaur, Vijay Mishra, Sachin Kumar Singh, Monica Gulati, Bhupinder Kapoor, Dinesh Kumar Chellappan, Gaurav Gupta, Harish Dureja, Krishnan Anand, Kamal Dua, et al. Harnessing amphiphilic polymeric micelles for diagnostic and therapeutic applications: Breakthroughs and bottlenecks. *Journal of Controlled Release*, 334:64–95, 2021.

[141] Conlin P O'Neil, André J van der Vlies, Diana Velluto, Christine Wandrey, Davide Demurtas, Jacques Dubochet, and Jeffrey A Hubbell. Extracellular matrix binding mixed micelles for drug delivery applications. *Journal of controlled release*, 137(2):146–151, 2009.

[142] Kwangjae Cho, XU Wang, Shuming Nie, Zhuo Chen, and Dong M Shin. Therapeutic nanoparticles for drug delivery in cancer. *Clinical cancer research*, 14(5):1310–1316, 2008.

[143] Marie-Christine Jones and Jean-Christophe Leroux. Polymeric micelles–a new generation of colloidal drug carriers. *European journal of pharmaceutics and biopharmaceutics*, 48(2):101–111, 1999.

[144] Christine Allen, Dusica Maysinger, and Adi Eisenberg. Nano-engineering block copolymer aggregates for drug delivery. *Colloids and Surfaces B: Biointerfaces*, 16(1-4):3–27, 1999.

[145] Suhong Wu, Huihui Kuang, Fanbo Meng, Yanjuan Wu, Xiaoyuan Li, Xiabin Jing, and Yubin Huang. Facile preparation of core cross-linked micelles from catechol-containing amphiphilic triblock copolymer. *Journal of Materials Chemistry*, 22(30):15348–15356, 2012.

[146] Diego A Chiappetta and Alejandro Sosnik. Poly (ethylene oxide)–poly (propylene oxide) block copolymer micelles as drug delivery agents: improved hydrosolubility, stability and bioavailability of drugs. *European Journal of Pharmaceutics and Biopharmaceutics*, 66(3):303–317, 2007.

[147] Zerrin Sezgin, Nilufer Yüksel, and Tamer Baykara. Preparation and characterization of polymeric micelles for solubilization of poorly soluble anticancer drugs. *European journal of pharmaceutics and biopharmaceutics*, 64(3):261–268, 2006.

[148] Nikken Wiradharma, Ying Zhang, Shrinivas Venkataraman, James L Hedrick, and Yi Yan Yang. Self-assembled polymer nanostructures for delivery of anticancer therapeutics. *Nano Today*, 4(4):302–317, 2009.

[149] Alexander V Kabanov, Elena V Batrakova, and Valery Yu Alakhov. Pluronic® block copolymers as novel polymer therapeutics for drug and gene delivery. *Journal of controlled release*, 82(2-3):189–212, 2002.

[150] Li-mei Han, Jie Guo, Li-jun Zhang, Qing-song Wang, and Xiao-ling Fang. Pharmacokinetics and biodistribution of polymeric micelles of paclitaxel with pluronic p123. *Acta Pharmacologica Sinica*, 27(6):747–753, 2006.

[151] Alexander V Kabanov, Elena V Batrakova, and Valery Yu Alakhov. Pluronic® block copolymers for overcoming drug resistance in cancer. *Advanced drug delivery reviews*, 54(5):759–779, 2002.

[152] Elena V Batrakova and Alexander V Kabanov. Pluronic block copolymers: evolution of drug delivery concept from inert nanocarriers to biological response modifiers. *Journal of controlled release*, 130(2):98–106, 2008.

[153] Alexander V Kabanov, Pierre Lemieux, Sergey Vinogradov, and Valery Alakhov. Pluronic® block copolymers: novel functional molecules for gene therapy. *Advanced drug delivery reviews*, 54(2):223–233, 2002.

[154] Alexander V Kabanov and Valery Yu Alakhov. Pluronic® block copolymers in drug delivery: From micellar nanocontainers to biological response modifiers. *Critical Reviews™ in Therapeutic Drug Carrier Systems*, 19(1), 2002.

[155] Nobuhiro Nishiyama and Kazunori Kataoka. Current state, achievements, and future prospects of polymeric micelles as nanocarriers for drug and gene delivery. *Pharmacology & therapeutics*, 112(3):630–648, 2006.

[156] Akbar, muhammad usman and zia, khalid mahmood and nazir, ahsan and iqbal, jamshed and ejaz, syeda abida and akash, muhammad sajid hamid. *AAPS PharmSciTech*, 19(6):2719—2739, 2018.

[157] Paschalis Alexandridis, Vassiliki Athanassiou, Shinya Fukuda, and T Alan Hatton. Surface activity of poly (ethylene oxide)-block-poly (propylene oxide)-block-poly (ethylene oxide) copolymers. *Langmuir*, 10(8):2604–2612, 1994.

[158] E Hecht and H Hoffmann. Interaction of aba block copolymers with ionic surfactants in aqueous solution. *Langmuir*, 10(1):86–91, 1994.

[159] Alexander V Kabanov, Irina R Nazarova, Irina V Astafieva, Elena V Batrakova, Valery Yu Alakhov, Alexander A Yaroslavov, and Victor A Kabanov. Micelle formation and solubilization of fluorescent probes in poly (oxyethylene-b-oxypropylene-b-oxyethylene) solutions. *Macromolecules*, 28(7):2303–2314, 1995.

[160] Gerd Wanka, Heinz Hoffmann, and Werner Ulbricht. Phase diagrams and aggregation behavior of poly (oxyethylene)-poly (oxypropylene)-poly (oxyethylene) triblock copolymers in aqueous solutions. *Macromolecules*, 27(15):4145–4159, 1994.

[161] Per Linse and Martin Malmsten. Temperature-dependent micellization in aqueous block copolymer solutions. *Macromolecules*, 25(20):5434–5439, 1992.

[162] Liu Yang, Xiaohan Wu, Feng Liu, Yourong Duan, and Suming Li. Novel biodegradable polylactide/poly (ethylene glycol) micelles prepared by direct dissolution method for controlled delivery of anticancer drugs. *Pharmaceutical research*, 26:2332–2342, 2009.

[163] Zukang Zhou and Benjamin Chu. Anomalous micellization behavior and composition heterogeneity of a triblock aba copolymer of (a) ethylene oxide and (b) propylene oxide in aqueous solution. *Macromolecules*, 21(8):2548–2554, 1988.

[164] Zukang Zhou and Benjamin Chu. Light-scattering study on the association behavior of triblock polymers of ethylene oxide and propylene oxide in aqueous solution. *Journal of colloid and interface science*, 126(1):171–180, 1988.

[165] Stuart L Nolan, Ronald J Phillips, Patricia M Cotts, and Stephanie R Dungan. Light scattering study on the effect of polymer composition on the structural properties of peo–ppo–peo micelles. *Journal of colloid and interface science*, 191(2):291–302, 1997.

[166] Kell Mortensen and Jan Skov Pedersen. Structural study on the micelle formation of poly (ethylene oxide)-poly (propylene oxide)-poly (ethylene oxide) triblock copolymer in aqueous solution. *Macromolecules*, 26(4):805–812, 1993.

[167] G Kwon, M Naito, M Yokoyama, T Okano, Y Sakurai, and K Kataoka. Block copolymer micelles for drug delivery: loading and release of doxorubicin. *Journal of controlled release*, 48(2-3):195–201, 1997.

[168] Xin D Guo, Jeremy PK Tan, Sung H Kim, Li J Zhang, Ying Zhang, James L Hedrick, Yi Y Yang, and Yu Qian. Computational studies on self-assembled paclitaxel structures: templates for hierarchical block copolymer assemblies and sustained drug release. *Biomaterials*, 30(33):6556–6563, 2009.

[169] Mohammad Ramezani and Jamal Shamsara. Application of dpd in the design of polymeric nanomicelles as drug carriers. *Journal of Molecular Graphics and Modelling*, 66:1–8, 2016.

[170] Paola Posocco, Maurizio Fermeglia, and Sabrina Pricl. Morphology prediction of block copolymers for drug delivery by mesoscale simulations. *Journal of Materials Chemistry*, 20(36):7742–7753, 2010.

[171] Gokhan Kacar. Molecular understanding of interactions, structure, and drug encapsulation efficiency of pluronic micelles from dissipative particle dynamics simulations. *Colloid and Polymer Science*, 297:1037–1051, 2019.

[172] Ammu Prhashanna, Saif A Khan, and Shing Bor Chen. Co-micellization behavior in poloxamers: dissipative particle dynamics study. *The journal of physical chemistry B*, 119(2):572–582, 2015.

[173] Ammu Prhashanna, Wee Kian Tan, Saif A Khan, and Shing Bor Chen. Co-micellization behavior of triblock copolymers in the presence of hydrophobic drug molecules: A simulation study. *Colloids and Surfaces B: Biointerfaces*, 148:299–307, 2016.

[174] Chufen Yang, Cong Yuan, Wenyao Liu, Jianwei Guo, Dachun Feng, Xueqiong Yin, Wenjing Lin, Peter S Shuttleworth, and Hangbo Yue. Dpd studies on mixed micelles self-assembled from mpeg-pdeaema and mpeg-pcl for controlled doxorubicin release. *Colloids and Surfaces B: Biointerfaces*, 178:56–65, 2019.

[175] Fabian A Garcia Daza and Allan D Mackie. Coarse-grained simulations of modified jeffamine ed900 micelles. *Molecular Simulation*, 44(6):470–477, 2018.

[176] Fabian A Garcia Daza and Allan D Mackie. Low critical micelle concentration discrepancy between theory and experiment. *The journal of physical chemistry letters*, 5(11):2027–2032, 2014.

[177] Asfaw Gezae Daful, Vladimir A Baulin, Josep Bonet Avalos, and Allan D Mackie. Accurate critical micelle concentrations from a microscopic surfactant model. *The Journal of Physical Chemistry B*, 115(13):3434–3443, 2011.

[178] Zaid A Al-Anber, Josep Bonet i Avalos, M Antonio Floriano, and Allan D Mackie. Sphere-to-rod transitions of micelles in model nonionic surfactant solutions. *The Journal of chemical physics*, 118(8):3816–3826, 2003.

[179] Rakesh K Sharma, Sofiya Shaikh, Debes Ray, and Vinod K Aswal. Binary mixed micellar systems of peo-ppo-peo block copolymers for lamotrigine solubilization: a comparative study with hydrophobic and hydrophilic copolymer. *Journal of Polymer Research*, 25:1–11, 2018.

[180] Lin Yang, Paschalis Alexandridis, David C Steytler, Matthias J Kositza, and Josef F Holzwarth. Small-angle neutron scattering investigation of the temperature-dependent aggregation behavior of the block copolymer pluronic l64 in aqueous solution. *Langmuir*, 16(23):8555–8561, 2000.

[181] Abhinav Maheswaran Pragatheeswaran, Shing Bor Chen, Chi-Fan Chen, and Bing-Hung Chen. Micellization and gelation of peo-ppo-peo binary mixture with non-identical ppo block lengths in aqueous solution. *Polymer*, 55(20):5284–5291, 2014.

[182] B Sheelarani, Prakash Karunanithi, and Sasmita Dash. Effect of valency of cation on micellization behaviour of pluronic mixed micelle f127 and l64. *Chemical Physics Letters*, 739:136956, 2020.

[183] Zhang Wei, Junguo Hao, Shi Yuan, Yajuan Li, Wu Juan, Xianyi Sha, and Xiaoling Fang. Paclitaxel-loaded pluronic p123/f127 mixed polymeric micelles: formulation, optimization and in vitro characterization. *International journal of pharmaceutics*, 376(1-2):176–185, 2009.

[184] Alexander L Borovinskii and Alexei R Khokhlov. Micelle formation in the dilute solution mixtures of block-copolymers. *Macromolecules*, 31(22):7636–7640, 1998.

[185] Mikhail Yu Kozlov, Nikolai S Melik-Nubarov, Elena V Batrakova, and Alexander V Kabanov. Relationship between pluronic block copolymer structure, critical micellization concentration and partitioning coefficients of low molecular mass solutes. *Macromolecules*, 33(9):3305–3313, 2000.

UNIVERSITAT ROVIRA i VIRGILI

MANCHESTER
1824
The University of Manchester